USGS
science for a changing world

Landslide Hazards Program

Map Depicting Susceptibility to Landslides Triggered by Intense Rainfall, Puerto Rico

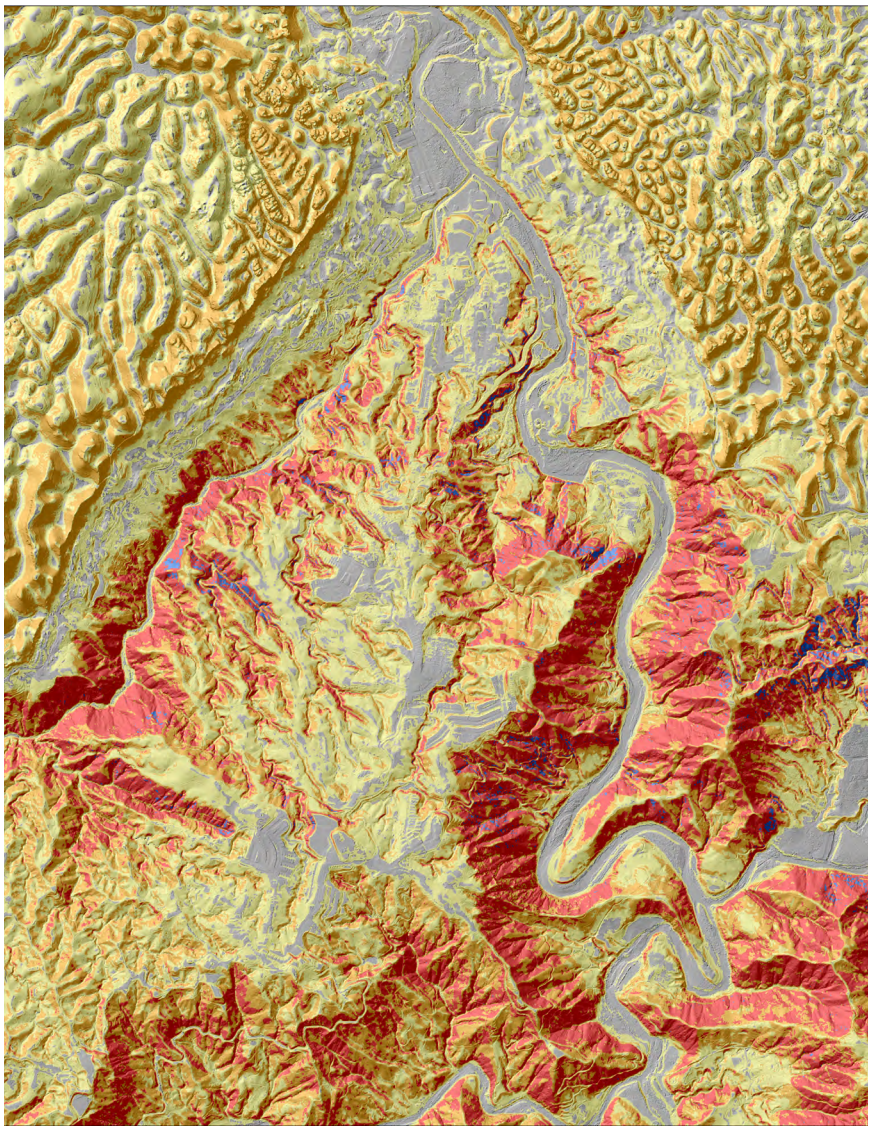

Open-File Report 2020–1022

U.S. Department of the Interior
U.S. Geological Survey

Cover. View from the landslide susceptibility map (plate 1) along the border between Ciales and Morovis municipalities, Puerto Rico.

Map Depicting Susceptibility to Landslides Triggered by Intense Rainfall, Puerto Rico

By K. Stephen Hughes and William H. Schulz

Landslide Hazards Program

Open-File Report 2020–1022

U.S. Department of the Interior
U.S. Geological Survey

U.S. Department of the Interior
DAVID BERNHARDT, Secretary

U.S. Geological Survey
James F. Reilly II, Director

U.S. Geological Survey, Reston, Virginia: 2020

Suggested citation:
Hughes, K.S., and Schulz, W.H., 2020, Map depicting susceptibility to landslides triggered by intense rainfall, Puerto Rico: U.S. Geological Survey Open-File Report 2020–1022, 91 p., 1 plate, scale 1:150,000, https://doi.org/10.3133/ofr20201022.

Associated data for this publication:
Hughes, K.S., and Schulz, W.H., 2020, Results from frequency-ratio analyses of soil classification and land use related to landslide locations in Puerto Rico following Hurricane María: U.S. Geological Survey data release, https://doi.org/10.5066/P9VK2FAL.

ISSN 2331-1258 (online)

Acknowledgments

The authors thank many colleagues and partners for their direct and indirect support of this project. K. Stephen Hughes (KSH) acknowledges the dedication of a terrific group of students in the Department of Geology at the University of Puerto Rico at Mayagüez who worked diligently to manually identify tens of thousands of landslide headscarps in aerial photographs taken across Puerto Rico after Hurricane María. These students include Sahira Cancel, Xavier García, Selena González, Edwin Irizarry, Raquel Lugo, Priscilla Ortiz, César Rodríguez, Amos Santiago, Yanira Santiago, Stephanie Soto, and Karla Torres. Additional support was provided by U.S. Department of Agriculture Natural Resource Conservation Service personnel Luis Aponte, Brendaly Rodríguez, and Misha Vargas. Special thanks to team members Desireé Bayouth and Gabriel Martínez who performed the tedious final verification of all landslide sites across the island. KSH is grateful to Chiara Lepore for sharing her previous susceptibility analysis data. KSH also thanks colleague James Joyce for helpful counsel in the subject matter in addition to the University of Puerto Rico at Mayagüez College of Arts and Sciences for providing release time to devote to the project.

KSH and William H. Schulz thank Arleen Reyes Rodriguez and Félix Rivera Santiago of the Puerto Rico Planning Board for their suggestions and assistance while developing the susceptibility map. Both authors also wish to thank Jim Hibbard and Félix Rivera Santiago for thoughtful and constructive review of the report. Desireé Bayouth is thanked for translating the report into Spanish. Both authors also thank Rex Baum, Jeffrey Coe, Eric Jones, and Robert Schmitt of the U.S. Geological Survey for their suggestions and assistance while developing the susceptibility map. Rex Baum and Jeffrey Coe are also thanked for their thoughtful and constructive review of the report.

Contents

Figures

Tables

Conversion Factors

U.S. customary units to International System of Units

Multiply	By	To obtain
	Area	
acre	0.004047	square kilometer (km^2)

International System of Units to U.S. customary units

Multiply	By	To obtain
	Length	
centimeter (cm)	0.3937	inch (in.)
millimeter (mm)	0.03937	inch (in.)
meter (m)	3.281	foot (ft)
kilometer (km)	0.6214	mile (mi)
	Area	
square kilometer (km^2)	247.1	acre
	Volume	
cubic meter (m^3)	264.2	gallon (gal)
cubic meter (m^3)	0.0002642	million gallons (Mgal)
cubic meter (m^3)	35.31	cubic foot (ft^3)
cubic meter (m^3)	1.308	cubic yard (yd^3)

Datum

Horizontal coordinate information is referenced to the World Geodetic System of 1984 (WGS84).

Abbreviations

°	degree
AUC	area under curve
DEM	digital elevation model
FR	frequency ratio
GAP	Gap Analysis Program
GIS	geographic information system
KSH	K. Stephen Hughes
lidar	light detection and ranging
MUKEY	mapunit key
NASA	National Aeronautics and Space Administration
ROC	receiver operating characteristic
SI	Susceptibility Index
SIA	aggregate *SI* value
SIA_m	the final modified *SI* value at each 5-meter pixel islandwide
SMAP	Soil Moisture Active Passive
USGS	U.S. Geological Survey

Map Depicting Susceptibility to Landslides Triggered by Intense Rainfall, Puerto Rico

By K. Stephen Hughes,[1] and William H. Schulz[2]

Executive Summary

Puerto Rico is vulnerable to landsliding. This report summarizes creation of a new high-resolution model of rainfall-induced landslide susceptibility for the main island. The main island of Puerto Rico was classified at 5-meter pixel scale into categories of Low, Moderate, High, Very High, or Extremely High susceptibility to landsliding during and soon after intense rainfall, such as is produced during tropical cyclones. The map data can be downloaded as georeferenced files in multiple formats by the public or government agencies and used in a geographic information system platform. The model is intended for use in planning, development, and emergency management. The map highlights areas susceptible to landsliding that may warrant further site-specific evaluation by licensed professionals.

This map product highlights an important collaboration between the U.S. Geological Survey and the Department of Geology at the University of Puerto Rico at Mayagüez that materialized after the destructive Hurricanes Irma and María in September 2017. An inventory of more than 70,000 mass wasting sites triggered by Hurricane María represents one of the initial products of this partnership and was an essential dataset in the modeling effort described in the report. Characteristics of the inventoried sites were statistically analyzed to produce Susceptibility Index values for various geospatial factors that were combined to form the new map product. The model output demonstrates how post-disaster data can be used to better understand risks and hazards for the future. The project benefited from diverse feedback among colleagues in the U.S. Geological Survey, at the University of Puerto Rico at Mayagüez, and government agencies in Puerto Rico. In addition, the inventory and present study satisfy sections (a), (b), (c), (d), and (i) of Article 4 in Puerto Rico Law 24 of 2008—Protocol for the Mitigation of Landslide Risks in Puerto Rico. The susceptibility map also represents an important step in understanding erosion, sedimentation, and hazards that arise from heavy rainfall in Puerto Rico and the tropics.

Abstract

Landslides in Puerto Rico range from nuisances to deadly events. Centuries of agricultural and urban modification of the landscape have perturbed many already unstable hillsides on the tropical island. One of the main triggers of mass wasting on the island is the high-intensity rainfall that is associated with tropical atmospheric systems. Puerto Rico's geographic position and rugged topography render millions of residents vulnerable to widespread landslide events. In this study, a high-resolution (5 meters), high-intensity rainfall-induced landslide susceptibility model was produced using the frequency-ratio method. Datasets utilized in the model included a complete-island landslide inventory created from imagery obtained after Hurricanes Irma and María impacted the island during September 2017, slope inclination, land-surface curvature, soil type, geologic terrane, mean annual precipitation, land use, soil moisture, and distance to roadways and streams. The final data product (plate 1) is a statistically viable representation of where landslides are likely to initiate during or soon after intense rainfall, with a robust receiver operating characteristic area-under-curve value of 0.87. The model output raster pixel values were binned into 100 equal-area quantiles and then classified into Low, Moderate, High, Very High, and Extremely High classes of susceptibility. The Extremely High susceptibility classification represents the most vulnerable 1 percent of the island, whereas Very High, High, Moderate, and Low classifications cover 9, 20, 30, and 40 percent of the island, respectively. The susceptibility map is intended to assist in planning future development, mitigation measures, and post-event emergency response; however, it is not a substitute for site-specific, slope-stability assessments performed by licensed geologists and engineers. Additionally, the map does not portray locations where landslide material may travel after mobilization, and which may be at extreme risk; nor does it necessarily portray where landslides may occur during earthquakes or mass wasting triggered by prolonged, relatively low-intensity rainfall.

[1]University of Puerto Rico, Mayagüez, Puerto Rico.

[2]U.S. Geological Survey.

Introduction

Puerto Rico (18.25°N., 66.50°W.) is an approximately 9,000-square kilometers (km^2) Caribbean territory of the United States and is the easternmost island of the Greater Antilles archipelago. Home to more than 3 million citizens, the archipelago's population density is the fourth highest of any U.S. State or State-equivalent jurisdiction, behind only the District of Columbia, New Jersey, and Rhode Island (U.S. Census Bureau, 2010). Unlike those locations, most of the Puerto Rican landscape is mountainous, a consequence of its location along the tectonically active North American-Caribbean plate boundary zone. A narrow, discontinuous coastal plain rings a rugged interior where the highest peaks on the main island are more than 1,300 meters (m) above sea level and lie within 150 kilometers (km) of the more than 8,000 m deep Puerto Rico trench, which marks the plate boundary. The island's terrain is demarcated by the east-west trending Cordillera Central (fig. 1), which is the main north-south fluvial divide, and the Sierra de Luquillo that lies in the northeast corner of the territory. Because of the high-relief, rugged topography that covers most of the land surface, and relatively higher risk of tectonic or climatic conditions that can induce landslides, millions of residents in Puerto Rico are disproportionately more likely to suffer the effects of mass wasting than their counterparts in the continental United States (Jibson, 1987).

The purpose of the landslide susceptibility map product presented herein (plate 1) is to provide high-resolution (5-m pixel) hazard data that can be directly used by citizens and government agencies to assess and plan effectively for future extreme precipitation events that induce widespread slope failure across the main island of the territory. Given that long-term tropical cyclone forecasts predict more frequent high-intensity events that will likely directly affect Puerto Rico in the future (Knutson and others, 2010; Jennings and others, 2014; Keellings and Hernández Ayala, 2019; Ramos-Scharrón and Arima, 2019), this landslide susceptibility map can be used as a tool to potentially avoid the loss of life and property.

Background

Mass Wasting in Puerto Rico

Mass movements present persistent hazards in Puerto Rico. Landslides, rockfalls, slumps, debris flows, and other mass movements are responsible for the loss of human life, private property, transportation routes, utility infrastructure, and the temporary isolation of remote communities across the densely populated, rugged Caribbean island (for example, Jibson, 1987; Larsen, 2012; Bessette-Kirton and others, 2019). For this report, the term "landslide" is used to include all types of slope failure. The mountainous interior of the island is most at risk from landslides; however, landslides also present risks in an extensive karst province and coastal zones marked by steep cliffs and terraces. The 1985 landslide disaster at Mameyes in Ponce (fig. 2), which claimed at least 129 lives, serves as a reminder of the vulnerability to landslides on the island and remains the deadliest landslide event to have occurred in any jurisdiction of the United States (Jibson, 1986; Silva-Tulla, 1986). Large block landslides like the Mameyes example exist at other locations across the island (figs. 3 and 4), including Cerca del Cielo (Wang, 2012, 2013; Rivera Santiago, 2015), Lago Guajataca Dam (Monroe, 1967; Silva-Tulla and others, 2018); El Yunque (Wang and others, 2013), Highway PR-10 in Utuado (Rodriguez-Pérez and others, 1988; Deere and others, 1989), Highway PR-9 in Ponce (García López, 2018), and scattered along the southern karst escarpment (Monroe, 1964). Much more frequent and widespread are shallow mass movements that usually mobilize into fast-moving channelized debris flows that deliver sediment directly to the fluvial network (figs. 5–9; Campbell and others, 1985; Jibson, 1986, 1989; Larsen and Simon, 1990, 1993; Simon and others, 1990; Larsen and Torres Sánchez, 1992; Larsen and Santiago Román, 2001; Pando and others, 2005; Larsen, 2012; Hughes and Morales Vélez, 2017; Morales Vélez and Hughes, 2018; Silva-Tulla and others, 2018; Bessette-Kirton and others, 2019). The introduction of liberated sediment into a river system also has negative consequences related to sedimentation, especially in watersheds that have impounded reservoirs (for example, Soler-López, 2000; Rodríguez Feliciano and others, 2019).

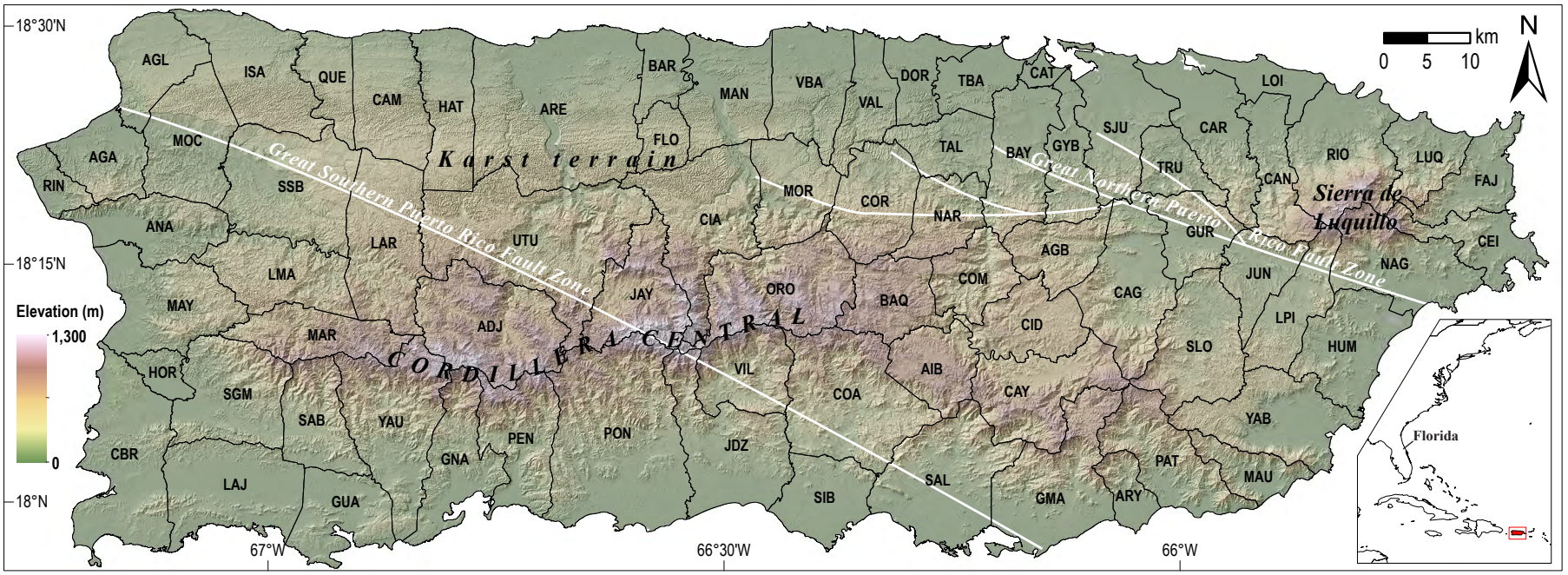

Figure 1. Topography of the U.S. territory of Puerto Rico (U.S. Geological Survey, 2017). The east–west trending Cordillera Central is the principal topographic feature on the island. It reaches more than 1,300 meters (m) above sea level and is the primary drainage divide between rivers to the north that drain to the Atlantic Ocean and rivers to the south that drain to the Caribbean Sea. The north coast karst terrain covers about 20 percent of the island's surface. The prominent Sierra de Luquillo in eastern Puerto Rico is the site of El Yunque National Forest. Puerto Rico is the easternmost of the Greater Antilles archipelago and lies approximately 1,600 kilometers (km) southeast of the State of Florida (see inset). Approximate locations of the Great Northern and Great Southern Puerto Rico Fault Zones are modified from Zachariasen and von Hillebrandt-Andrade (2005). Explanation of municipality abbreviations can be found in appendix 1.

Figure 2. Headscarp and body of the large block landslide in 1985 at Mameyes, Ponce, Puerto Rico (18.024, –66.619). Photograph taken October 1985 by James Joyce, University of Puerto Rico at Mayagüez, used with permission. View is looking west.

Figure 3. Large block landslide along Highway PR–9 in Ponce, Puerto Rico (18.032, –66.636). Photograph taken on 4 September 2018 by Stephen Hughes, University of Puerto Rico at Mayagüez. View is looking southeast.

Figure 4. Large block failure along uncompleted section of PR–385 in Peñuelas, Puerto Rico (18.051, –66.724). Photograph taken by the Puerto Rico Autoridad de Carreteras y Transportación on 20 November 2005. View is looking south.

Figure 5. Debris flows (light-colored linear features on the hillslopes) triggered by Hurricane Georges along the Rio Grande de Arecibo in Utuado, Puerto Rico (18.222, –66.717). Photograph taken on 1 October 1998, courtesy of Cheryl Hapke, U.S. Geological Survey. View is looking north.

Figure 6. Landslide along Highway PR–4131 in the municipality of Lares, Puerto Rico (18.250, –66.884). Photograph taken on 15 October 2017 by the Civil Air Patrol (2017). View is looking west.

Figure 7. Abundant shallow mass movements and debris flows on the eastern side of the upper reach of Lago Caonillas, Puerto Rico (18.252, –66.644). Photograph taken by the Civil Air Patrol (2017) on 17 October 2017. View is looking northeast.

Figure 8. Landslide that transitioned to debris flow along Highway PR–143 in Barranquitas, Puerto Rico (18.176, –66.338). Photograph taken by the Civil Air Patrol (2017) on 12 October 2017. View is looking west.

Figure 9. Shallow failure in Río Blanco watershed of Naguabo, Puerto Rico (18.266, –65.789). Photograph taken on 26 March 2018 by Stephen Hughes, University of Puerto Rico at Mayagüez. View is looking east–southeast.

General Geology of Puerto Rico

The geology of the island is complex. In its simplest conceptualization, two main components include (1) an Eocene and older basement arc complex (Jolly and others, 1998a, 1998b) that is unconformably overlain by (2) a late Oligocene to Pliocene carbonate cover sequence (Monroe, 1980a; Ortega-Ariza and others, 2015). The basement rocks include volcaniclastic units, granodiorite plutons, serpentinite, and other rock types. Since the Pliocene, the island has experienced uplift, which continues to the present (Taggart and Joyce, 1989; Brocard and others, 2015); adjustment to this tectonic forcing has promoted topographic disequilibrium. Fluvial incision into low-relief erosional surfaces has shaped a deeply dissected landscape where hillslopes are oversteepened and drainage divides are susceptible to piracy. Erosion is also controlled in many places by the local bedrock geology. For example, karstification of carbonate rocks that underlie about 20 percent of the island has resulted in a topographic expression distinct from that of other geologic units on the island. In these karst zones, most water movement is subterranean, but elsewhere, surficial fluvial processes have exploited the abundance of faulted contacts in the island's older basement arc complex. Pronounced valley systems mark both the Great Northern and Southern Puerto Rico Fault Zones. Classic graben and half-graben fault systems are also expressed in the topography of western Puerto Rico (Grindlay and others, 2005; Mann and others, 2005; Prentice and Mann, 2005; Moul-Bogunovic, 2019). Chemical weathering is accelerated in most of the territory due to the prevalent humid tropical climate.

Natural Landslide-Provoking Phenomena in Puerto Rico

The island is particularly exposed to tropical cyclone activity because of its latitude and ocean setting. The most devastating atmospheric events to affect Puerto Rico usually originate near the Cape Verde islands in the eastern Atlantic Ocean and travel west-northwest towards the Lesser and Greater Antilles (Ramos-Scharron and Arima, 2019). The most destructive hurricanes that have affected Puerto Rico since U.S. occupation in 1898 are San Ciriaco (1899) and María (2017). Because of vast differences in the political and societal landscape of the island during each event, direct comparison of the impacts of the two storms is difficult. However, both storms caused historic flooding, destruction of infrastructure, extensive loss of cultivated lands, and loss of life. Hurricane San Ciriaco resulted in the death of more than 3,000 residents and left more than 200,000 residents of the total population of about 950,000 homeless and facing starvation (Sanger and others, 1900; Schwartz, 1992). Hurricane María also caused the death of an estimated 3,000 citizens and triggered the outmigration of about 8 percent (about 280,000 people) of the island population in the months after the storm (Milken Institute School of Public Health, 2018).

The archipelago lies at the seismically active interface of the North American and Caribbean tectonic plates. Widespread slope failures can also be triggered by seismic shaking. A swarm of earthquakes with magnitude as great as 6.4 occurred from December 2019 to January 2020 generally offshore of the Guanica municipality (fig. 1) and triggered rockfalls from steep slopes in limestone bedrock near the epicentral area (Lopez and others, 2020). Prior to this, the 1918 magnitude 7.2 Mona Passage earthquake (Doser and others, 2005) initiated mostly rockfalls that were generally reported in areas underlain by limestone bedrock units in the northwest portion of the island, closest to the inferred epicenter zone offshore (Reid and Taber, 1919).

Anthropogenic Topographic Perturbations

Since colonization in the late 15th century, diverse societal factors in Puerto Rico have contributed to an increase in the failure susceptibility of hillslopes, many of which were already naturally vulnerable. During the 19th century under Spanish control, almost all of the usable Puerto Rican landscape was developed for agricultural crops such as sugarcane, coffee, and plantains (Dietz, 1986). In the decades after U.S. acquisition in 1898, a shift towards industrialization occurred, and in the latter 60 years of the 20th century, forests increased from only 10 percent coverage of the island to more than 40 percent (Grau and others, 2003). This statistic represents the abandonment of agricultural practices for the majority of the population and the movement towards urbanization. Both the agricultural and industrial phases of land use practice have involved extensive road networks. For the agrarian phase, a dense and tangled web of improvised roads was developed across montane plantations, and during the urbanization phase, construction of dense residential communities expanded into the hills and mountains surrounding population centers. Excavation and fill placement associated with road building throughout the development of the island has led to an increase in landslide susceptibility along and near roadways (for example, Larsen and Torres-Sanchez, 1992).

Previous Landslide Susceptibility Studies for Puerto Rico

Puerto Rico has been the focus of many landslide-related investigations given that it is a geographically, topographically, and climatologically unique jurisdiction under U.S. control. Puerto Rico-specific rainfall intensity thresholds have been empirically derived for historical storms that triggered widespread mass wasting (Larsen and Simon, 1993; Pando and others, 2005). Island-wide estimations of high landslide vulnerability zones have been carried out in the past at 1:240,000 and 1:60,000 scales (Monroe, 1979; Kamal, 2008; Lepore and others, 2012). Monroe's hand-drawn map (1979) was developed based upon extensive bedrock and surficial mapping carried out across the island and showcases zones susceptible to large and deep bedrock failures along prominent escarpments in the island's northern carbonate region (fig. 10). The vast majority of the interior of the island was classified as moderately susceptible, without much differentiation. Kamal (2008) and Lepore and others (2012) used a robust bivariate statistical method and partial landslide inventories available in central and eastern Puerto Rico to derive a susceptibility model (fig. 11) superior to Monroe's map (1979). The same general bivariate approach is used in this study, with modification.

Some regionally focused landslide susceptibility maps have been prepared for individual municipalities, including Ponce (PON; Larsen and others, 2004) and Comerío (COM; Larsen and Parks, 1998) at 1:30,000 and 1:20,000 scale, respectively. Both of these maps were prepared using a subjective matrix methodology and regional mass movement inventories. In addition, a seismic-triggered landslide susceptibility map was prepared for seven municipalities in the San Juan metropolitan area (TBA, CAT, BAY, SJU, GYB, CAR, and TRU; Santiago and Larsen, 2001).

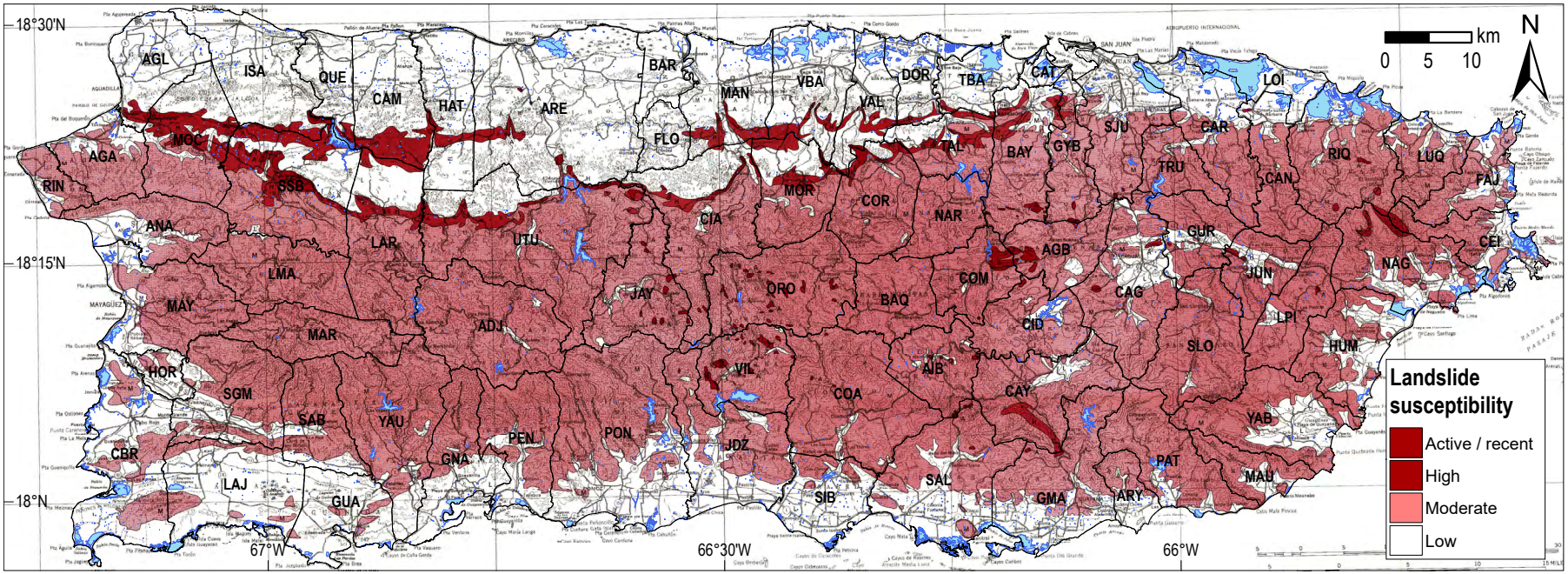

Figure 10. Hand-drawn landslide susceptibility map (1:240,000) modified from Monroe (1979). Most zones of active movement and high susceptibility lie within and at the margin of the northern carbonate province. Explanation of municipality abbreviations can be found in appendix 1. (km, kilometer)

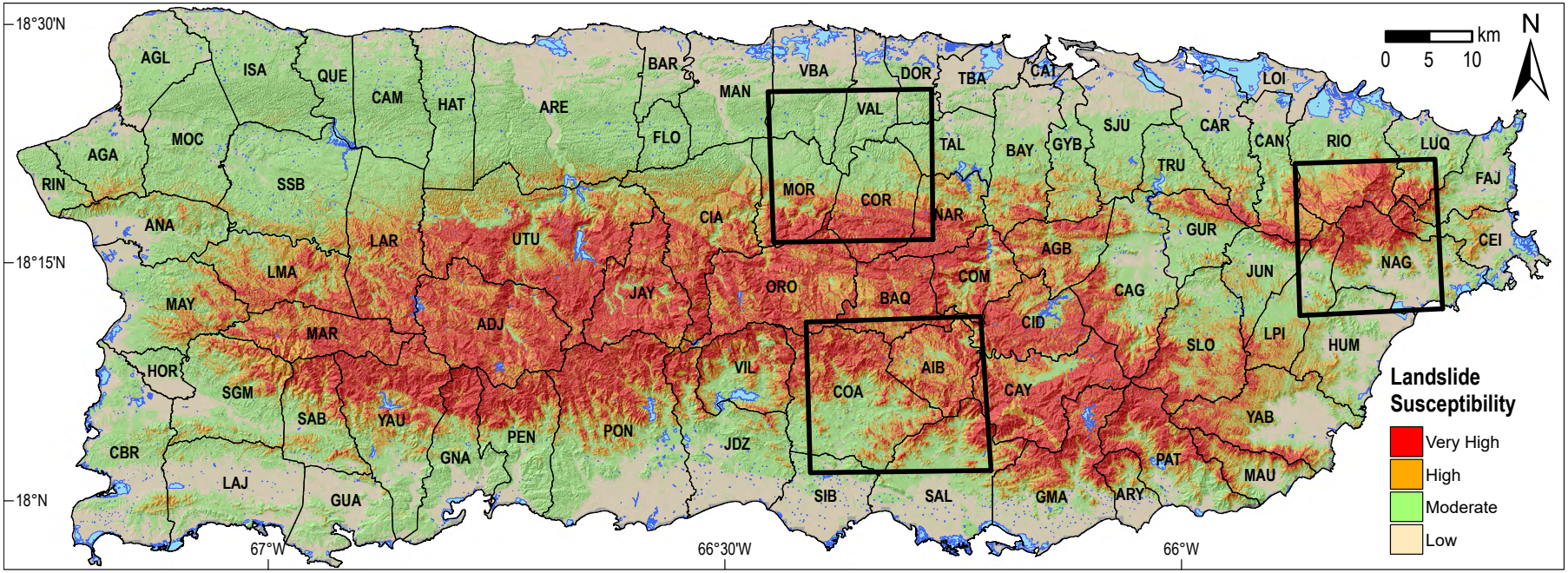

Figure 11. Landslide susceptibility map modified from Lepore and others (2012). Inventory areas used to inform their model are delineated by the three boxes. Explanation of municipality abbreviations can be found in appendix 1. (km, kilometer)

Datasets and Methodology

The landslide susceptibility model described herein utilizes the Hurricane María digital landslide inventory (figs. 12 and 13; Hughes and others, 2019) as well as a host of other geospatial data. The inventory includes 71,431 points that correspond to the centers of headscarps formed at failure initiation sites. The sites were manually identified using high-resolution, georeferenced, post-event aerial and satellite imagery. The dataset appears to represent the largest rainfall-induced event slope failure inventory to date. The smaller municipalities of Culebra and Vieques that lie offshore of the main island were not incorporated in the model because they do not present considerable sites for slope failure and there were no landslides on these islands in the Hurricane María post-event inventory (Hughes and others, 2019). In addition, other minor outlying islands off the coast of Puerto Rico, including Caja de Muertos, Desecheo, Mona, and Monito, were not included in the analysis.

Various data in this study are classified by their correlation with María slope-failure sites and combined into a comprehensive model. The method employed is the frequency-ratio (FR) bivariate approach (Lee and Pradhan, 2006; Lee and others, 2007; He and Beighley, 2008; Lepore and others, 2012; Chalkias and others, 2014). Like other empirical assessments, FR analysis assumes that landslides are likely to occur in locations that have very similar conditions to previous failure sites (Brabb, 1984; Varnes, 1984; Sidle and Ochiai, 2006). The use of FR modeling requires that quantitative target factors (such as slope, curvature, aspect, and so on) are classified into ranges or bins. Then the percentage of total study area covered by that bin range is compared to the total percentage of events (landslides in this case) from some empirical dataset that are geospatially coincident with the locations where the bin range exists in the study area. A FR value for each bin (*i*) of each characteristic (*f*) is calculated using equation 1 (modified from He and Beighley, 2008; Lepore and others, 2012; and Chalkias and others, 2014):

$$FR_{fi} = \frac{N_{Lfi} / N_L}{A_{fi} / A}, \tag{1}$$

where:

FR_{fi} is the frequency-ratio value for each bin (*i*) of each characteristic (*f*),

N_{Lfi}/N_L is the ratio of the number of landslides in a bin (for example, slope of 0 degrees [°] –5°) to the total number of landslides, and

A_{fi}/A is the ratio of any area with the same bin characteristic to the total study area.

The value of FR_{fi} is interpreted to indicate higher correlation of the event dataset to the geospatial factor dataset if it is greater than 1. FR_{fi} values cannot be 0 or negative. Equation 2 was used to convert FR_{fi} values to Susceptibility Index (*SI*) values because equally opposite FR_{fi} values are not symmetrically distributed about the neutral value of 1:

$$SI_{fi} = ln\ (FR_{fi}), \tag{2}$$

where:

SI_{fi} is the *SI* value for each bin (*i*) of each characteristic (*f*).

Once converted to *SI* values, the neutral value is now 0, and negative numbers represent anti-correlation and positive numbers represent correlation between the event dataset and the geospatial factor dataset. Table 1 shows an example of hypothetical FR_{fi} values converted to SI_{fi} values. The use of SI_{fi} values allows for the simple summing of classified factor raster datasets in the final model output.

Only a random 75 percent of the Hurricane María slope failure event inventory (Hughes and others, 2019) was used to calculate the *SI* values for the landslide susceptibility model. The remaining 25 percent was used to examine the viability of the model using a receiver operating characteristic (ROC) curve (see "Results and Discussion" section). Although landslide inventories were created following other events (Jibson, 1989; Larsen and Torres-Sanchez, 1992), we were unable to obtain georeferenced versions of these inventories with which to test our model. We attempted to georeference the inventories from the publications, but results indicated inconsistent mislocations as great as several hundred meters between mapped landslides and their apparent true locations revealed by a light detection and ranging- (lidar-) derived digital elevation model (DEM; U.S. Geological Survey [USGS], 2017). Once the *SI* values for each of the factors described below were calculated, they were combined using equation 3 to obtain an aggregate *SI* value (*SIA*) for each pixel at 5-m resolution across the main island of Puerto Rico (fig. 14):

$$SIA = (SI_{f1} + SI_{f1} + SI_{f1} + SI_{f4}\ ...) + X(SI_{fs}), \tag{3}$$

where:

SIA is the aggregate *SI* value,

SI_{fn} is the *SI* value for nonslope factor *n*,

X is the number of nonslope factors, and

SI_{fs} is the *SI* value for the slope factor.

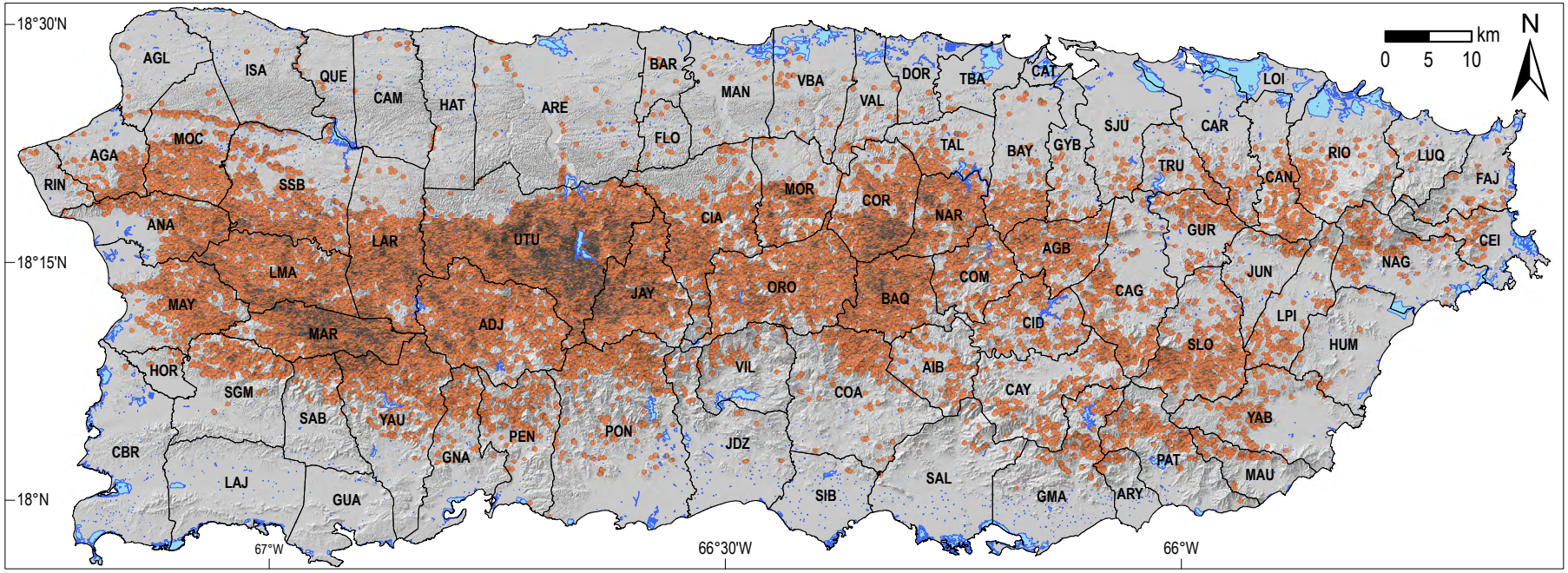

Figure 12. Hurricane María event slope failure inventory (Hughes and others, 2019). Each small circle represents one landslide site. There are 71,431 sites in the inventory. Explanation of municipality abbreviations can be found in appendix 1. (km, kilometer)

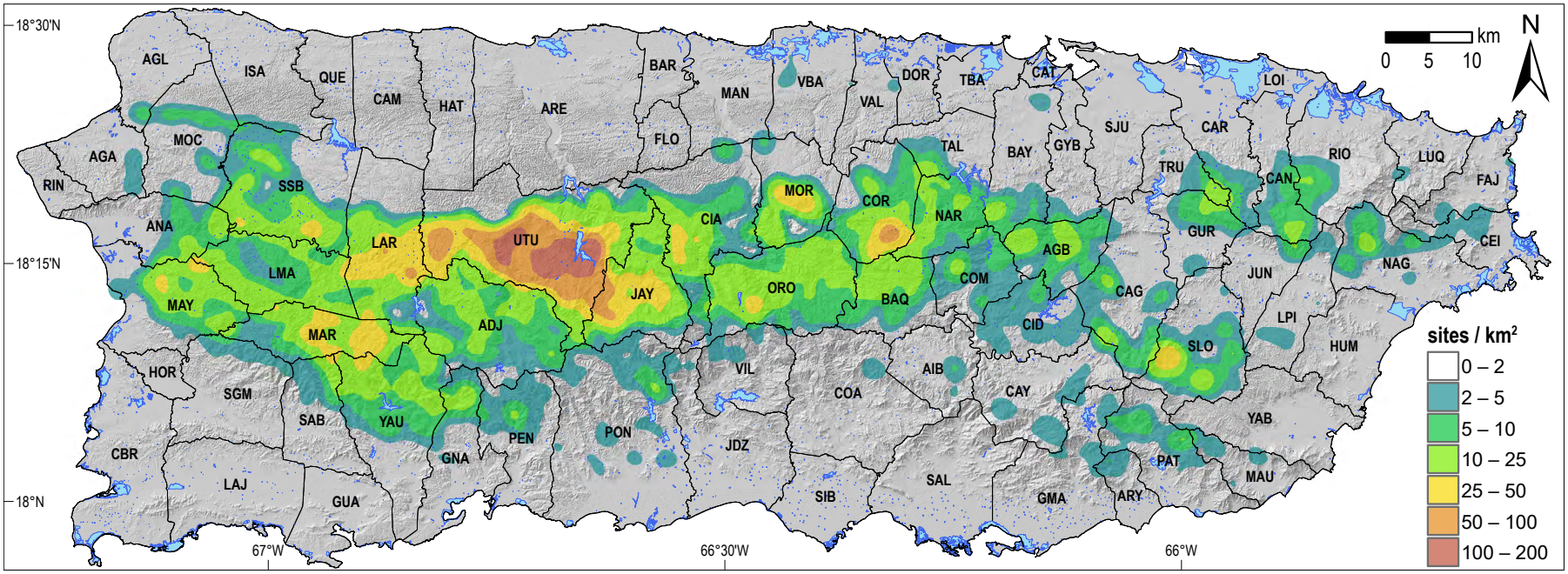

Figure 13. Density of landslide sites from the Hurricane María event inventory. Point data from Hughes and others (2019) were used to determine the spatial density of the points, which is shown in the figure. The figure was created with kernel density technique using a 2-km-diameter window. Explanation of municipality abbreviations can be found in appendix 1. (km, kilometer; km^2, square kilometer)

Table 1. Hypothetical examples of a set of frequency-ratio (FR) values and corresponding Susceptibility Index (*SI*) values for a given bin (*i*) of any characteristic (*f*). Cooler colors represent increasingly less correlation between the characteristic bin and inventory sites. Warmer colors represent increasingly greater correlation between the characteristic bin and inventory sites. A FR value of 1 and *SI* value of 0 are neutral. *SI* is the natural log of FR.

[FR_{fi}, the frequency-ratio value for each bin (*i*) of each characteristic (*f*); SI_{fi}, the *SI* value for each bin (*i*) of each characteristic (*f*)]

Ratio	FR_{fi}	SI_{fi}
1:5	0.2	-1.61
1:4	0.25	-1.39
1:3	0.33	-1.11
1:2	0.5	-0.69
1:1	1	0
2:1	2	0.69
3:1	3	1.1
4:1	4	1.39
5:1	5	1.61

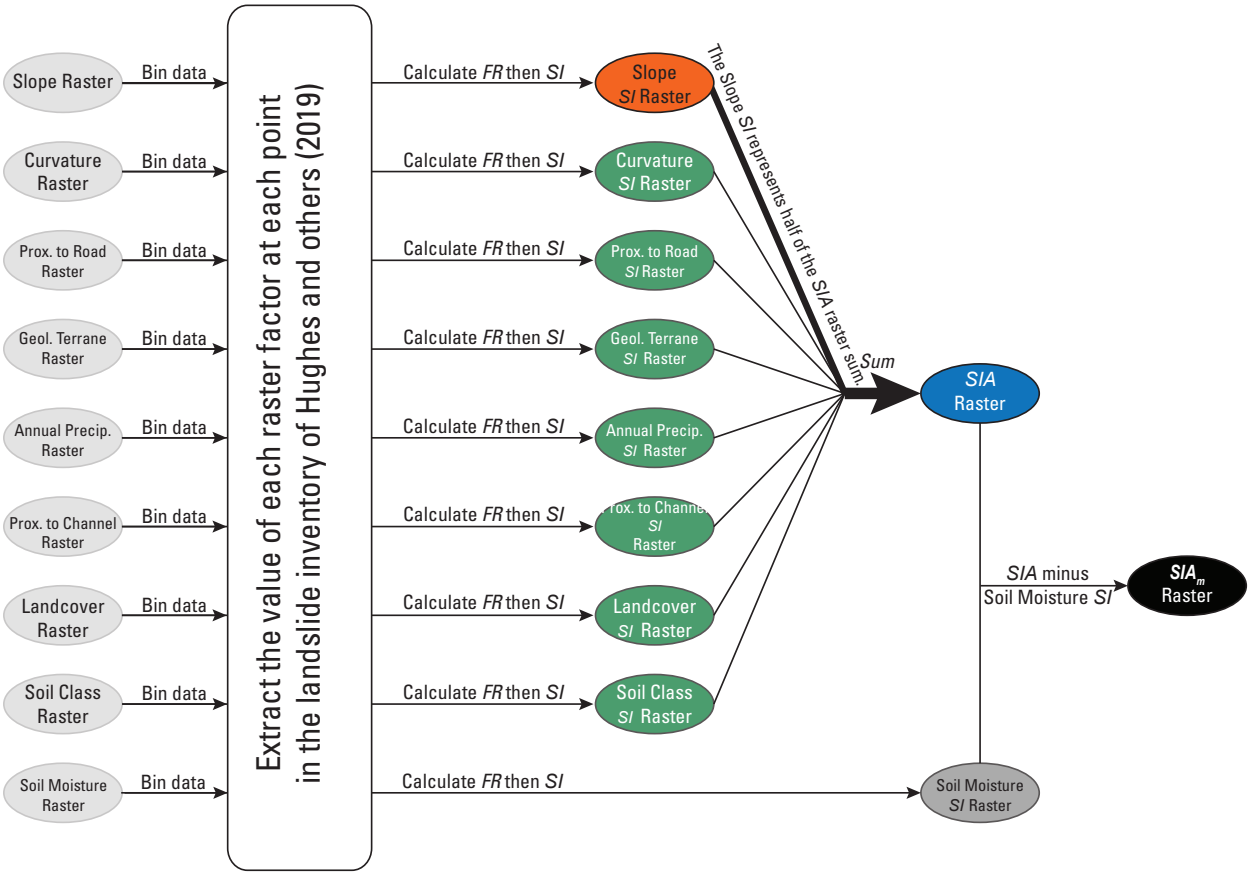

Figure 14. Flowchart depicting the process followed to develop the SIA_m raster, which forms the basis for the landslide susceptibility map (geol., geological; precip., precipitation; prox., proximity; FR, frequency ratio; *SI*, Susceptibility Index; *SIA*, aggregate Susceptibility Index; SIA_m, aggregate Susceptibility Index modified by soil moisture)

Table 2. Data utilized in the frequency-ratio analyses.

[USGS, U.S. Geological Survey: lidar, light detection and ranging; NHD, National Hydrography Dataset; GAP, Puerto Rico Gap Analysis Program; USDA, U.S. Department of Agriculture; NRCS, Natural Resources Conservation Service; NASA, National Aeronautics and Space Administration]

Factor[1]	Data source	Original resolution	Final resolution	Interpolation
Slope	2015–2016 USGS lidar[2]	1 meter	5 meters	No
Curvature	2015–2016 USGS lidar[2]	1 meter	5 meters	No
Proximity to road surface	U.S. Census Bureau Tiger/Line Shapefile[3]	Polyline vector	5 meters	No
Geology	USGS/Puerto Rico Office of Management & Budget[4]	1:20,000 polygon vector	5 meters	No
Mean annual precipitation	Fick and Hijmans, 2017	900 meters	5 meters	No
Proximity to fluvial channel	USGS NHD Flowline[5]	Polyline vector	5 meters	No
Land cover	USDA GAP Land Cover[6]	15 meters	5 meters	No
Soil classification	USDA NRCS[7]	Polygon vector	5 meters	No
Soil moisture	NASA Soil Moisture Active Passive[8]	9,008 meters	5 meters	Yes

[1]Factors are highlighted in bolded text when first described in the following paragraphs.

[2]USGS, 2017.

[3]U.S. Census Bureau, 2015.

[4]Puerto Rico Oficina de Gerencia y Presupuesto, 2018.

[5]USGS, 2019.

[6]Gould and others, 2008.

[7]USDA, 2018.

[8]NASA, 2017.

The factors used in the analysis are recorded in table 2. The resultant output model has the slope *SI* values as half of the input and all other combined factors as the remaining half of the input. This weighting of slope input was selected by trial-and-error evaluations of effects on regions known to have historically high and low landslide susceptibility.

In order to make the susceptibility map applicable for any intense rainfall event, an attempt was made to temper any bias resulting from variable rainfall and soil moisture conditions unique to the Hurricane María event because the model was derived from that single rainfall event inventory. Bessette-Kirton and others (2019) found that the spatial density of landslides triggered by Hurricane María correlated well with remotely sensed root zone soil moisture data from the National Aeronautics and Space Administration (NASA) Soil Moisture Active Passive (SMAP) mission collected 1 day after the event (NASA, 2017), and did not correlate as well with rainfall estimates. Using equation 4, we calculated *SI* values for the same SMAP data and subtracted these from the *SIA* values to account for soil moisture variability following the hurricane:

$$SIA_m = SIA - SI_{SMAP}, \tag{4}$$

where:

SIA_m is the final modified *SI* value at each 5-m pixel islandwide, and

SI_{SMAP} is the *SI* value calculated based on the root zone soil moisture content estimated for 21 September 2017.

The SMAP dataset is discussed further below, as is an approach to utilize future SMAP data along with the landslide susceptibility map data to improve forecasts of the locations of landslides triggered by specific events (in the "Use and Limitations of the Landslide Susceptibility Map" section.)

Slope angle is usually considered one of the most important factors with regards to mass wasting, especially for shallow failures (for example, Carson and Petley, 1970). Values of slope at 5-m pixel resolution were binned into 5° intervals for analysis. All slopes greater than 45° were combined into one group. The distribution of slope bins across the island is presented in table 3 and figure 15. About 40 percent of the island has a slope of less than 10°, another 40 percent has a slope between 10–30°, and the remaining 20 percent is greater than 30° inclination. The lowest slopes are generally coastal; however, broad alluvial valleys are present in some interior zones along rivers such as the Rio Gurabo, Rio Grande de Arecibo, and others. The north coast karst province is a zone of especially high slopes along the flanks of mogotes, sinkholes, zanjones, and other dissolution features. Where the karst is covered by blanket sand deposits, the north coast has very low slopes. Along the Cordillera Central, slopes on the southern flank are generally higher, on average, given that the rivers destined for the Caribbean Sea have shorter distances to descend to base level from the divide. Notable high-slope topographic features across the island include the Lares escarpment along the southern edge of the karst province, river gorges incised into the karst terrain (Rio Guajataca, Rio Camuy, Rio Tanamá, Rio Grande de Arecibo, Rio Grande de Manatí), and the Cañon San Cristobal. Not all high slope zones are confined to the higher elevation interior as there are prominent sea cliffs in both northwestern and southeastern corners of the island, in addition to other locations. Although most urban centers are positioned in lower slope areas, the population density across the rugged interior remains high. Lakes and reservoirs were classified as areas with 0° slope.

Hillslope **curvature** is classified as convex, concave, or planar. Ridge tops are generally convex but hollows are concave. Curvature was calculated at 5-m pixel resolution using the combination of profile and planform profiles (standard curvature function). Positive values represent convexities and negative values represent concavities. The amount of convex versus concave topography across Puerto Rico is approximately equal (about 35 percent each) and pixels classified as planar and near-planar represent the remaining approximately 30 percent (fig. 16). Curvature values are binned as shown in table 3. Lakes and reservoirs are classified as planar areas.

Both slope and curvature metrics are calculated from a pre-María 1-m resolution lidar-derived DEM raster (USGS, 2017) that was resampled to 5-m resolution. Using lidar data has been shown to be far superior for landslide investigations than traditional, low-resolution DEMs created with photogrammetric methods (for example, Schulz, 2007). The lidar-derived DEM is almost complete for the island. Data do not exist for approximately 55 km^2 (less than 1 percent of the island) located in the vicinity of Lago Carite in southeastern Puerto Rico (fig. 17). The three polygonal zones without data are mostly in Cayey and Guayama municipalities with much less expression in Salinas, Patillas, San Lorenzo, and Yabucoa municipalities. Within these zones, the gaps were seamlessly filled with older, non-lidar data extracted from a 5-m resolution DEM (Puerto Rico Centro de Recaudación de Ingresos Municipales, 1998). The DEM used to fill the data gaps results in a less-detailed slope and curvature product in those specific areas because the DEM was produced using aerial imagery photogrammetry, which reveals less ground surface detail than a lidar survey.

Roadway construction often involves cutting and filling of the natural landscape. If Puerto Rico were an independent nation, its road density (kilometer/square kilometer) would rank ninth globally (NationMaster, 2017). Larsen and Parks (1997) showed that **proximity to road surfaces** in mountainous regions of Puerto Rico increases the likelihood of mass wasting. This correlation is a result of stress redistribution from cutting and filling, and alteration of surface and subsurface drainage paths, all of which can result in decreased slope stability. In addition, many rural roads are not constructed using best practices for reducing slope instability (Larsen and Parks, 1997). The correlation between landslides and the presence of roads was explored using the Hurricane María

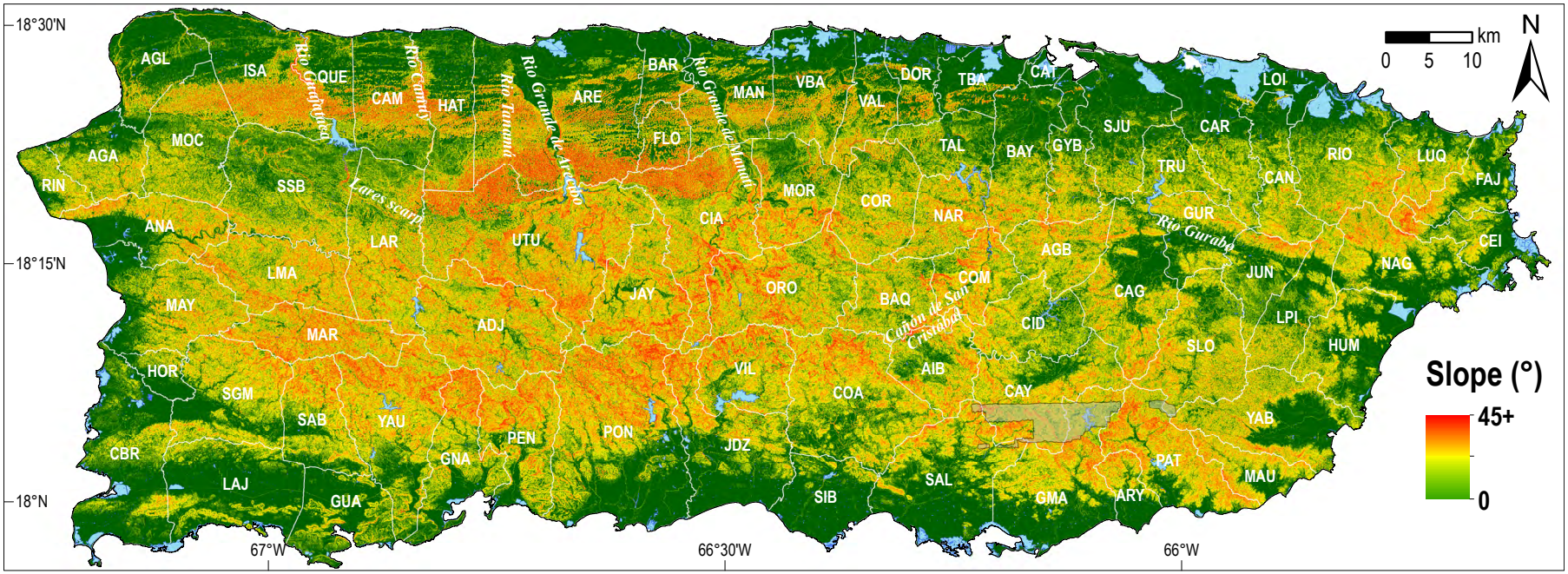

Figure 15. Slope map for the island of Puerto Rico. Values calculated from lidar-derived digital elevation model (U.S. Geological Survey, 2017). Resolution is 5 meters. The shaded polygonal zones mostly within Cayey (CAY) and Guayama (GMA) in the southeast are explained in the text and shown on figure 17. Explanation of municipality abbreviations can be found in appendix 1. (km, kilometer; °, degree]

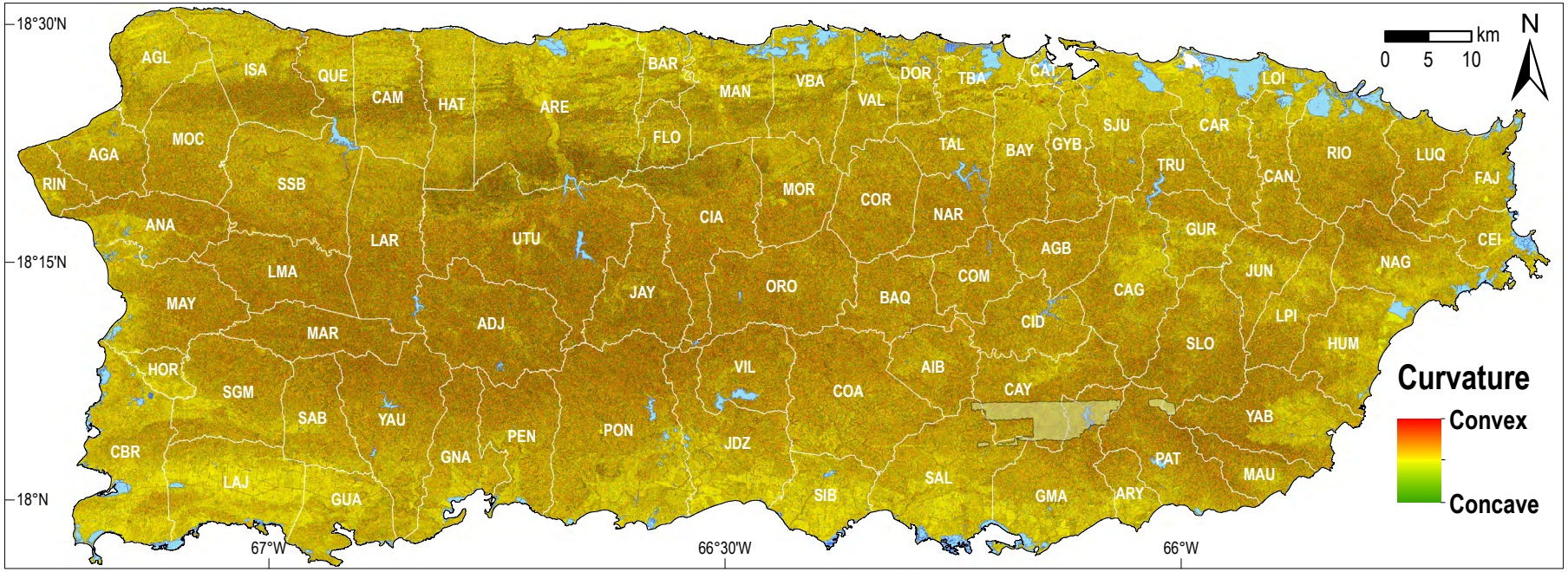

Figure 16. Curvature values calculated from lidar-derived digital elevation model for the island of Puerto Rico (U.S. Geological Survey, 2017). Resolution is 5 meters. The shaded polygonal zones mostly within Cayey (CAY) and Guayama (GMA) in the southeast are explained in the text and shown on figure 17. Explanation of municipality abbreviations can be found in appendix 1. (km, kilometer)

Table 3. Results from frequency-ratio analyses of potential landslide-contributing factors.

[Values may not sum due to rounding. °, degree; km², square kilometer; %, percent; #, number; FR, frequency ratio; *SI*, Susceptibility Index; —, not applicable; m, meter; <, less than; >, greater than; K-T, Cretaceous and Tertiary; wv/sv, water volume/soil volume]

Bin	Area (km²)	Area (%)	Landslides[1] (#)	Landslides[1] (%)	FR	*SI*
			Slope			
0–5°	2,477.5	28.5	415	0.8	0.03	−3.60
5–10°	924.1	10.6	660	1.2	0.12	−2.15
10–15°	821.8	9.4	1,114	2.1	0.22	−1.51
15–20°	867.6	10.0	2,157	4.0	0.40	−0.91
20–25°	924.8	10.6	4,116	7.7	0.72	−0.32
25–30°	908.5	10.4	7,726	14.4	1.38	0.32
30–35°	773.5	8.9	12,403	23.2	2.61	0.96
35–40°	545.4	6.3	13,316	24.9	3.97	1.38
40–45°	282.1	3.2	8,468	15.8	4.88	1.59
45–90°	181.9	2.1	3,198	6.0	2.86	1.05
Total	**8,707.2**	**100.0**	**53,573**	**100.1**	—	—
			Curvature			
<−50 (0.01/m)	7.2	0.1	42	0.08	0.95	−0.05
−50–−25 (0.01/m)	66.4	0.8	882	1.60	2.16	0.77
−25–−10 (0.01/m)	446.9	5.1	6,551	12.20	2.38	0.87
−10–−5 (0.01/m)	681.4	7.8	7,285	13.60	1.74	0.55
−5–−1 (0.01/m)	1,845.2	21.2	8,293	15.50	0.73	−0.31
−1–1 (0.01/m)	2,489.4	28.6	4,739	8.80	0.31	−1.17
1–5 (0.01/m)	1,876.8	21.6	8,029	15.00	0.70	−0.36
5–10 (0.01/m)	785.5	9.0	7,453	13.90	1.54	0.43
10–25 (0.01/m)	462.8	5.3	9,166	17.10	3.22	1.17
25–50 (0.01/m)	38.9	0.4	1,114	2.10	4.66	1.54
>50 (0.01/m)	6.6	0.1	19	0.04	0.47	−0.76
Total	**8,707.1**	**100.0**	**53,573**	**99.92**	—	—
			Proximity to road surface			
0–10 m	1,051.7	12.1	7,256	13.50	1.12	0.12
10–25 m	1,140.6	13.1	8,902	16.60	1.27	0.24
25–50 m	1,363.1	15.6	9,809	18.30	1.17	0.16
50–75 m	1,012.9	11.6	6,968	13.00	1.12	0.11
75–100 m	782.1	9.0	5,049	9.40	1.05	0.05
100–200 m	1,798.0	20.6	10,319	19.30	0.93	−0.07
200–400 m	1,119.3	12.8	4,471	8.40	0.65	−0.43
400–1,000 m	397.2	4.6	772	1.40	0.32	−1.15
1,000+ m	52.4	0.6	27	0.05	0.08	−2.48
Total	**8,717.3**	**100.0**	**53,573**	**99.95**	—	—
			Geologic terrane			
Quaternary alluvium	1,875.1	21.5	438	0.80	0.040	−3.27
Tertiary cover sequence	1,496.9	17.2	1,102	2.10	0.120	−2.12
Cretaceous non-igneous	61.1	0.7	9	0.02	0.020	−3.73
Tertiary intrusive	285.5	3.3	2,829	5.30	1.610	0.48
Cretaceous intrusive	654.2	7.5	15,149	28.30	3.760	1.33

Table 3. Results from frequency-ratio analyses of potential landslide-contributing factors.—Continued

[Values may not sum due to rounding. °, degree; km², square kilometer; %, percent; #, number; FR, frequency ratio; *SI*, Susceptibility Index; —, not applicable; m, meter; <, less than; >, greater than; K-T, Cretaceous and Tertiary; wv/sv, water volume/soil volume]

Bin	Area (km²)	Area (%)	Landslides[1] (#)	Landslides[1] (%)	FR	*SI*
K-T volcaniclastic	3,506.5	40.3	31,514	58.80	1.460	0.38
Hydrothermic/metamorphic	112.0	1.3	588	1.10	0.850	−0.16
Basalts, cherts, others	355.4	4.1	1,297	2.40	0.590	−0.52
Serpentinite/amphibolite	115.1	1.3	408	0.80	0.580	−0.55
Quaternary landslide	53.2	0.6	232	0.40	0.710	−0.34
Surficial water	193.8	2.2	7	0.01	0.006	5.14
Total	**8,708.8**	**100.0**	**53,573**	**100.03**	—	—
Mean annual precipitation						
0–250 mm	0.0	0.0	0	0.000	—	—
250–500 mm	0.0	0.0	0	0.000	—	—
500–750 mm	0.0	0.0	0	0.000	—	—
750–1,000 mm	484.3	5.6	1	0.002	0.00	[2]8.00
1,000–1,250 mm	589.0	6.8	98	0.200	0.03	−3.61
1,250–1,500 mm	705.7	8.1	148	0.300	0.03	−3.38
1,500–1,750 mm	1,859.8	21.3	3,190	6.000	0.28	−1.28
1,750–2,000 mm	3,149.4	36.1	20,498	38.700	1.06	0.06
2,000–2,250 mm	1,637.9	18.8	23,469	43.800	2.33	0.85
2,250–2,500 mm	290.8	3.3	6,169	11.500	3.45	1.24
Total	**8,716.9**	**100.0**	**53,573**	**100.502**	—	—
Proximity to fluvial channel						
0–10 m	309.9	3.6	780	1.5	0.41	−0.89
10–25 m	388.2	4.5	2,091	3.9	0.88	−0.13
25–50 m	602.6	6.9	4,941	9.2	1.33	0.29
50–75 m	578.8	6.6	4,354	8.1	1.22	0.20
75–100 m	552.6	6.3	3,930	7.3	1.16	0.15
100–200 m	1,939.6	22.3	13,916	26.0	1.17	0.15
200–400 m	2,405.4	27.6	17,694	33.0	1.20	0.18
400–1,000 m	1,333.6	15.3	5,778	10.8	0.70	−0.35
1,000+ m	605.4	7.0	89	0.2	0.02	−3.73
Total	**8,716.1**	**100.0**	**53,573**	**100.0**	—	—
Land cover[3]						
Moist grasslands and pastures	2,184.6	25.10	14,547	27.20	1.08	0.08
Montane wet evergreen abandoned/active coffee plantation	548.9	6.30	13,920	26.00	4.12	1.42
Young secondary lowland moist noncalcareous evergreen forest	530.5	6.10	3,077	5.70	0.94	−0.06
High density urban development	522.8	6.00	38	0.10	0.01	−4.44
Mature secondary moist limestone evergreen and semideciduous forest	464.6	5.30	130	0.20	0.05	−3.09
Montane wet noncalcareous evergreen shrubland and woodland	241.1	2.80	5,831	10.90	3.93	1.37
Young secondary montane wet noncalcareous evergreen forest	216.7	2.50	4,018	7.50	3.02	1.10

Table 3. Results from frequency-ratio analyses of potential landslide-contributing factors.—Continued

[Values may not sum due to rounding. °, degree; km², square kilometer; %, percent; #, number; FR, frequency ratio; *SI*, Susceptibility Index; —, not applicable; m, meter; <, less than; >, greater than; K-T, Cretaceous and Tertiary; wv/sv, water volume/soil volume]

Bin	Area (km²)	Area (%)	Landslides[1] (#)	Landslides[1] (%)	FR	*SI*
Montane west alluvial shrubland and woodland	9.0	0.10	120	0.20	2.17	0.77
Mature secondary montane wet alluvial evergreen forest	6.1	0.07	80	0.20	2.12	0.75
Wet serpentine shrubland and woodland	3.6	0.04	42	0.08	1.91	0.64
Total	**8,713.5**	**100.00**	**53,573**	**100.00**	—	—
Soil classification[4]						
Mucara clay (326695) 40–60% slopes	298.9	3.40	2,154	4.0	1.17	0.16
Tanamá Rock Outcrop (326474) 12–60% slopes	239.4	2.80	46	0.1	0.03	−3.47
Caguabo clay loam (326645) 40–60% slopes	218.5	2.50	877	1.6	0.65	−0.43
Consumo clay (326530) 40–60% slopes	157.6	1.80	4,863	9.1	5.02	1.61
Caguabo clay loam (326863) 20–60% slopes	128.6	1.50	297	0.6	0.38	−0.98
Pellejas clay loam (326463) 40–60% slopes	98.9	1.10	8,524	15.9	14.01	2.64
Maricao clay (326577) 20–60% slopes	3.8	0.04	295	0.6	12.65	2.54
Lirios clay loam (326445) 40–60% slopes	59.1	0.70	3,802	7.1	10.47	2.35
Los Guineous clay (326566) 20–60% slopes	6.9	0.08	374	0.7	8.78	2.17
Lirios clay loam (326444) 20–40% slopes	3.0	0.04	146	0.3	7.85	2.06
Total	**8,713.8**	**100.00**	**53,573**	**100.0**	—	—
Soil moisture						
0.14–0.15 wv/sv	7.1	0.08	13	0.02	0.30	−1.21
0.15–0.20 wv/sv	318.4	3.65	787	1.47	0.40	−0.91
0.20–0.25 wv/sv	260.4	2.99	576	1.08	0.36	−1.02
0.25–0.30 wv/sv	1,081.4	12.41	988	1.84	0.15	−1.91
0.30–0.35 wv/sv	2,118.2	24.30	2,852	5.32	0.22	−1.52
0.35–0.40 wv/sv	3,150.9	36.15	19,051	35.56	0.98	−0.02
0.40–0.45 wv/sv	1,571.6	18.03	22,477	41.96	2.33	0.84
0.45–0.50 wv/sv	208.7	2.39	6,829	12.75	5.33	1.67
Total	**8,716.7**	**100.00**	**53,573**	**100.00**	—	—

[1]Only a random 75 percent of the Hurricane María slope failure inventory was used to calculate the FR and *SI* values. The remaining 25 percent was used to test the final model. The total number of sites in the inventory is 71,431.

[2]The minimum *SI* value used in the model creation was −5.00. *SI* values less than this limit were set to −5.00. This was employed in order to avoid incorporating anomalously low *SI* values in the model due to low factor areal extent.

[3]The Puerto Rico Gap Analysis Program dataset includes 66 distinct land cover classifications across Puerto Rico. Only the top five most widespread and top five FR value classes are shown here. The full data and results are in appendix 2 and Hughes and Schulz (2020).

[4]The U.S. Department of Agriculture Natural Resources Conservation Service soils dataset includes 697 unique soil unit numerical key code (mapunit key [MUKEY]) classes for the island of Puerto Rico. Only the top five most widespread and top five FR value classes are shown here. The full data and results are in appendix 3 and Hughes and Schulz (2020). The number in parenthesis listed for each soil class is the corresponding MUKEY.

event inventory and the U.S. Census Bureau TIGER line shapefile (fig. 18; U.S. Census Bureau, 2015). A raster populated with Euclidean distances to road surfaces was created at 5-m resolution. The results of this exercise, summarized in table 3, reveal that more than 50 percent of the island lies within 75 m of a roadway and only about 5 percent of the island lies more than 400 m from a road surface. The study by Larsen and Parks (1997) showed that mountainous terrain within 85 m of a roadway is at least 5 times more likely to suffer landsliding. Importantly, the TIGER line shapefile does not include many of the improvised and densely constructed farm and hacienda roads (fig. 19). In the early 20th century, Dorsey and others (1903) described the interior of the island to have "many trails which penetrate the island in almost every direction" (p. 839). These trails, paths, and roads have been shown to be primary sources of erosion and sedimentation within the Cordillera Central (Ramos-Scharrón and LaFevor, 2016).

Bedrock composition is very diverse across Puerto Rico (Jolly and others, 1998b). The rock type combined with the varying effects of tropical chemical weathering result in distinct regolith products with varying susceptibility to mass movement. A digitized compilation of geologic quadrangle maps at 1:20,000 scale prepared by the USGS in the latter half of the 20th century was utilized in this study (Puerto Rico Oficina de Gerencia y Presupuesto, 2018). For the quadrangles that were not published at 1:20,000 scale (Rincón, Guánica, and Sabana Grande), both unpublished 1:20,000 scale maps and published 1:100,000 map data were used for the digitization. The hundreds of geological units were binned according to the 10 terranes assigned by Bawiec (1998). The 10 terranes, as well as surficial water, are shown on figure 20. The data in table 3 show that about 20 percent of the island is classified as Quaternary alluvium. An almost equal area is underlain by the Tertiary cover sequence rocks. About 40 percent of the island is the volcaniclastic basement complex with an additional almost 10 percent of Cretaceous and Tertiary intrusive igneous rocks. The less than 1 percent of the island mapped as Quaternary landslides includes mostly deep bedrock features mapped along the southern margin of the karst province by Watson Monroe and associates (Monroe, 1963, 1967, 1969a, 1969b; Berryhill, 1965; Briggs, 1965, 1968; Nelson, 1967; Nelson and Tobisch, 1968; Pease, 1968; McIntyre, 1971; Tobisch and Turner, 1971). The digitized 1:20,000 polygon shapefile was rasterized and reclassified to terrane at a 5-m resolution.

Although measuring only 170 km x 60 km, the main island of the Puerto Rican archipelago is home to several microclimates. Topographic features across the island, namely the Sierra de Luquillo and the Cordillera Central, coupled with the prevailing trade winds create both orographic rainfall and rain shadows. The prominent El Yunque rainforest in the eastern region and the central western interior are the wettest zones with more than 2 m of annual rainfall; the Guánica dry forest and other zones of the arid south coast receive less than 1 m of precipitation yearly (fig. 21; Fick and Hijmans, 2017). Areas with higher **annual precipitation** are more likely to be subjected to more intense chemical weathering in the humid tropical climate. The effect of chemical weathering is important in bedrock decomposition and soil development, both of which can influence hillslope stability. Additionally, because of orographic effects that result in higher precipitation at higher elevation, precipitation generally may partially serve as a proxy to represent mountainous areas, which are more likely to host landslides. Analysis of the precipitation dataset shows about 6 percent of the island with less than 1 m of annual rainfall, approximately 70 percent of the island between 1 m and 2 m of annual precipitation, and just over 20 percent with greater than 2 m of yearly rainfall (table 3). For the FR calculations, the dataset was binned into 0.25-m intervals. The original resolution of the dataset is 900 m, but it was resampled—not interpolated or smoothed—to 5-m pixel size to be consistent with the other factor raster datasets.

The principal agent of erosion in Puerto Rico is landsliding (Larsen, 2012), much of which occurs as a topographic adjustment to fluvial incision. Locally forced by tectonic uplift, fluvial downcutting results in oversteepened hillslopes that are primed for failure. Much like the distance to the road surface is used as an input to the model, proximity to fluvial channel is also incorporated. This factor addresses drainage network density, and distinguishes between the "normal" topographic terrain where surficial drainage dominates and the large karst province in the northern region of Puerto Rico, where there are very limited surficial drainage expressions in the landscape. The dataset used for the fluvial channels is the USGS National Hydrography Dataset flowline shapefile archive (fig. 22; USGS, 2019). Similar to the TIGER line shapefile for roads, Euclidean distance to the flowline shapefile features was generated at 5-m pixel resolution. The resultant raster dataset reveals that just under 30 percent of the island lies within 100 m of a fluvial channel as defined by the USGS, 50 percent of the island is between 100 m and 400 m from a fluvial channel, about 15 percent lies between 400 m and 1,000 m of a fluvial channel, and 7 percent of the island is more than 1,000 m from a fluvial channel (table 3). The areas of the island that lie farthest from fluvial channels are mostly in the northern karst zone, where many flow paths are subterranean. The bins for this dataset are set at the same intervals as the proximity-to-roads analysis.

The 20th century in Puerto Rico was a time of extended transition from a primarily agrarian civilization after 400 years of Spanish rule to a more modern, urbanized society (Dietz, 1986). The natural environment had been intensively modified by anthropomorphic activity prior to the island's acquisition by the United States. More recently, vast swaths of cultivated land have been abandoned and left to nature, resulting in reforestation across the island (Grau and others, 2003). **Land cover** is also integrated into the FR analysis because it reflects the type of local terrain and land-use styles that can control the topographic response to environmental forcings (Philpott and others, 2008). The Puerto Rico Gap Analysis Program (GAP) land cover raster (Gould and others, 2008) was chosen for the study and is resampled—not interpolated—from 15-m resolution to 5-m resolution in order to be compatible with the other model input datasets. The GAP data raster includes 66 distinct classifications (fig. 23), which were used during the analysis without combining the different classifications. The GAP data (table 3; app. 2; Hughes and

Figure 17. Missing zones for the 2015–2016 airborne lidar survey of Puerto Rico (U.S. Geological Survey, 2017) are shown as red polygons in the southeastern quadrant of the island. The gaps in coverage occur in portions of the municipalities of Salinas (SAL), Cayey (CAY), Guayama (GMA), Patillas (PAT), San Lorenzo (SLO), and Yabucoa (YAB). The data holes were patched with a preexisting 5-meter digital elevation model generated by the Puerto Rico Centro de Recaudación de Ingresos Municipales (1998). Explanation of municipality abbreviations can be found in appendix 1. (km, kilometer)

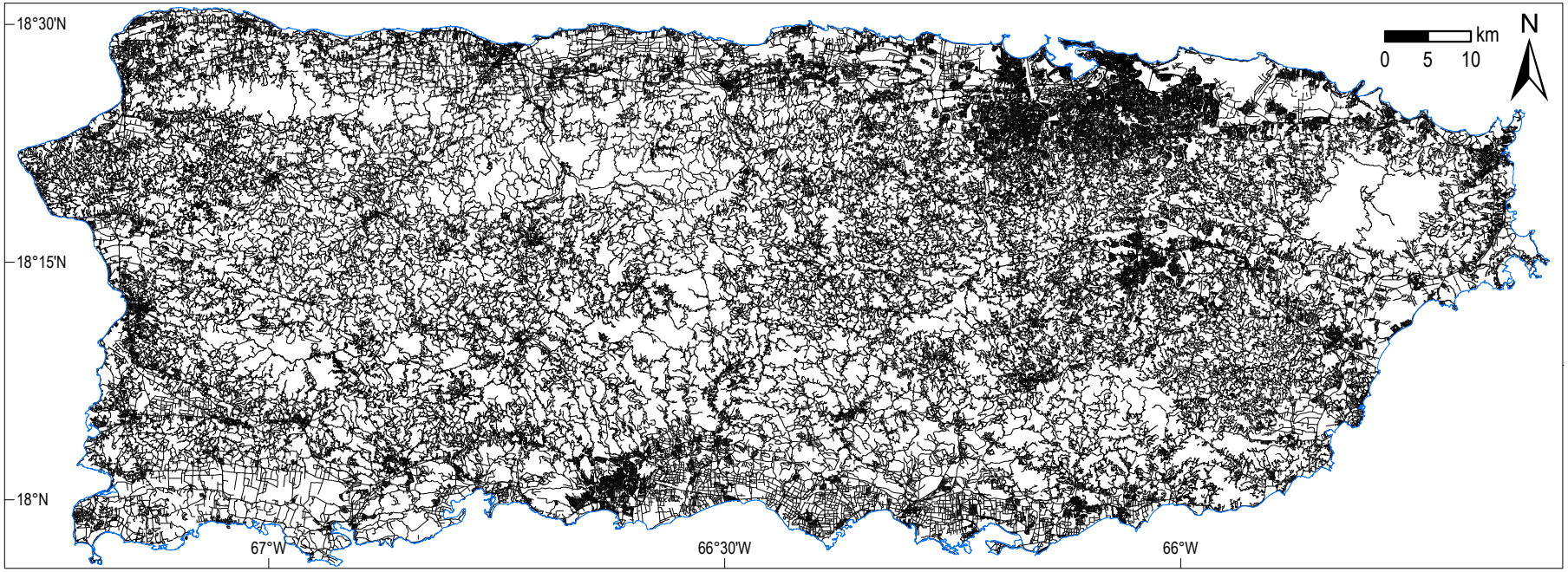

Figure 18. Paved roads on the island of Puerto Rico (U.S. Census Bureau, 2015). The densest population centers of San Juan (metro area), Caguas, and Ponce are distinct. Zones with very few roads are in the northwestern karst interior and in the Sierra de Luquillo (fig. 1) in the northeast of the island. The U.S. Census Bureau TIGER shapefile roads do not include dense farm road networks (see fig. 19). (km, kilometer)

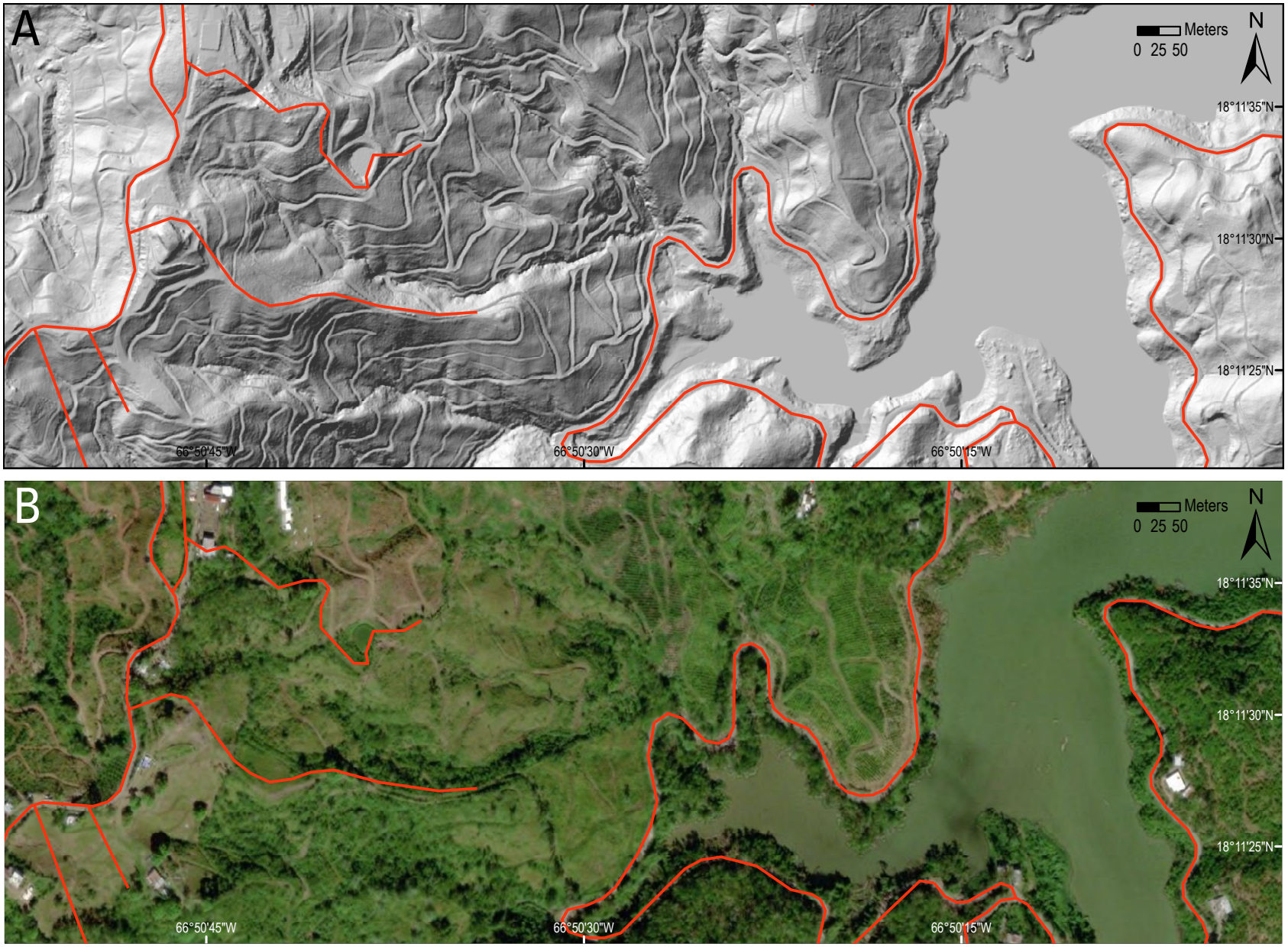

Figure 19. Example of dense improvised farm road network that is not digitized as part of the U.S. Census Bureau (2015) TIGER roads shapefile (shapefile roads shown as red lines). *A,* Hillshade raster from lidar-derived digital elevation model (U.S. Geological Survey, 2017) reveals very dense unpaved paths and trails that have been built across much of the mountainous interior of Puerto Rico and *B,* Aerial photograph of the same area. Location (18.190, -66.840) is Hacienda Buena Vista near Castañer at the upper end of Lago Guayo in the municipality of Lares. (m, meter)

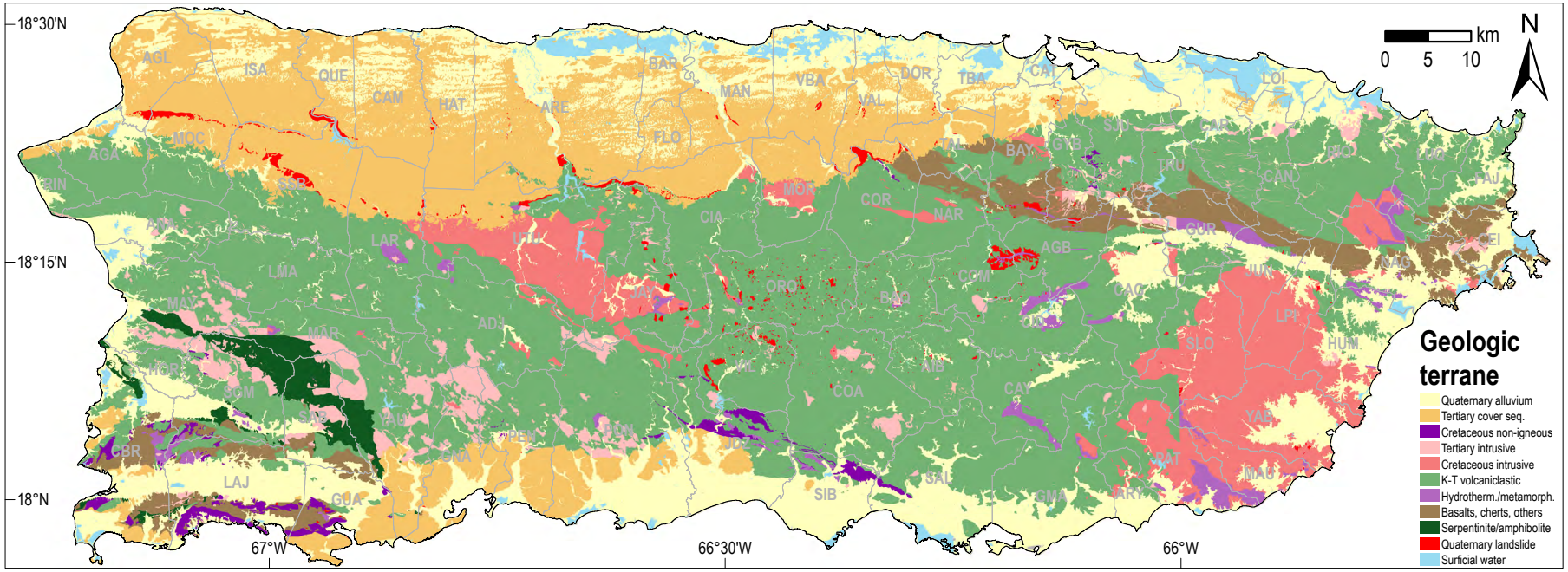

Figure 20. Digitized 1:20,000 geologic map units of Puerto Rico (from U.S. Geological Survey quadrangle maps) categorized using the scheme of Bawiec (1998). The bedrock basement complex of the island is mostly volcaniclastic rocks intruded by small to large plutons. Basement rocks in the north and south parts of the island are unconformably overlain by a sequence of mostly limestone units. Explanation of municipality abbreviations can be found in appendix 1. (km, kilometer; seq., sequence; hydrotherm., hydrothermal; metamorph., metamorphic)

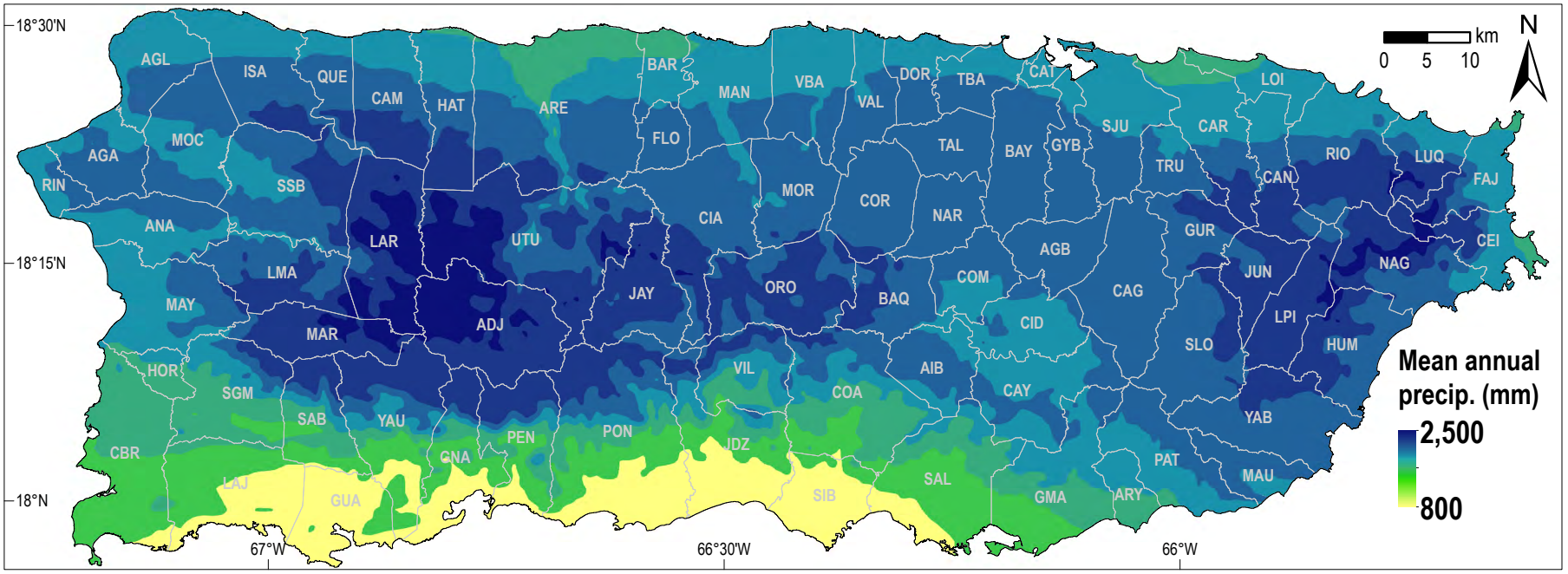

Figure 21. Mean annual precipitation in Puerto Rico (modified from Fick and Jijmans, 2017). The highest yearly rainfall amounts are in the Sierra de Luquillo and in the western interior regions of the island. The south coast is a more arid, rain shadow zone. Explanation of municipality abbreviations can be found in appendix 1. (km, kilometer; mm, millimeter; precip., precipitation)

Schulz, 2020) reveal that "Moist grasslands and pastures" cover 25 percent of the island and the next highest classifications of "Montane wet evergreen abandoned/active coffee plantation," "Young secondary lowland moist noncalcareous evergreen forest," and "High density urban development" each represent about 6 percent of the island's total area.

Soils in Puerto Rico are diverse, and include 10 of the 12 taxonomic classes (Muñoz and others, 2018). The only soils not found on the island are permafrost-related and active volcano-related soils. Detailed soil surveys of the island were started after U.S. acquisition (Dorsey and others, 1903) and continued throughout the remainder of the 20th century and into the 21st century (Roberts, 1942; Carter, 1965; Gierbolini, 1975; Boccheciamp, 1977, 1978; Gierbolini, 1979; Acevido, 1982; Huffaker, 2002; Lugo-Camacho, 2008). The result of the compilation and digitization of soils data by the U.S. Department of Agriculture Natural Resources Conservation Service is a high-resolution soils dataset of the complete island. The soil class vector file was rasterized to 5-m resolution and used in the analysis for this study (fig. 24). The soil unit numerical key code (mapunit key [MUKEY]) is used to define unique soil units because similar names and acronyms exist for distinct soil classes in separate study regions. The dataset includes 697 unique MUKEY values (table 3; app. 3; Hughes and Schulz, 2020). Some of these MUKEY values are assigned to identical soil units that exist in more than one regional soil survey area. However, the distinct MUKEY classes were not aggregated for the analysis so that as much spatial diversity could be explored as possible. The soils that are most widespread are the Mucara clay (40–60 percent slopes), the Tanamá complex rock outcrop (12–60 percent slopes), and the Caguabo clay loam (40–60 percent slopes) that cover 3.4, 2.8, and 2.5 percent of the island, respectively. Approximately 3 percent of the island is classified as "No Digital Data Available" or "Not Public Information." These locations mostly lie in urban areas and (or) closed Federal lands and were analyzed as independent soil units consistent with all soil unit analyses. For the purpose of this study, the actual composition of the local soils is not of importance, given that each area has an individual MUKEY classification and can be analyzed for landslide correlation.

Typically, landslide occurrence initiated by intense rainfall positively correlates with the cumulative rainfall amount because infiltration of precipitation elevates pore-water pressures, which consequently decrease effective normal stress and shear strength within potential shear zones (Terzaghi, 1950). Hurricane María produced rainfall amounts sufficient to trigger landsliding across all mountainous areas of Puerto Rico (Bessette-Kirton and others, 2019), making it an opportune event for the analysis of landslide susceptibility. However, precipitation amounts from Hurricane María were spatially variable, as they were from Hurricane Irma about 2 weeks prior, which can create event-specific bias in the results of susceptibility analyses such as the one described herein. In an attempt to account for and remove this bias from the susceptibility map, FR analysis of the landslide inventory and root-zone (0–100 centimeters [cm] depth) **soil moisture** estimated by the NASA SMAP mission for 9:30 am Atlantic Standard Time on 21 September 2017 (the day after Hurricane María; NASA, 2017), was carried out. As described by equation 4, the *SI* results for SMAP data were removed from the aggregate Susceptibility Index and resulting susceptibility map. Because of the failure of the local Doppler radar (National Weather Service Public Information Sheet, 2017) and many rain gage stations at various times during the passage of the storm, the precipitation estimates across the island for the event are quite variable (Bayouth García and others, 2018). In addition, soil moisture is a subsurface parameter that represents interception of precipitation, runoff, and infiltration and is a more accurate proxy for pore-water pressure conditions than rainfall data. Bessette-Kirton and others (2019) found stronger correlation between María-induced landslide density and the SMAP data than with available rainfall data. Figure 25 shows the SMAP data, which depict volumetric water content (volume of water/volume of soil) on a 9-km gridded basis. For the chosen sensor pass, soil moisture was generally higher in the mountainous interior of the island than around the perimeter, although high amounts were also present along the north-central and northwestern coastlines. The raw SMAP data were resampled to 5-m pixel size and interpolated using cubic convolution to provide a more realistic, smoother distribution of soil moisture values for use in this analysis (fig. 26).

In addition to all datasets being set to 5-m resolution, they were all processed in the same projection: WGS 84/UTM Zone 19N. The final data product is also registered in the same coordinate system. Certain datasets were analyzed but not used in the final model. Among others, these include hillslope aspect, elevation above sea level, and proximity to faults. Aspect was not used to preclude bias from event-specific conditions. In addition, a pilot study of the inventory dataset and a full island aspect map resulted in very little distinction with regards to aspect (Lugo Bendezú and others, 2018). This analysis also revealed that almost equal numbers of hillslopes are facing each cardinal direction on the island. Generally, tropical cyclones approach Puerto Rico from the east-southeast, which is important in terms of wind effects across ridge crests. However, the data used in this study do not demonstrate that directional rainfall had any effect on slope failure control. Elevation was rejected as a model input because there are notable low-relief upland zones (Lobeck, 1922; Meyerhoff, 1927; Monroe, 1980b; Brocard and others, 2015; Santiago-Pérez and others, 2019) as well as coastal cliff areas across the island; increase or decrease in altitude alone has no control on landslide potential. Relief rasters with various radii were explored, but this metric was also not included as a model input because relief over any given distance does not represent site-specific hillslope conditions as well as slope inclination. Proximity to a fault trace was not incorporated in the model due to the variability of fault mapping from quadrangle to quadrangle and the unknown positional precision of mapped faults.

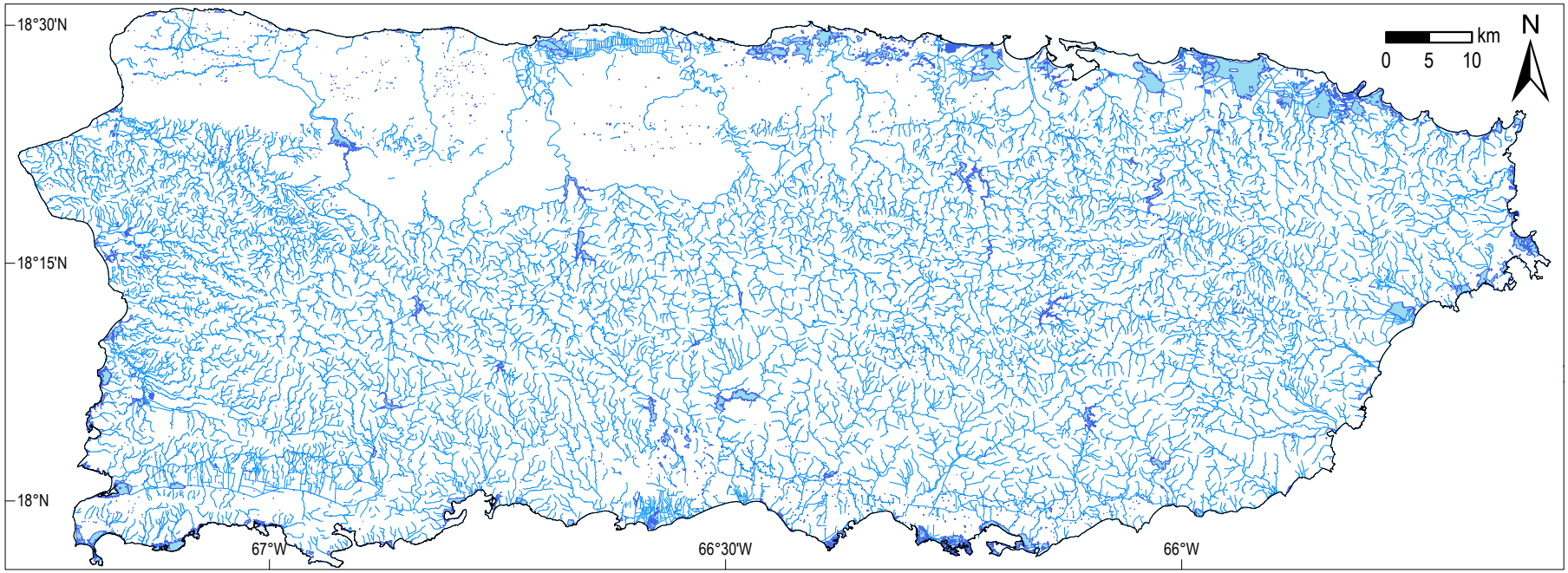

Figure 22. Fluvial channels for Puerto Rico from the National Hydrography Dataset geodatabase file (U.S. Geological Survey, 2019). The northcentral/northwest coast is characterized by sinking streams and subterranean flow through the karst region. Most of the remainder of the island has dendritic drainage patterns. Rivers follow prominent fault zones at various locations across the island. (km, kilometer)

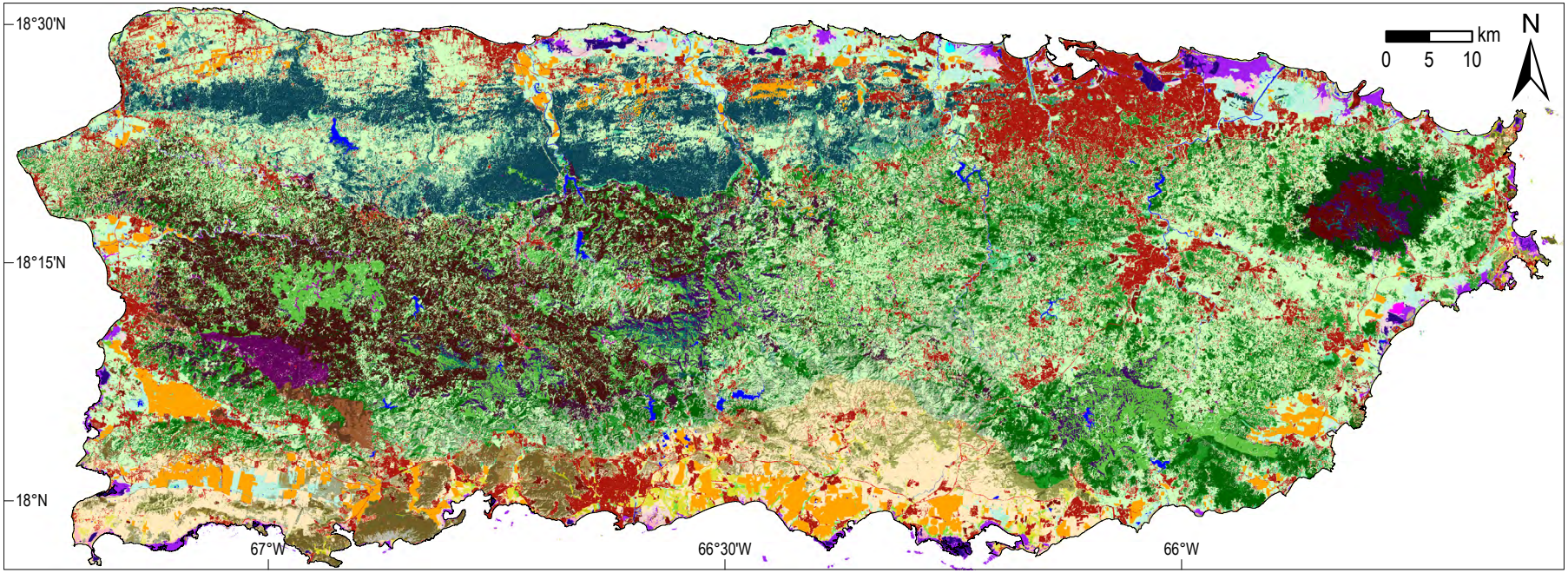

Figure 23. Puerto Rico Gap Analysis Program land cover dataset (modified from Gould and others, 2008). Data are derived from Landsat analysis and include 66 unique classes. Legend not included as map is intended to show diversity of land cover classifications, not exact classes. (km, kilometer)

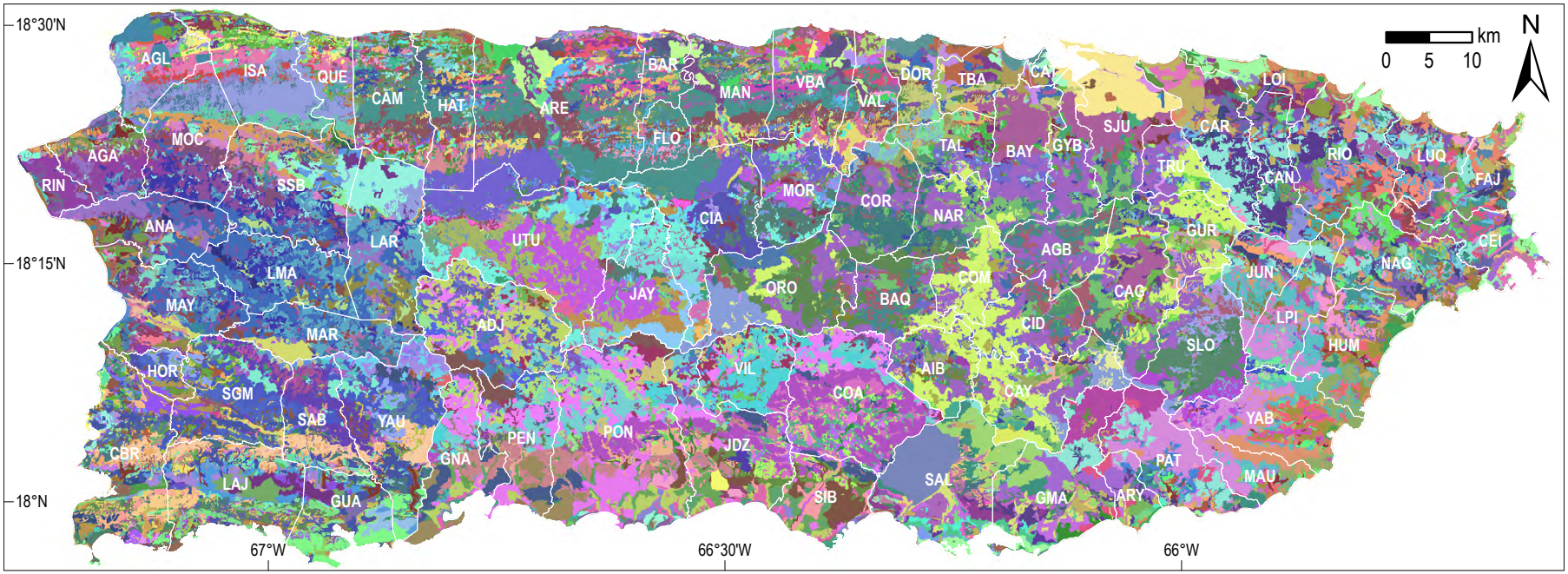

Figure 24. U.S. Department of Agriculture (USDA) Natural Resources Conservation Service soil classification map for the island of Puerto Rico (USDA, 2018). Color is based on mapunit key (MUKEY) classifications which yield 697 unique classes. Similar colors across the map do not necessarily indicate similar soils. This is because of the large number of classes, which results in colors being repeated for dissimilar units. Explanation of municipality abbreviations can be found in appendix 1. (km, kilometer)

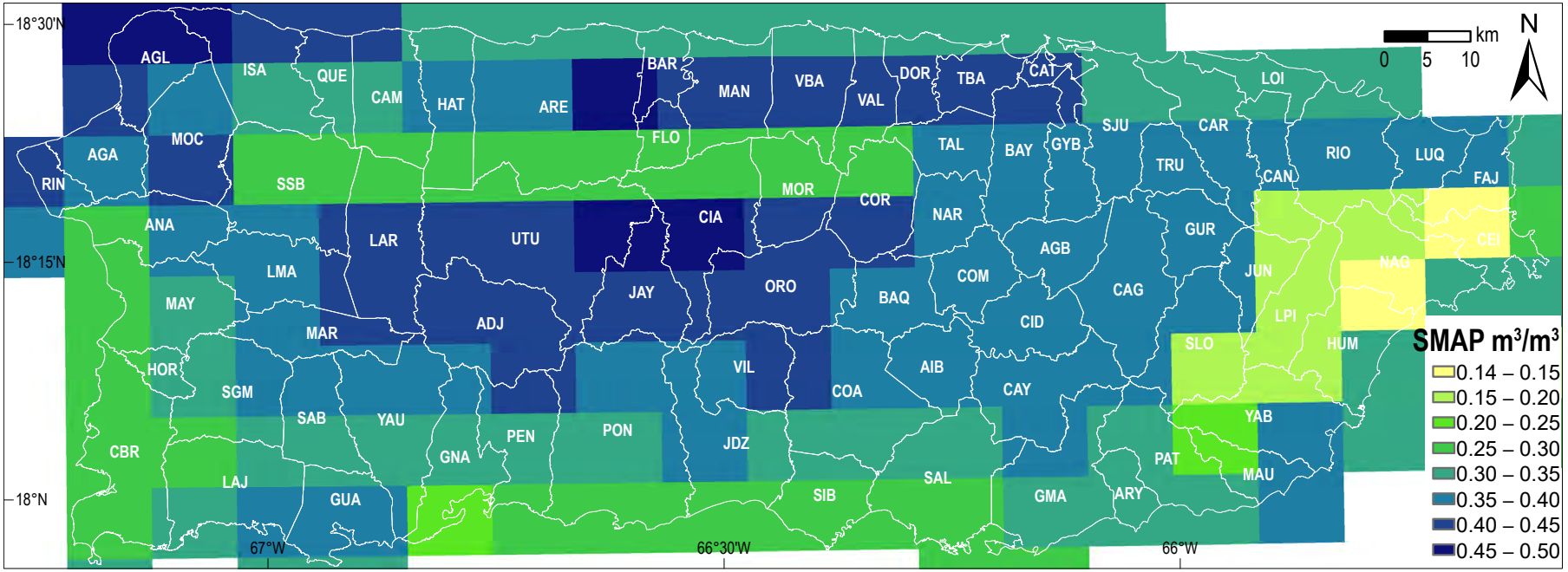

Figure 25. Raw Soil Moisture Active Passive (SMAP) root zone soil moisture data for 9:30 a.m. Atlantic Standard Time on 21 September 2017 (National Aeronautics and Space Administration, 2017). Soil moisture is reported as volumetric water content (volume of water/volume of soil). Explanation of municipality abbreviations can be found in appendix 1. (km, kilometer; m^3, cubic meter)

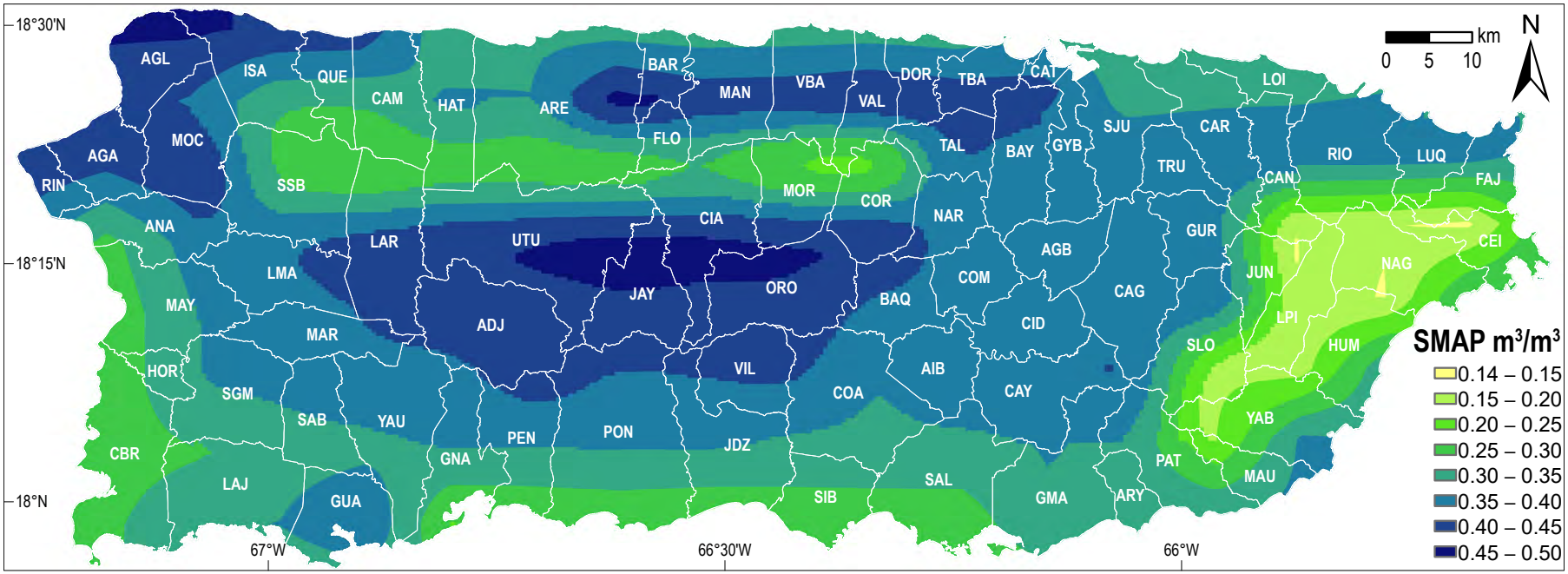

Figure 26. Interpolated root zone soil moisture data from Soil Moisture Active Passive (SMAP) at 9:30 a.m. Atlantic Standard Time on 21 September 2017. Soil moisture is reported as volumetric water content (volume of water/volume of soil). Explanation of municipality abbreviations can be found in appendix 1. (km, kilometer; m^3, cubic meter)

Results and Discussion

The results of the FR analyses and the corresponding landslide *SI* values are reported in table 3, appendixes 2 and 3, and figures 27–35. A summary of the *SI* values and cumulative SIA_m is shown in table 4. In general, the results follow expected factor correlations, which act as a form of independent check on the quality of the inventory product used. The *SI* color scheme for figures 27–35 is consistent with a range of 5.00 to −5.00, such that 0 lies at the neutral color. Full maximum and minimum color saturation is at *SI* values of 2.00 and −2.00. The highest *SI* value calculated for any factor bin is 2.64 (Pellejas clay loam soil unit) and the lowest *SI* values were limited to −5.00. These criteria were used to temper the effect of (1) extremely negative *SI* values that may have been a result of very small bin areas or (2) bins that had a FR value of 0.

Factor Performance

Results of analyses of slope inclination and the landslide inventory (table 3, fig. 27*A–B*) show that landslides were more numerous as slope inclination increased to 45°. Slope values of less than 25° have *SI* values less than 0, indicating they are less likely to fail. Slopes between 25° and 45° show linear increase in *SI* (logarithmic increase in FR) to a maximum value of 1.59 for the 40–45° bin. Slopes between 45° and 90° represent only 2 percent of the island and have a lower *SI* value at 1.05. The lower *SI* in this highest slope bin may be a result of a combination of the failure mechanism and identification potential of landslides at very steep sites. As slope increases, the depth of landslide-susceptible soil decreases and the potential for rockfalls becomes higher than the potential for slumps, slides, or flows. Rockfalls are often less evident than debris flows when using aerial photographs to catalog failure sites. Another potential contributing factor for the lower *SI* value for slopes greater than 45° is that vertical or near-vertical limestone cliffs in the northern karst province represent much of the bin values for the island and landslides were relatively rare in this region (Hughes and others, 2019). Specific results of the geologic substrate analysis are discussed in the following three paragraphs.

Results from the curvature analysis (table 3, fig. 28*A–B*) show that planar or nearly planar areas have the lowest correlation with landslides in the inventory. Pixels that were classified as planar or nearly planar have a *SI* value of −1.17, which is the lowest for the factor. For slopes that are either more concave (+) or more convex (−), the *SI* values increase to maxima of 1.54 and 0.87, respectively, indicating that landslides commonly occurred in valleys and on ridges. The most extreme values of concavity and convexity have neutral to negative *SI* values (table 3).

Table 4. Susceptibility Index (*SI*) values for potential landslide-contributing factors.

[max, maximum; min, minimum; std. dev., standard deviation; SIA_m, final modified *SI* value at each 5-m pixel islandwide]

Factor	*SI* max	*SI* min	*SI* range	*SI* mean	*SI* std. dev.
Slope	1.59	−3.60	5.19	−0.32	1.62
Curvature	1.54	−1.17	2.71	0.24	0.80
Proximity to road surface	0.24	−2.48	2.72	−0.38	0.85
Geologic terrane	1.33	[1]−3.73	[1]5.06	[1]−0.85	[1]1.57
Mean annual precipitation	1.24	[2]−8.00	[2]6.24	[2]−1.59	[2]2.26
Proximity to fluvial channel	0.29	−3.73	4.02	−0.46	1.21
Land cover	1.42	([3])	[3]6.42	[3]−2.78	[3]2.25
Soil classification	2.64	([3])	[3]7.64	[3]−3.00	[3]2.20
Event soil moisture	1.67	−1.91	3.58	−0.51	1.16
Cumulative SIA_m	1.97	−4.84	6.81	−1.36	1.74

[1]The −5.14 value for surficial water bodies category is not included.

[2]*SI* values less than −5.00 were set to −5.00 to minimize the statistical influence of subfactors that cover very small areas and (or) include very few landslides. The range, mean, and standard deviation above were calculated using −5.00 as a minimum value.

[3]Some categories of land cover and soil classification included sites with no landslides. The resultant frequency-ratio value is 0 and the natural log of 0 goes to negative infinity. In these cases, the *SI* value was set to −5.00. The range, mean, and standard deviation above were calculated using −5.00 as a substitute for all negative infinity returns. More detailed data results are in table 3 and appendixes 2 and 3.

Similar to the results from Larsen and Parks (1997), the analysis of the landslide inventory with respect to **road surface proximity** shows that sites within 100 m of a road were more likely to correlate with landsliding than those farther away. The highest *SI* values are 0.12 and 0.24, which correlate with bins that represent pixels within 0–10 m and 10–25 m, respectively, of a paved road surface. The results are tabulated in table 3 and displayed visually in figure 29*A–B*.

The results from the analysis of geologic substrate (table 3, fig. 30) show that local geology was important to mass wasting susceptibility during Hurricane María. Of the 11 terrane classifications (including surface water), only 3 show positive correlation to the landslide inventory. The Cretaceous intrusive rock category shows the most correlation and has a *SI* value of 1.33. The majority of this category is made up of the mostly granodiorite Utuado and San Lorenzo plutonic bodies. The Cretaceous-Tertiary volcaniclastic terrane, which is the most widespread geologic classification on the island, has a positive *SI* value of 0.38. Most classes are negatively correlated, including the Tertiary cover sequence rocks (−2.12) and Quaternary alluvium (−3.27). The surficial water body classification (−5.14) includes seven sites (less than 0.01 percent of the inventory dataset) in the mass wasting catalog. These sites represent locations on the lateral limit of water bodies where the geologic mapping overextended the extent of water coverage. Zones mapped as Quaternary landslides yield an *SI* value of −0.34, indicating that these zones of deep mass movements mostly mapped by Monroe (1979) did not frequently produce landslides during Hurricane María. The highest landslide correlation for the Cretaceous intrusive rocks classification is linked to the manner in which these plutonic rocks react to chemical weathering in Puerto Rico, which has been shown to be among the most rapid in the world (White and Blum, 1995). Specifically, as the granodiorite rock suffers chemical weathering in the humid tropical environment, most minerals experience dissolution or hydrolysis and are transported away in groundwater solution (White and others, 1998; Porder and others, 2015). However, the abundant quartz in the bedrock remains mostly unaffected and the result is a sandy residuum (Mattson, 1968). This product has very low cohesion and is more vulnerable to mobilization when pore-water pressures increase due to rainwater (or other) saturation. The regolith generated from rock types other than the granodiorite is generally more clay rich and more cohesive.

Mean annual precipitation shows a strong correlation with landslide sites. Only one landslide site was cataloged in zones that receive less than 1,000 millimeters (mm) of rain annually. The 1,750–2,000 mm bin is nearly neutral with a *SI* value of 0.06 and the highest bin of 2,250–2,500 mm has the highest *SI* value of 1.24. In general, areas that receive more rainfall are more prone to experience hillslope failure due to the increased rates of chemical weathering and (or) fluvial incision resulting from higher rainfall amounts. These results are summarized in table 3 and shown graphically in figure 31*A–B*.

The analysis of **proximity to fluvial channel** (table 3, fig. 32*A–B*) reveals that sites within 25 m and in excess of 400 m from a flow line representing each channel are statistically less likely to experience mass wasting. Bins of between 25-m and 400-m distance show correlation with failure sites. The lower *SI* values for sites within 25 m of fluvial channels is interpreted to result from some of this distance being the channel itself (the hydrographic data provide a line near channel axes) and low-susceptibility floodplains that are associated with many fluvial channels. Most of the island that is more than 400 m from a fluvial channel is in the topographically complex northern limestone and karst region where landslides were rare during Hurricane María (Hughes and others, 2019).

Land cover analysis shows variability among the 66 distinct categories classified as part of the GAP dataset (table 3; fig. 33; app. 2; Hughes and Schulz, 2020). The "Montane wet evergreen abandoned/active coffee plantation" class yields the highest *SI* value of 1.42. This high correlation is likely due to the disturbance of natural slopes by centuries of agricultural activity, especially the creation of improvised, rudimentary farm roads throughout the mountainous areas where coffee is cultivated (Philpott and others, 2008; Ramos-Scharrón and LaFevor, 2016). The "Montane wet noncalcareous evergreen shrubland and woodland" category has a similar *SI* value of 1.37. Twenty-three land cover classes did not include any landslide sites; these are generally wetland, beach, water, and arid categories.

Soil class (table 3; fig. 34; app. 3; Hughes and Schulz, 2020) is perhaps the best nonslope factor to distinguish zones susceptible to mass wasting. In addition, the highest *SI* values for any factor of the study are related to specific soil types. Both the "Pellejas clay loam (40–60 percent slopes)" and "Maricao clay (20–60 percent slopes)" classes yield *SI* values greater than 2.5. Another 28 soil classes have *SI* values greater than 1.0 and an additional 58 classes have *SI* values greater than 0. Of the 697 total classes, 317 have no association with any landslide in the inventory. The detailed soil classification is an important model input and acts as an effective discriminator within zones that fall in the same geological terrane classification.

The **soil moisture** analysis (table 3; fig. 35) shows that the wettest two bins (0.40–0.45 cubic meters [m^3] and 0.45–0.50 m^3) correlate best with the Hurricane María inventory dataset. The high correlation is because much of the wettest SMAP data registered in the central municipalities of Utuado, Jayuya, Ciales, and Orocovis where many landslides occurred. A comparison with the density map in figure 13 highlights this correlation, especially in the vicinity of Lago Caonillas in east-central Utuado. The results here generally concur with the analysis made by Bessette-Kirton and others (2019). However, the FR relationship between SMAP values and landslide sites does not follow a consistent trend (table 3) considering values of soil moisture less than 0.25; *SI* increases with increasing soil moisture greater than 0.25. This suggests that soil moisture of 0.25 or greater was required to initiate widespread landsliding.

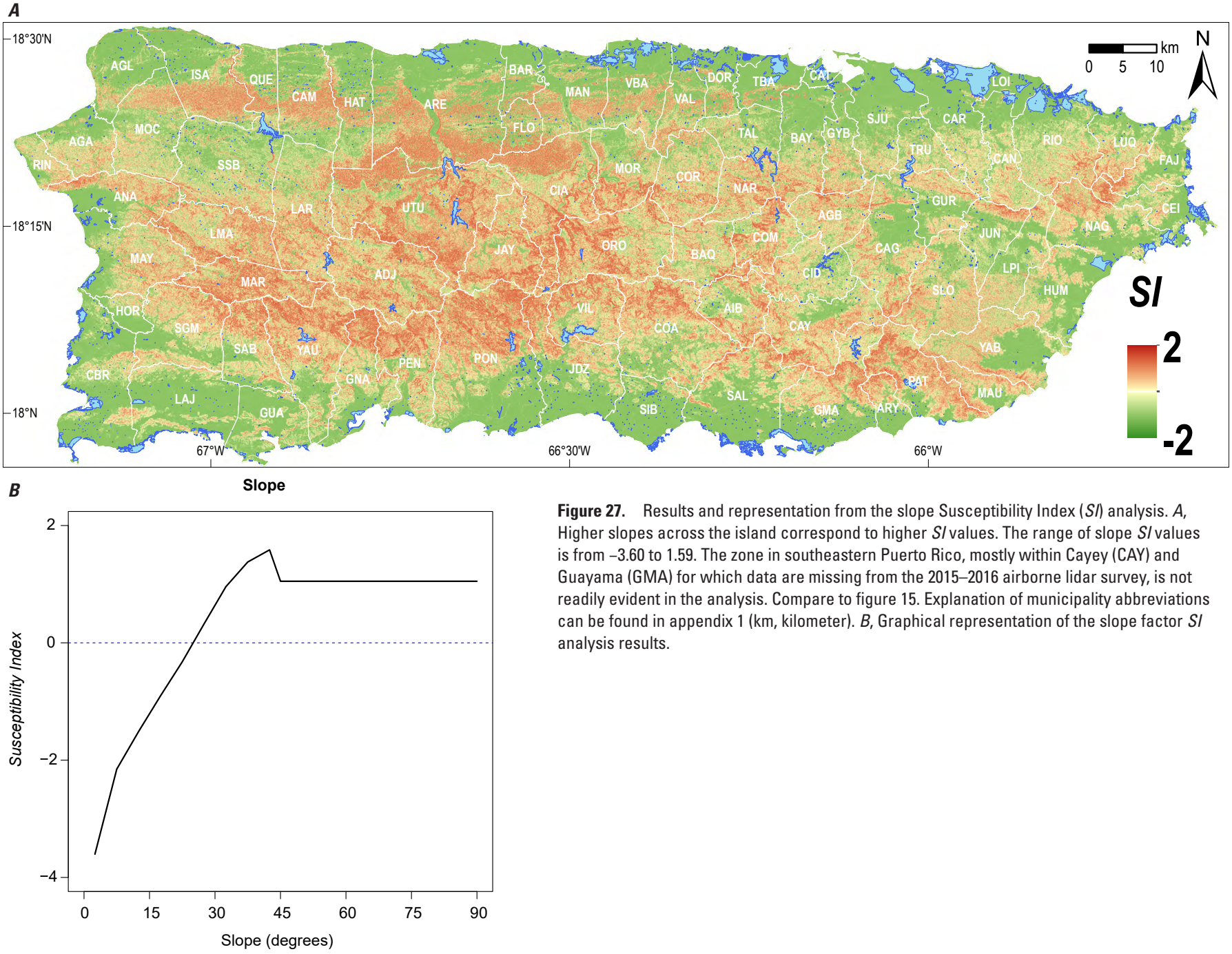

Figure 27. Results and representation from the slope Susceptibility Index (*SI*) analysis. *A*, Higher slopes across the island correspond to higher *SI* values. The range of slope *SI* values is from –3.60 to 1.59. The zone in southeastern Puerto Rico, mostly within Cayey (CAY) and Guayama (GMA) for which data are missing from the 2015–2016 airborne lidar survey, is not readily evident in the analysis. Compare to figure 15. Explanation of municipality abbreviations can be found in appendix 1 (km, kilometer). *B*, Graphical representation of the slope factor *SI* analysis results.

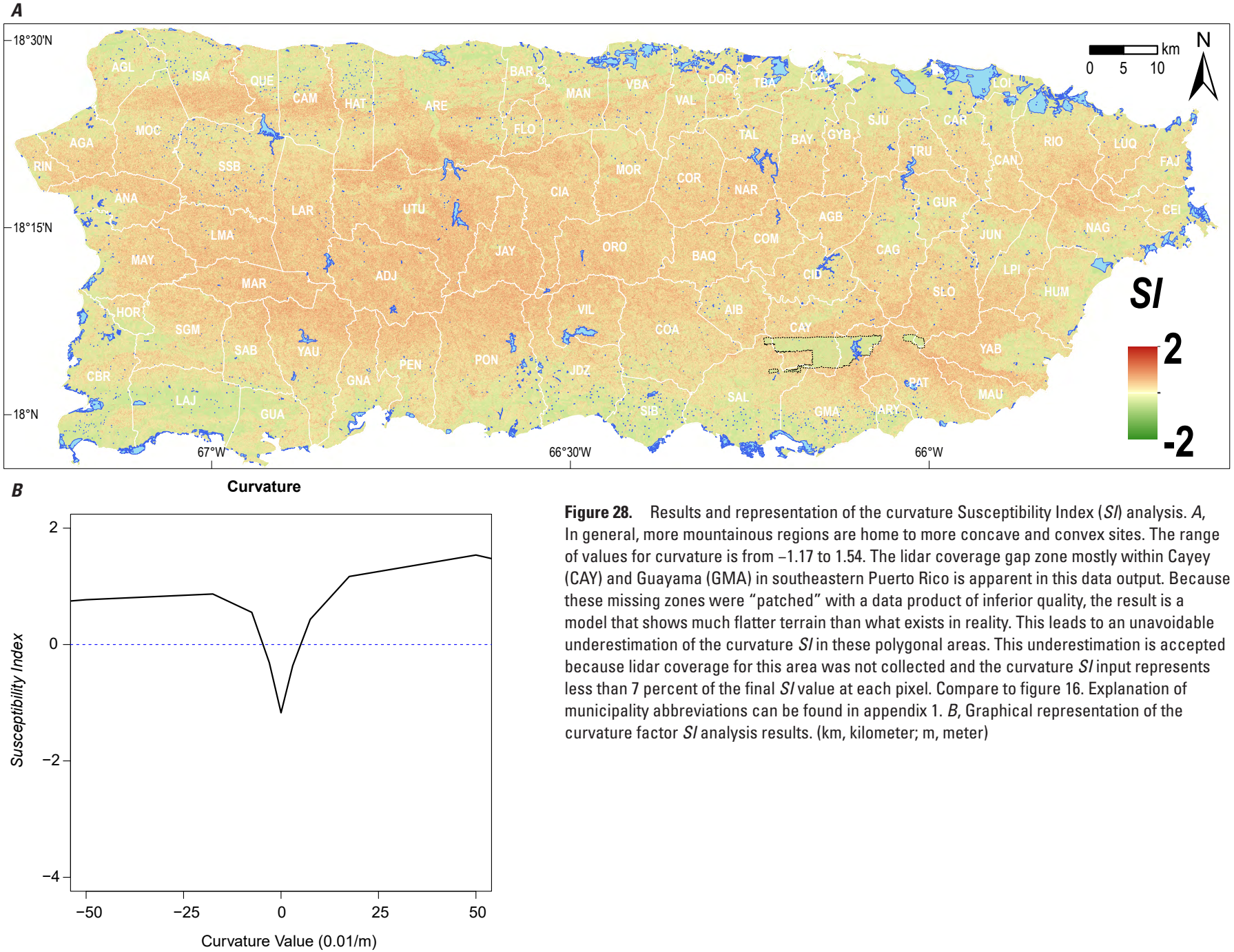

Figure 28. Results and representation of the curvature Susceptibility Index (*SI*) analysis. *A*, In general, more mountainous regions are home to more concave and convex sites. The range of values for curvature is from –1.17 to 1.54. The lidar coverage gap zone mostly within Cayey (CAY) and Guayama (GMA) in southeastern Puerto Rico is apparent in this data output. Because these missing zones were "patched" with a data product of inferior quality, the result is a model that shows much flatter terrain than what exists in reality. This leads to an unavoidable underestimation of the curvature *SI* in these polygonal areas. This underestimation is accepted because lidar coverage for this area was not collected and the curvature *SI* input represents less than 7 percent of the final *SI* value at each pixel. Compare to figure 16. Explanation of municipality abbreviations can be found in appendix 1. *B*, Graphical representation of the curvature factor *SI* analysis results. (km, kilometer; m, meter)

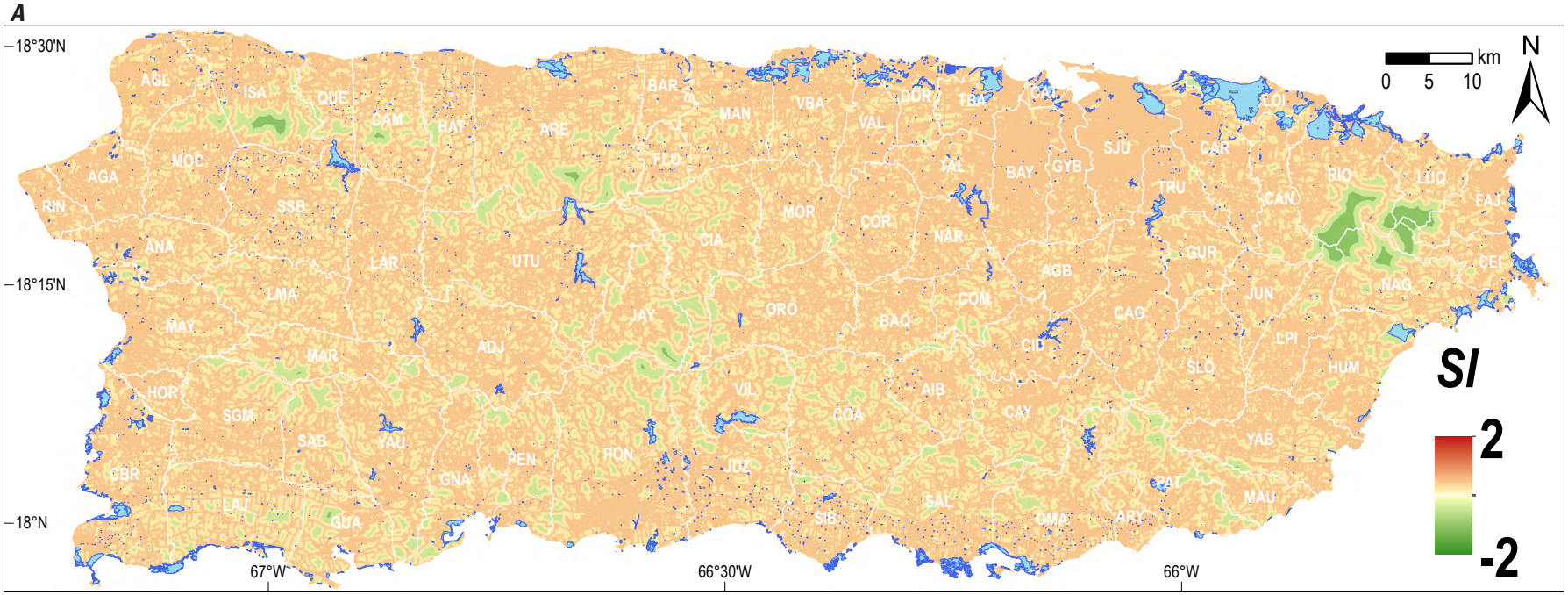

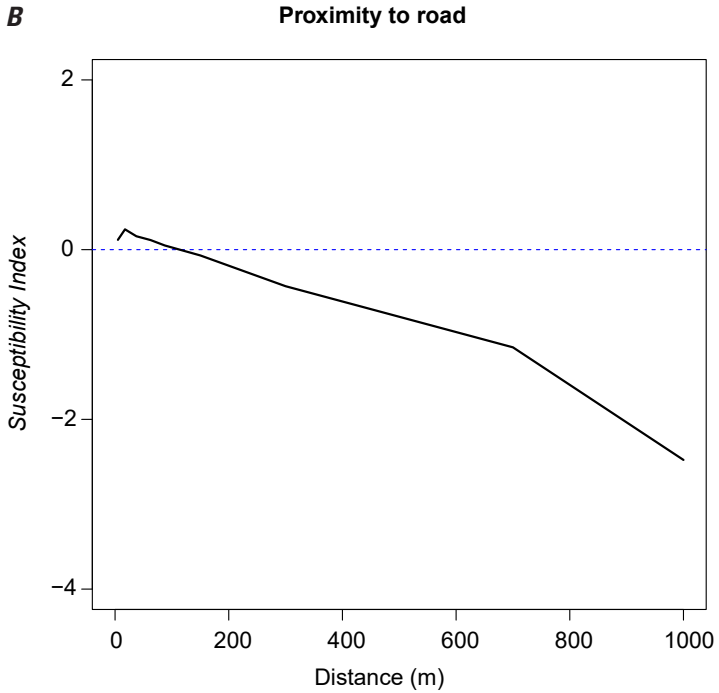

Figure 29. Results and representation from the road proximity analysis. *A*, Sites closer to road surfaces yield higher Susceptibility Index (*SI*) values. Sites more than 1 kilometer from a road have the lowest *SI* value at –2.45 whereas sites within 100 meters of a road have *SI* values greater than 0. Compare to figure 18. Explanation of municipality abbreviations can be found in appendix 1. *B*, Graphical representation of the proximity to road factor *SI* analysis results. (km, kilometer; m, meter)

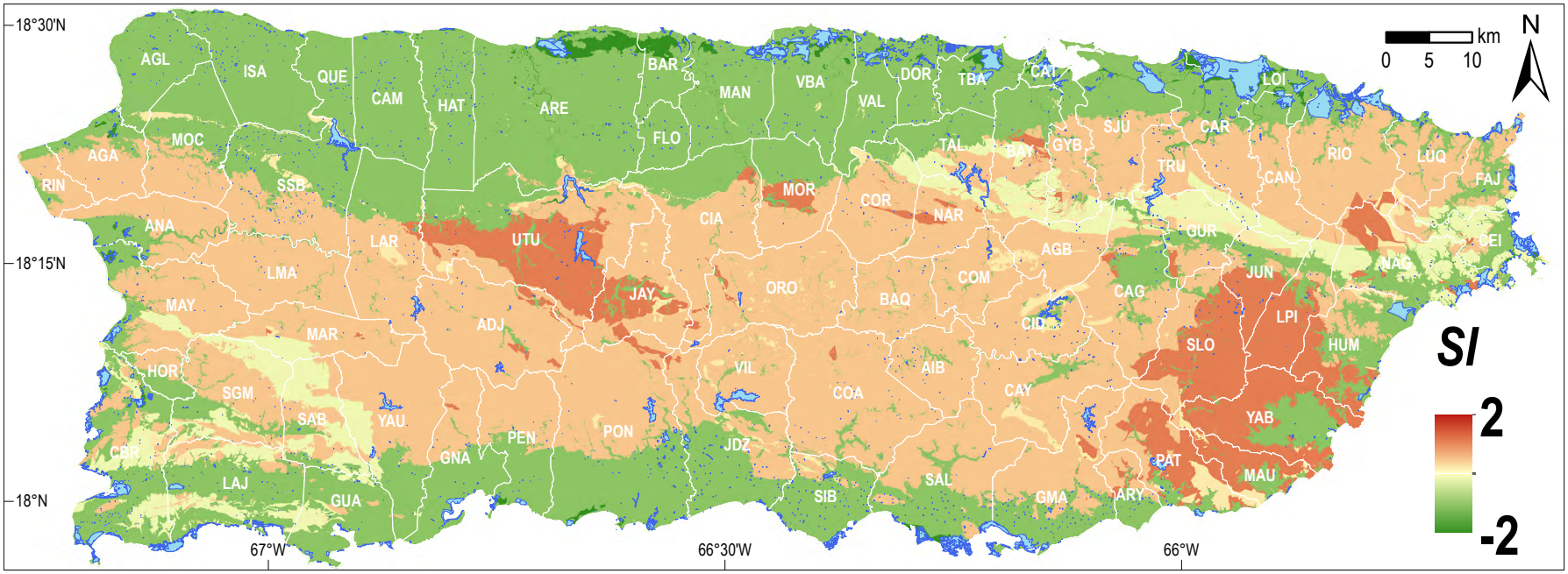

Figure 30. Susceptibility Index (*SI*) results for geological terranes as defined by Baiwec (1998). The Cretaceous intrusive classification shows the strongest correlation with the landslide inventory. The extensive Cretaceous–Tertiary volcaniclastic terrane yields a positive correlation as well. Compare to figure 20. Explanation of municipality abbreviations can be found in appendix 1. (km, kilometer)

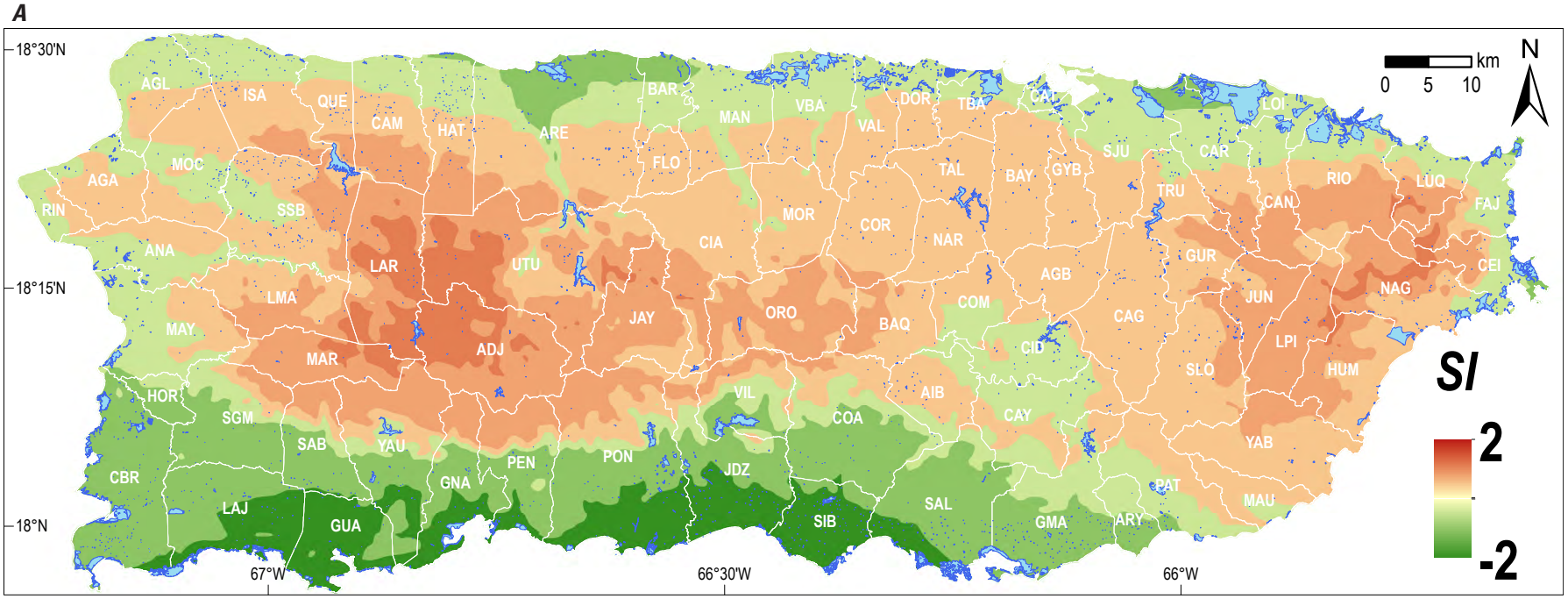

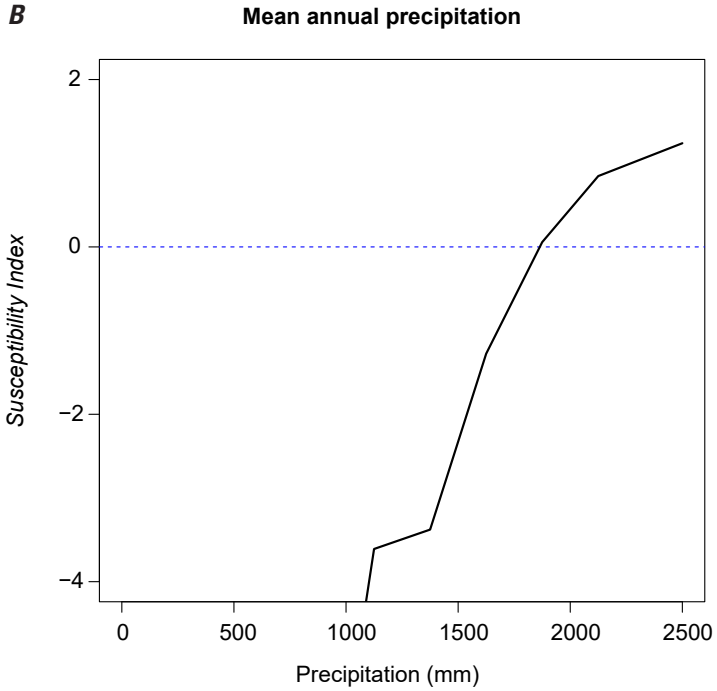

Figure 31. Results and representation from Susceptibility Index (*SI*) analysis of mean annual precipitation. *A*, Zones of higher mean annual precipitation are more positively correlated to mass wasting sites. The wettest regions in the Sierra de Luquillo and western interior have the highest *SI* values. The arid south coast region has the lowest correlation with landslide sites in the inventory. Compare to figure 21. Explanation of municipality abbreviations can be found in appendix 1. *B*, Graphical representation of the mean annual precipitation factor *SI* analysis results. (km, kilometer; mm, millimeter)

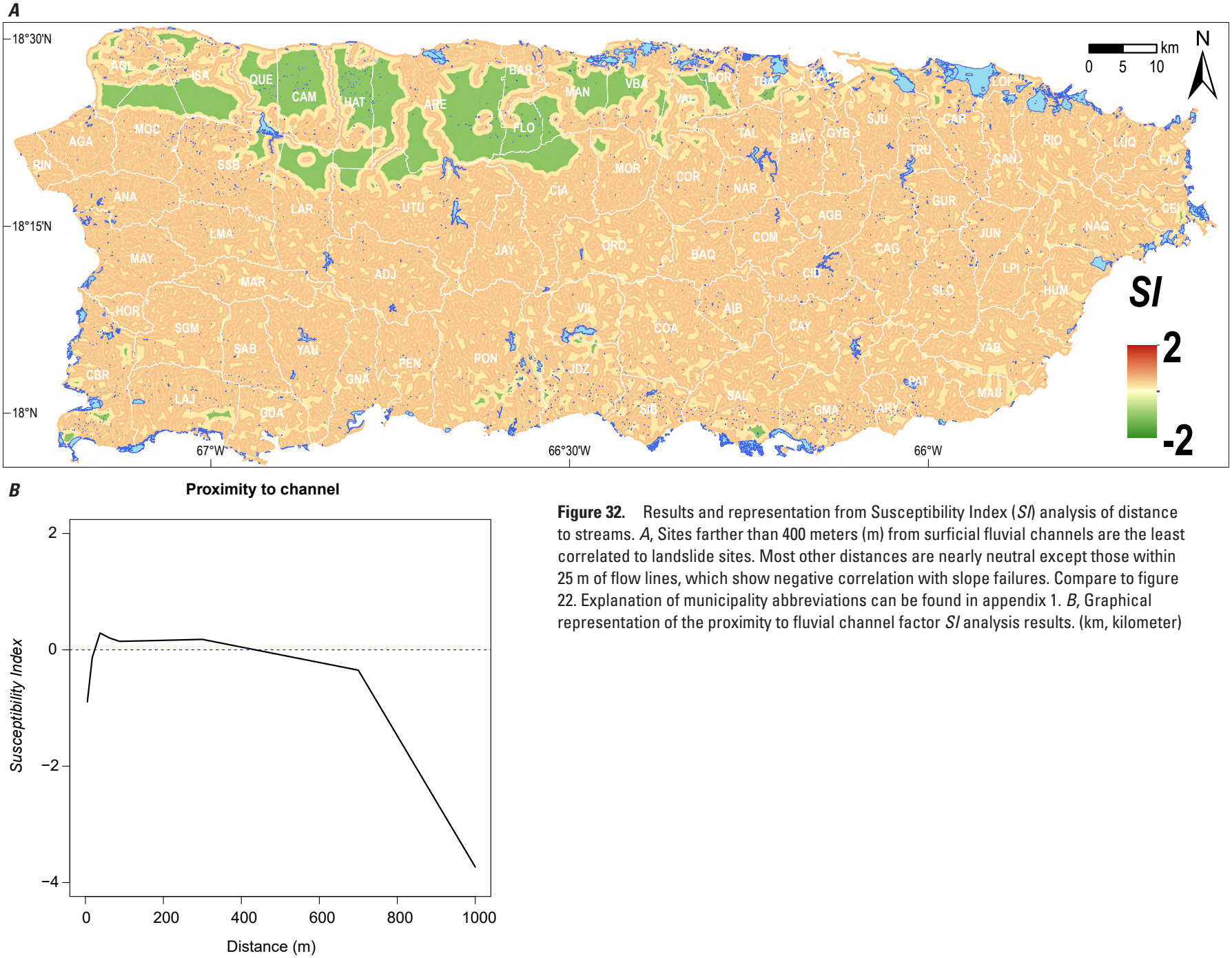

Figure 32. Results and representation from Susceptibility Index (*SI*) analysis of distance to streams. *A*, Sites farther than 400 meters (m) from surficial fluvial channels are the least correlated to landslide sites. Most other distances are nearly neutral except those within 25 m of flow lines, which show negative correlation with slope failures. Compare to figure 22. Explanation of municipality abbreviations can be found in appendix 1. *B*, Graphical representation of the proximity to fluvial channel factor *SI* analysis results. (km, kilometer)

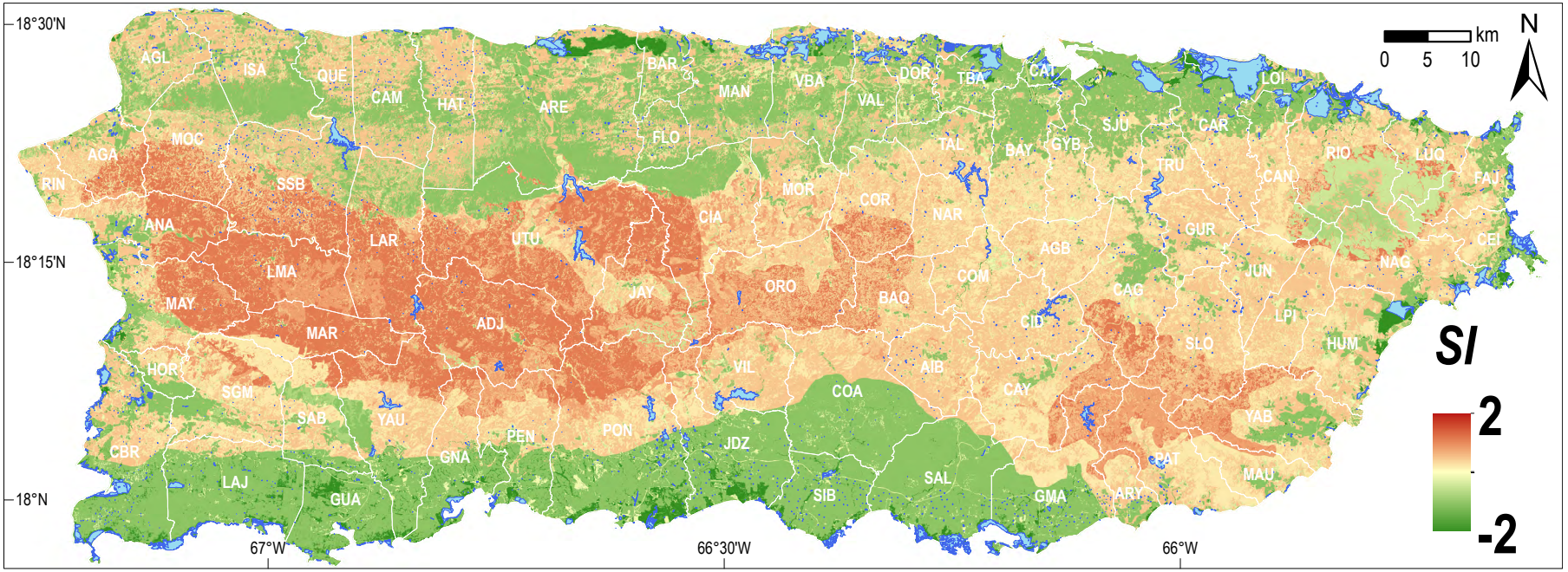

Figure 33. Results from analysis of Susceptibility Index (*SI*) values for the 66 unique land cover classes. The highest *SI* value is for abandoned and active coffee farms, which cluster in the rugged western interior of the island. The Sierra de Luquillo is characterized by neutral to negative *SI* values ringed by a zone of land cover areas that have higher *SI* values. Wetlands, urban areas, and beaches return very negative *SI* values. Compare to figure 23. (km, kilometer)

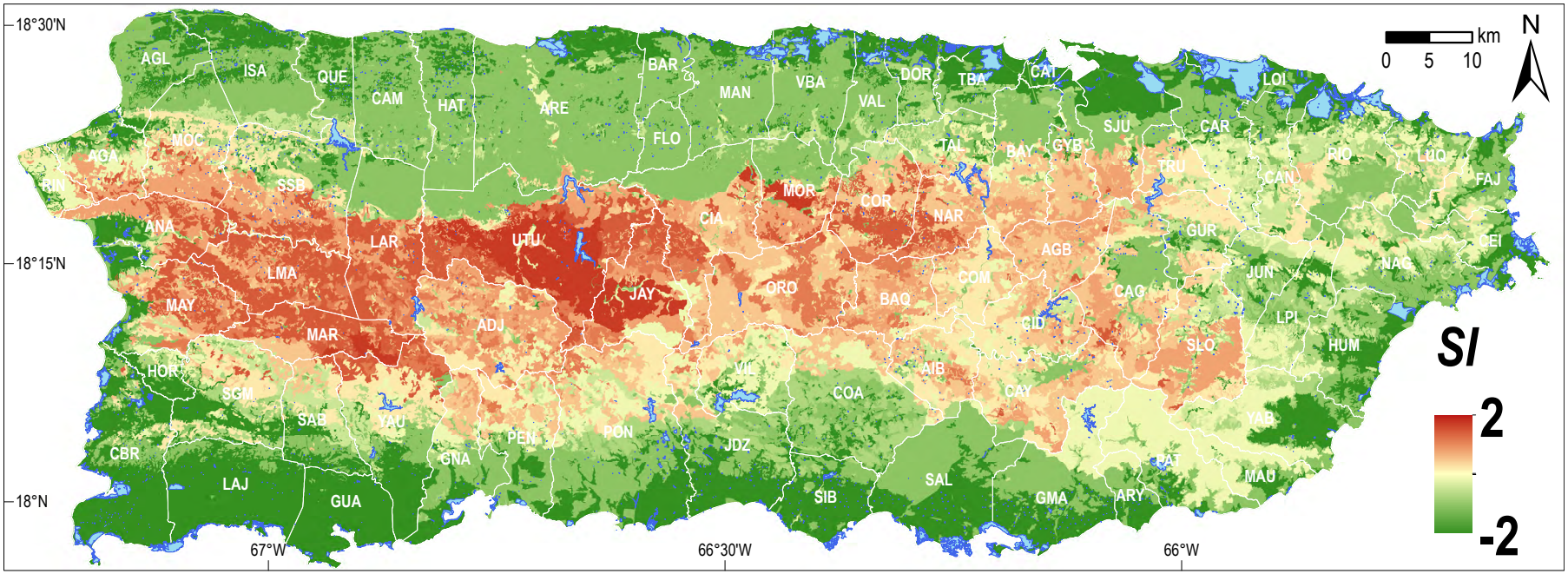

Figure 34. Results from Susceptibility Index (*SI*) analysis of 697 soil classes. The Pellejas clay loam has the highest *SI* value of any factor in the study at 2.64 and mostly correlates with the Utuado granodiorite pluton. Compare to figure 24. Explanation of municipality abbreviations can be found in appendix 1. (km, kilometer)

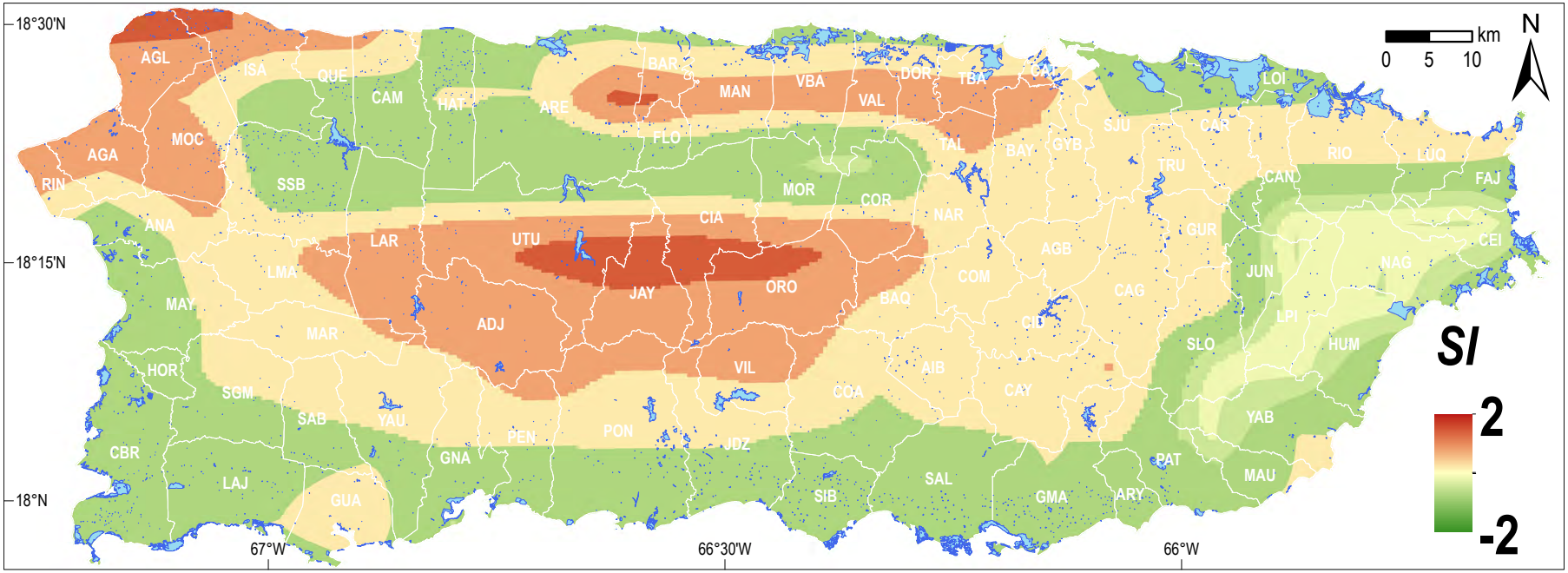

Figure 35. Results from Susceptibility Index (*SI*) analysis of Soil Moisture Active Passive data. The areas of highest root zone soil moisture estimated for 21 September 2017 correlate best with landslide sites. The *SI* values for SMAP values were subtracted from the final model output as shown in equation 4. This technique was used to minimize the effect of using one single-event inventory for a comprehensive susceptibility model. Compare to figure 26. Explanation of municipality abbreviations can be found in appendix 1. (km, kilometer)

Map Performance

Convention and experience indicate that landslide susceptibility maps are best understood when susceptibility is classified into several groups. Rankings of Low, Moderate, High, Very High, and Extremely High landslide susceptibility were assigned after binning the SIA_m raster data into 100 equal-area quantiles. The categorization scheme is shown in table 5. The lower 40 percent of pixel values islandwide are considered representative of areas of low susceptibility. The 40th–70th percentile range corresponds to zones of moderate susceptibility. The 70th–90th percentile range is classified as having high susceptibility. The highest 10–1 percent of pixel values are classified as having very high vulnerability and the highest 1 percent are classified as having extremely high potential for failure. The ranking scheme was scrutinized in detail throughout the island at known sites and is consistent with the authors' field experience. The final map is provided as plate 1.

The final *SIA* and SIA_m model values were calculated using only 75 percent of the landslide inventory. The remaining 25 percent of the sites were used to independently test the validity of the model. The data were used to generate ROC plots to calculate area under curve (AUC) values, which are commonly used to evaluate slope hazard modeling (for example, Lepore and others, 2012; Xu and others, 2012; Li and others, 2016; Regmi and Poudel, 2016). The ROC plots were generated at increments of 5 for the full range (−50 to 20) of SIA/SIA_m values. The true positive rate for a given boundary of SIA/SIA_m values was the number of landslides with SIA/SIA_m values greater than any given increment (true positives) divided by the total number of landslides. The false positive rate for a given increment of SIA/SIA_m values was the total number of pixels in the SIA/SIA_m raster from which the number of landslides (true positives) and the number of pixels with values lower than the boundary were subtracted, and this difference was divided by the total number of pixels in the SIA/SIA_m raster. AUC values can vary from 0.5 to 1.0 and quantify the false versus true predictions from a model. A value of 1.0 indicates perfect model performance and a value of 0.5 corresponds to a model that is equivalent to random prediction (Fawcett, 2006). The AUC value for *SIA* and SIA_m were compared to the AUC for the slope factor alone (fig. 36). Analysis of slope alone yields an AUC value of 0.83. The AUC for *SIA* and SIA_m are higher at 0.88 and 0.87, respectively. The AUC of the composite *SI* of all nonslope and non-SMAP factors (figs. 36 and 37) is 0.94. This verification indicates that the model is both statistically viable and provides an improved prediction versus a slope-only model. Slope represents almost 50 percent of the final model. The nonslope and non-SMAP factors also represent almost 50 percent of the final susceptibility model and considered together yield the highest AUC value of the analysis. A composite map of these seven factors (curvature, proximity to road surface, geologic terrane, mean annual precipitation, proximity to fluvial channel, land cover, and soil classification) shows the highest correlating zones to be in the western interior region (fig. 37). Even though it has a much higher AUC value (0.94), the nonslope composite *SI* model was not adopted as the preferred model because the importance of slope cannot be overlooked in any mass movement model (for example, Carson and Petley, 1970). The lower performance of the slope-only dataset indicated by its lowest AUC value is likely due to the abundance of very high slopes on the flanks of mogotes, sinkholes, zanjones, and gorges in the karst terrain that do not usually suffer the same weathering and mass wasting processes as the remainder of the island, and because of factors described previously that are captured by inclusion of nonslope and non-SMAP factors. The decrease in AUC from *SIA* to SIA_m shows that the incorporation of SMAP data in the model slightly decreases its performance against the Hurricane María event inventory, as expected. Incorporation of the SMAP factor in SIA_m was intended to buffer the influence of site-specific conditions related to the single event used for developing the predictive map. SMAP data incorporation also permits evaluation of variable soil moisture from future events and its effect on landsliding, as described in the "Use and Limitations of the Landslide Susceptibility Map" section.

Table 5. Results from comparison of the susceptibility map to locations of landslides in the Hurricane María inventory.

[*SI*, Susceptibility Index; km², square kilometer; %, percent; #, number; —, not applicable]

Susceptibility ranking	Approximate *SI* range	Percentile	Area (km²)	Area (%)	Landslides in category (#)[1]	Landslides in category (%)[1]	Density (landslides/km²)[1]
Low	−4.84–−1.6	0–40	3481.2	40	843	1.2	0.2
Moderate	−1.6– −0.1	40–70	2609.3	30	7,108	10.0	2.7
High	0.1–0.9	70–90	1740.5	20	20,988	29.4	12.1
Very High	0.90–1.40	90–99	782.7	9	31,850	44.6	40.7
Extremely High	1.40–1.97	99–100	86.5	1	10,642	14.9	123.0
Total	—	—	**8,700.2**	**100**	**71,431**	**100.1**	—

[1]Values calculated using the Hurricane María event inventory (Hughes and others, 2019).

The model generated in this study was compared with the Lepore and others (2012) model and the raster model output was provided by C. Lepore (written commun., 2018). The pixel resolution of the Lepore and others' study (2012) was 30 m, whereas our model resolution is 5 m, which is advantageous because of its higher resolution and is possible because of the recent availability of a high-resolution lidar DEM dataset for the island. To quantitatively compare the models, Lepore and others' model output (2012) was grouped into 100 equal-area quantile classes in the same manner as our dataset. A raster output of the difference of quantile value from our model and their model is shown in figure 38. Within the 2 standard deviation (σ) confidence interval, the similarity between the two models is only as good as ±37 quantiles. This metric indicates that the difference between the two model products is considerable. Table 6 shows a breakdown of which factors were used for each model's generation. Because elevation was not incorporated into our model, the Lepore and others' model (2012) tends to rank higher-elevation pixels with much higher susceptibility than our model. This effect is most evident in the high plateau area in the vicinity of the municipalities of Cidra, Cayey, Aibonito, and Barranquitas (fig. 38). In addition, the Lepore and others' methodology (2012) did not calculate *SI* values by taking the natural log of the FR numbers. Their model output was a sum of FR values, which unevenly gives more weight to positive correlating factors than negative correlating factors. Many areas in figure 38, where our model ranks susceptibility higher than does Lepore and others (2012) result from higher slope *SI* values, which are almost one-half of our model input but only make up 12 percent of Lepore and others' model input (2012).

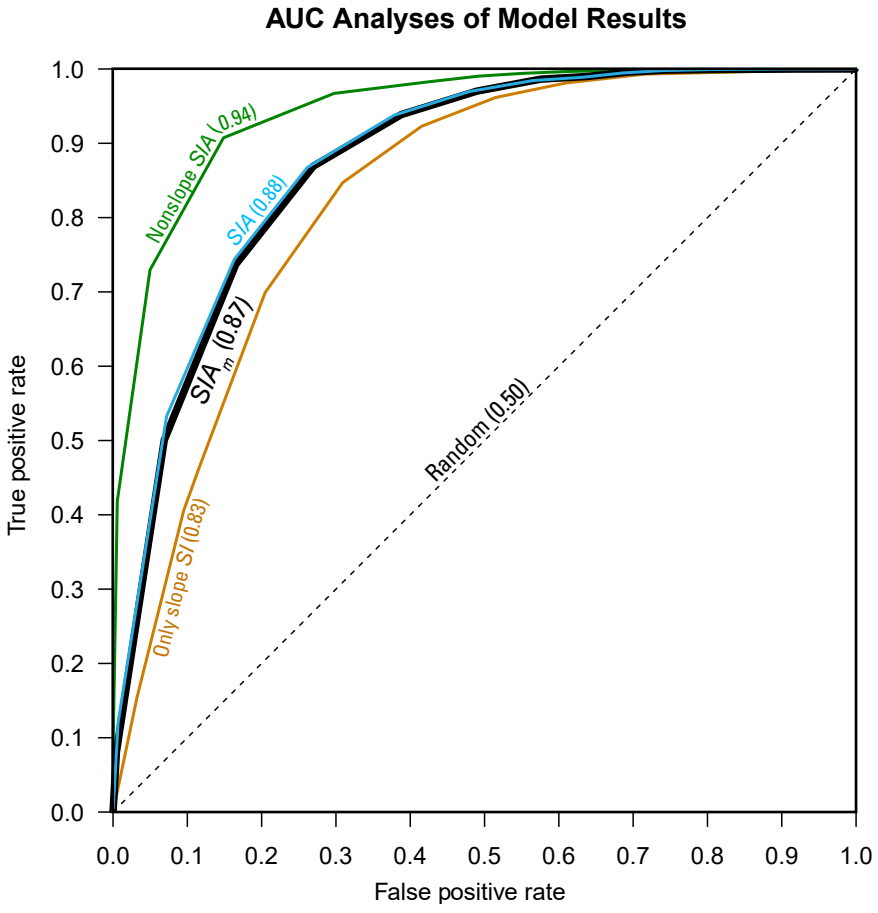

Figure 36. Receiver operating characteristic (ROC) area under curve (AUC) analyses for different combinations of data results. *SI* indicates Susceptibility Index, *SIA* indicates aggregate Susceptibility Index, and SIA_m indicates aggregate Susceptibility Index modified by soil moisture. The final model chosen is the SIA_m output.

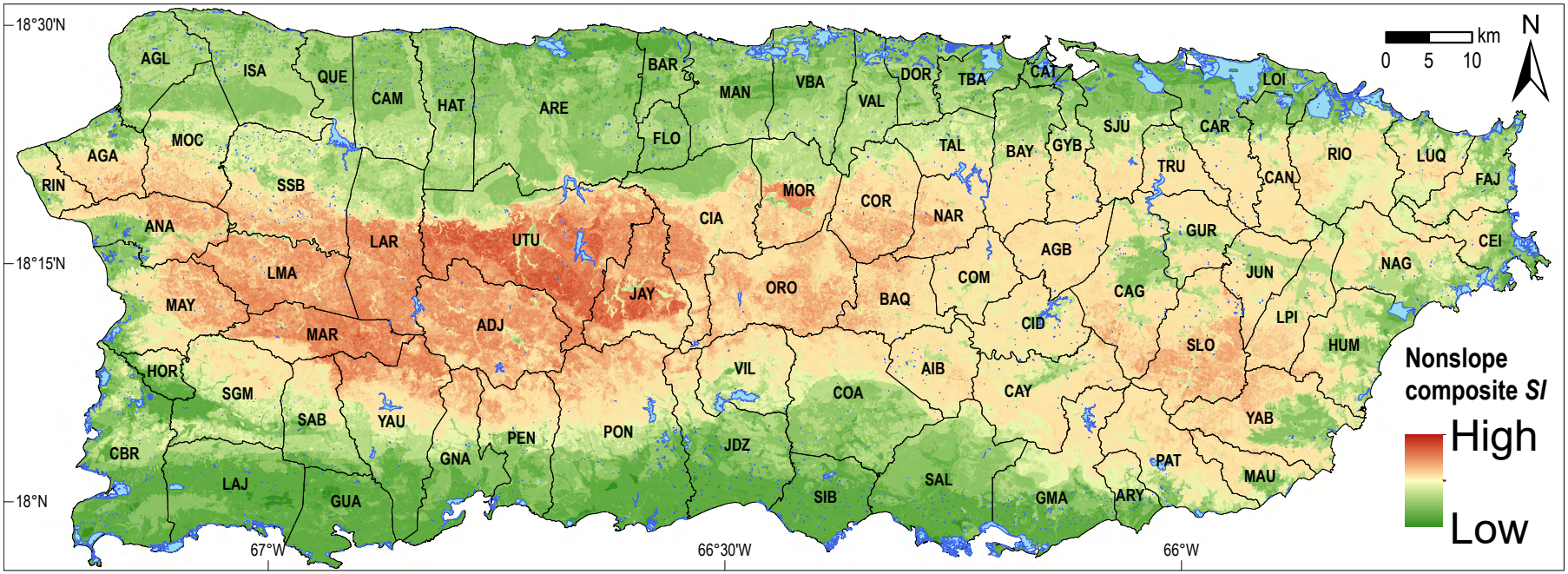

Figure 37. Composite Susceptibility Index (*SI*) map of the seven nonslope and non-Soil Moisture Active Passive datasets used in the analysis. A neutral *SI* score of 0 is shown as the neutral tan color. The combination of these factors yields a higher area under curve (AUC) value than slope alone (fig. 36). Explanation of municipality abbreviations can be found in appendix 1. (km, kilometer)

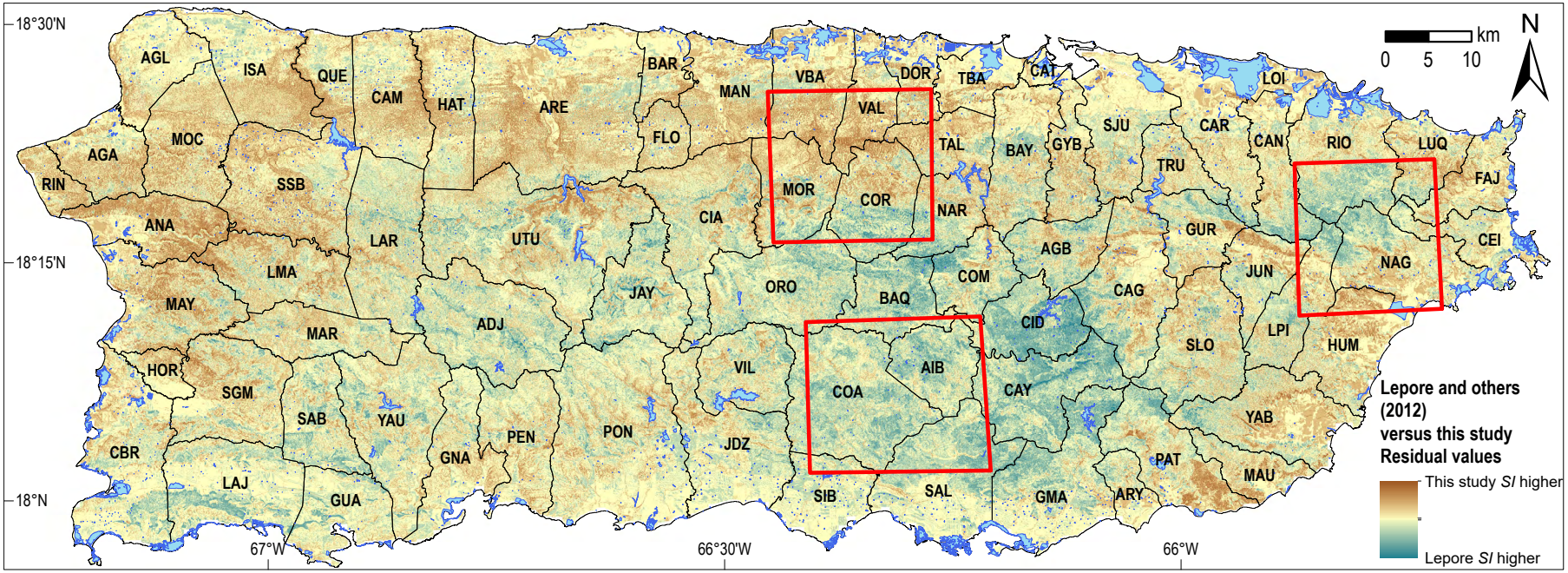

Figure 38. Residual values of Susceptibility Index (*SI*) model output from this study compared with the frequency ratio (FR) model output of Lepore and others (2012). Blue areas (nonwater) represent zones where the normalized Lepore model values are at least 10 percent higher than our normalized values. Orange pixels represent areas where our normalized values were at least 10 percent higher than those of Lepore and others (2012). Both models were standardized using quantiles in order to compare. The three red outlined areas show the extent of the landslide inventories used by Lepore and others (2012) to guide their whole-island susceptibility model. Explanation of municipality abbreviations can be found in appendix 1. (km, kilometer)

Table 7 provides a summary of the density of landslides from the Hurricane María inventory (Hughes and others, 2019) for each of the susceptibility classification ranges of the susceptibility maps produced for the entire island (Monroe, 1979; Lepore and others, 2012; this study). The density values in the Low, Moderate, and High categories of both the current study and those of Lepore and others (2012) are strikingly similar; however, the current study model displays much higher density within the Very High susceptibility category and also includes an Extremely High category, which was well represented by the spatial density of landslides triggered by Hurricane María. Additionally, the model presented herein indicates Low susceptibility over an area more than twice as large as the corresponding area of Lepore and others (2012), and Very to Extremely High susceptibility over an area about one-half the size of the Lepore and others' Very High susceptibility area (2012).

Some specific notable landslide sites are presented here as examples of how the susceptibility model represents susceptibility at local scale:

- The Villa España Urbanization in the municipality of Bayamón was the site of a landslide on the southern flank of a mogote in August 2013 (fig. 39). Failure of the limestone material caused several houses to be condemned and eventually demolished. The analysis of the site in the current study shows that the area is classified as having High landslide susceptibility.

Table 6. Factors considered in quantitative Puerto Rico landslide susceptibility maps.

[x, factor considered in study, —, factor not considered in study]

Factor	This study	Lepore and others study (2012)
Slope	x	x
Aspect	—	x
Elevation	—	x
Curvature	x	x
Distance from faults	—	x
Distance from roads	x	x
Distance from rivers	x	—
Geology	x	x
Soil	x	—
Land cover	x	x
Annual precipitation	x	—
Event soil moisture	x	—

- The Las Lomas Urbanization in the municipality of Ceiba suffered a landslide during October 2015 (fig. 40). The failure left several houses partially hanging over a new headscarp feature. This landslide was surveyed by the lidar campaign of 2015–2016 and the landslide susceptibility model produced by this study classifies the current site as having High to Very High landslide susceptibility. It is likely that the unfailed slope would have been classified as having High susceptibility, given the ranking of slopes adjacent to the failure.
- During the passing of Hurricane María in September 2017, a large landslide at km 56.2 of Highway PR-143 in the municipality of Barranquitas transitioned into a debris flow (figs. 8 and 41). The susceptibility model output of this study shows that the site had Very High to Extremely High landslide potential before the hurricane.
- In the urban center of the town of Utuado, a landslide caused by Hurricane María on a cut-bank between two houses resulted in the death of three elderly sisters (fig. 42; Irizarry Álvarez, 2017). The model output shows this site as having Very High to Extremely High landslide susceptibility prior to the hurricane.
- In December 2017, a cut slope at km 209.8 of Highway PR-2 in the municipality of Guayanilla failed and caused the road to be closed temporarily and traffic was diverted for many months (fig. 43). The model analysis in this study shows that this location registers as a site with Moderate to High landslide potential.

Table 7. Comparison of performance of Puerto Rico landslide susceptibility maps against the Hurricane María inventory.

[km², square kilometer; —, not applicable]

Classification	Density of Hurricane María landslides (sites/km²)[1]					
	Monroe (1979)		Lepore and others (2012)		This study	
	Area (km²)	Density	Area (km²)	Density	Area (km²)	Density
Low	5,051	0.3	1,617	0.1	3,481	0.2
Moderate	3,472	19.7	3,561	2.6	2,609	2.7
High	272	4.0	1,649	12.8	1,741	12.1
Very High	78	6.8	1,764	23.3	783 ([2]870)	40.7 ([2]48.9)
Extremely High	—	—	—	—	87	123.0

[1]Hurricane María landslides from inventory of Hughes and others (2019).

[2] This is the value of the combination of the Very High and Extremely High classifications from the current study.

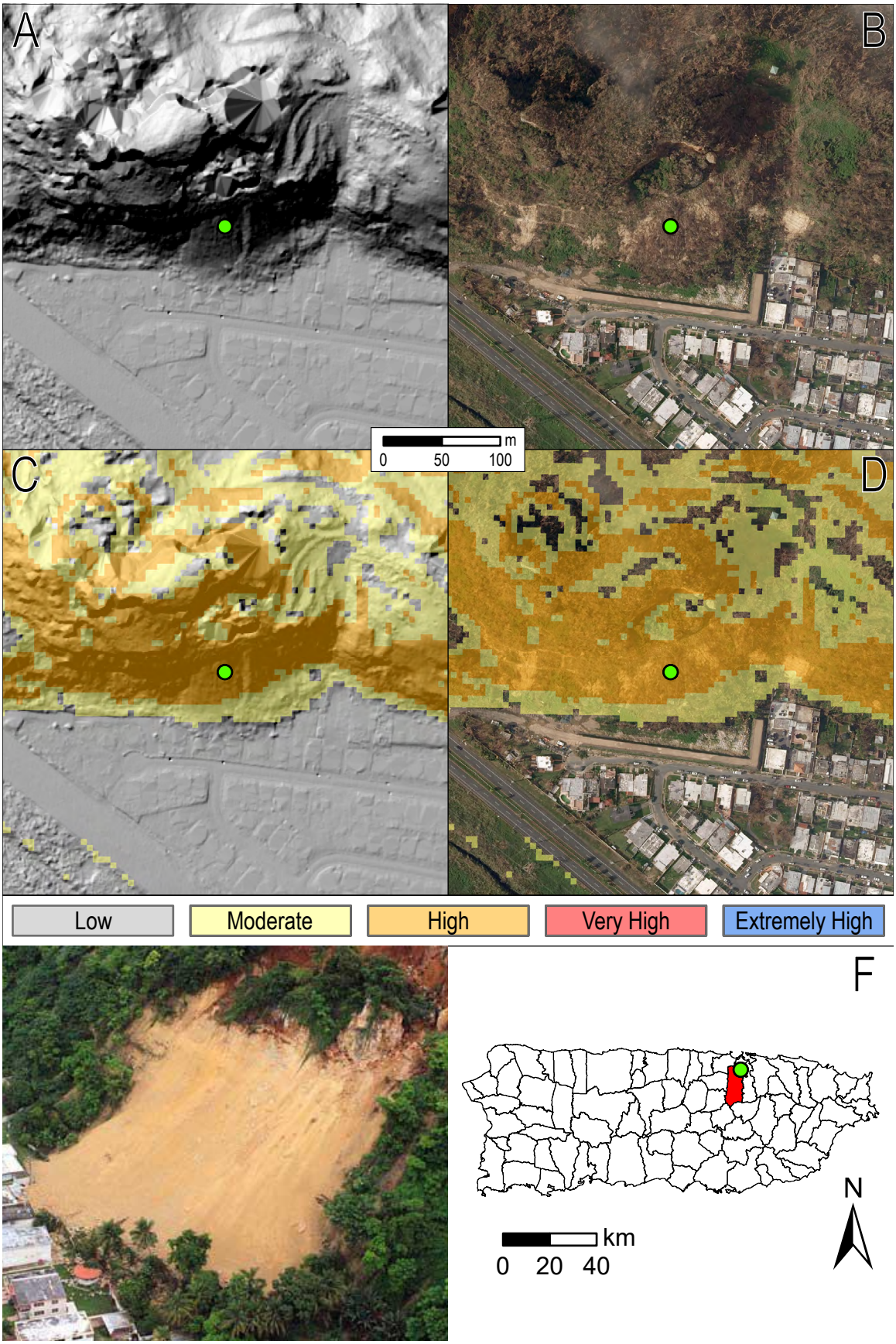
A
B
C
D
m
0 50 100
Low
Moderate
High
Very High
Extremely High
F
N
km
0 20 40

Figure 39 (previous page). Example of the Susceptibility Index model output for the Santa Ana mogote landslide at the Villa España Urbanization in the municipality of Bayamón, Puerto Rico. This site (18.405, –66.144) failed on 20 August 2013. Panes A–D show the same extent. The green marker is presented in the center of each image and does not necessarily correspond to any landslide feature. *A*, Hillshade raster of the 2016 lidar survey data. *B*, Aerial view of the same location. The imagery was acquired on 8 October 2017 and shows the presence of a mitigation berm that was constructed at the site after the demolition of several houses. *C*, The final susceptibility map dataset overlayed on the hillshade raster. The site is classified as having High landslide susceptibility. *D*, The final susceptibility map dataset overlayed on the aerial imagery. *E*, An oblique aerial photograph of the site in 2013, shortly after the failure (Vazquez Torres, 2013). *F*, Location map of the area with the municipality of Bayamón highlighted in red, and the location of the Villa España site denoted by the green marker. (m, meter; km, kilometer)

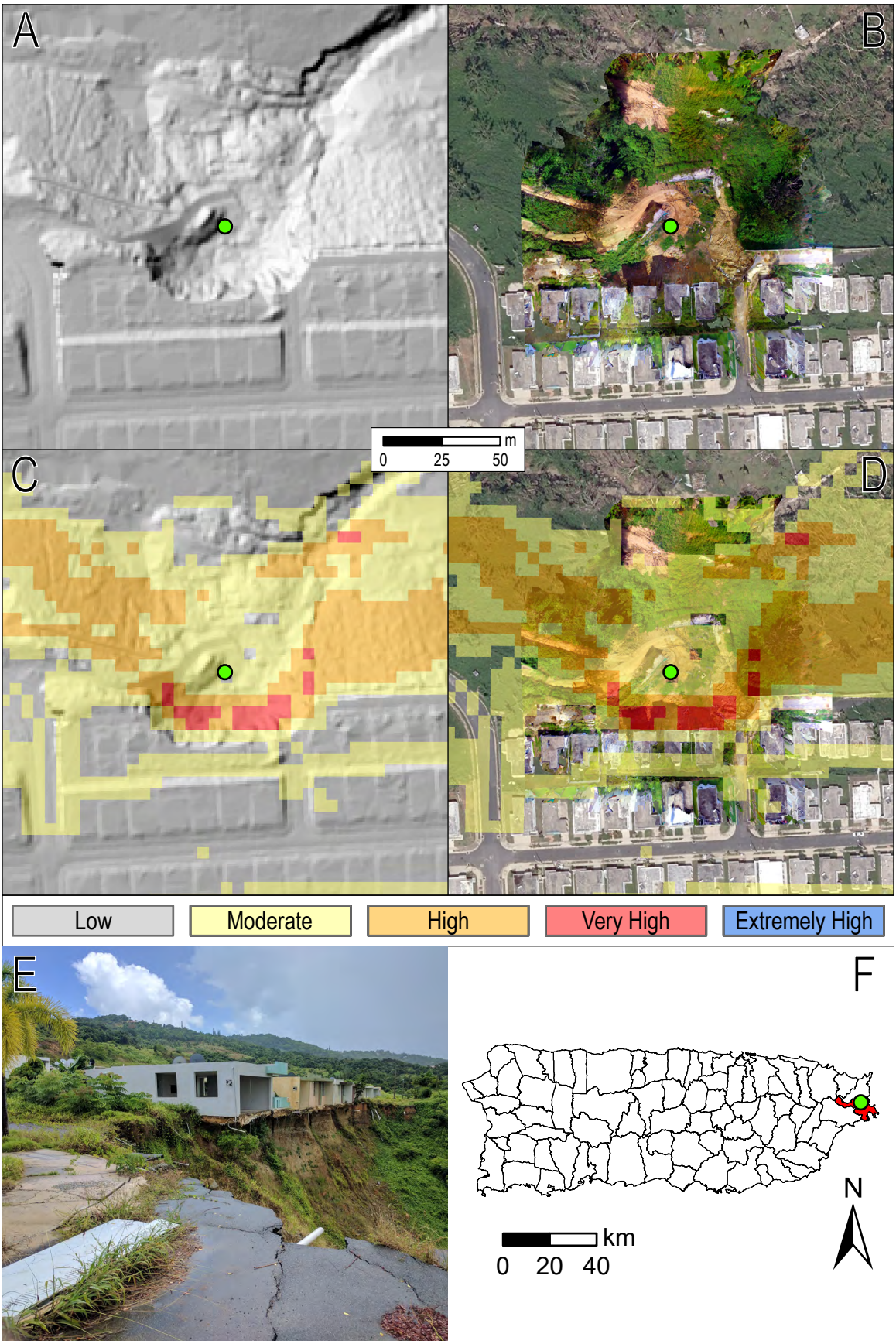
A
B
C
D
m
0 25 50
Low
Moderate
High
Very High
Extremely High
E
F
N
km
0 20 40

Figure 40 (previous page). Example of the Susceptibility Index model output for the Las Lomas Urbanization failure (18.2708, –65.6615) in the municipality of Ceiba, Puerto Rico. Panes A–D show the same extent. The green marker is presented as the center of the area and does not necessarily correspond to any landslide feature. *A*, Hillshade raster of the 2016 lidar survey data. The scar where fill material that collapsed on 4 October 2015 and undermined several houses is visible. *B*, Aerial view of the same location. The imagery in the center is from a drone survey on 5 February 2017 by K.S. Hughes, and the outer imagery is from Federal Emergency Management Agency imagery of 27 October 2017. *C*, The final susceptibility map dataset overlayed on the hillshade raster. The headscarp left behind by the 2015 failure registers as a zone of Very High landslide susceptibility, and the adjacent, unfailed slopes register as High susceptibility; it is likely that this High susceptibility zone would have extended across the landslide site prior to its occurrence. *D*, The final susceptibility map dataset overlayed on the aerial imagery. *E*, A photograph taken by K.S. Hughes of the headscarp on 17 June 2017. *F*, Location map of the area with the municipality of Ceiba is highlighted in red and the location of the Las Lomas site is denoted by the green marker. (m, meter; km, kilometer)

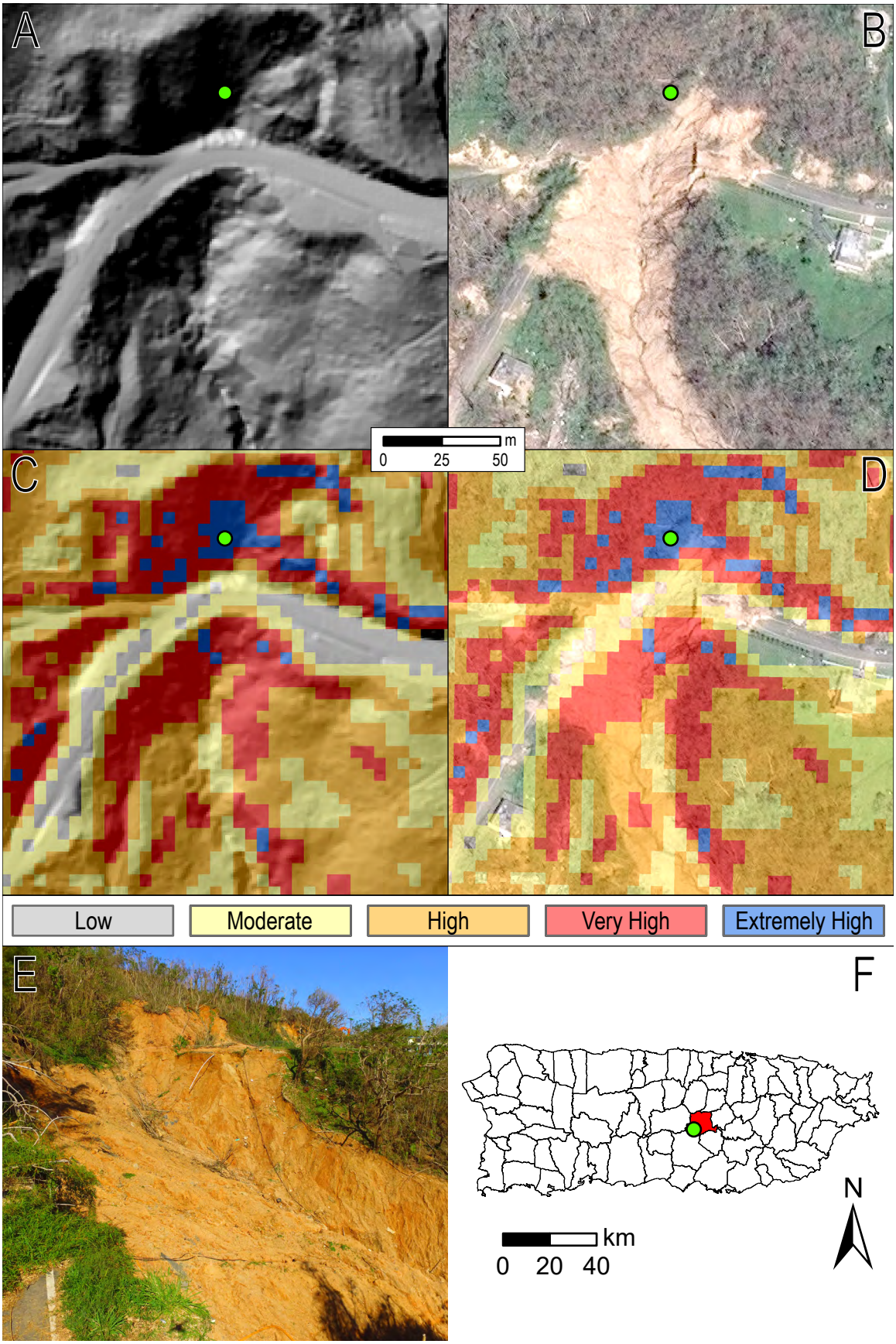
A
B
m
0 25 50
C
D
Low
Moderate
High
Very High
Extremely High
E
F
N
km
0 20 40

Figure 41 (previous page). Example of the Susceptibility Index model output for the PR–143 kilometer 56.2 landslide site in the municipality of Barranquitas, Puerto Rico. This location (18.176, –66.338) failed during Hurricane María (20 September 2017). Panes A–D show the same extent. The green marker is presented as the same location in each image and does not necessarily correspond to any landslide feature. *A*, Hillshade raster of the 2016 lidar survey data. The site has likely experienced previous landslide events. *B*, Aerial view of the same location. The imagery is a mosaic of photos that were acquired via aerial drone on 2 March 2018 by K.S. Hughes. *C*, The final susceptibility map dataset overlayed on the hillshade raster. The site is classified as having Very High to Extremely High landslide susceptibility. *D*, The final susceptibility map dataset overlayed on the satellite imagery. *E*, A photograph taken by K.S. Hughes looking east across the headscarp on 1 November 2017. The white pipe in the upper center of the image was about 80 meters away from the photographer. *F*, Location map of the area with the municipality of Barranquitas is highlighted in red and the location of the PR–143 kilometer 56.2 site is denoted by the green marker. This site is also shown in figure 8. (m, meter; km, kilometer)

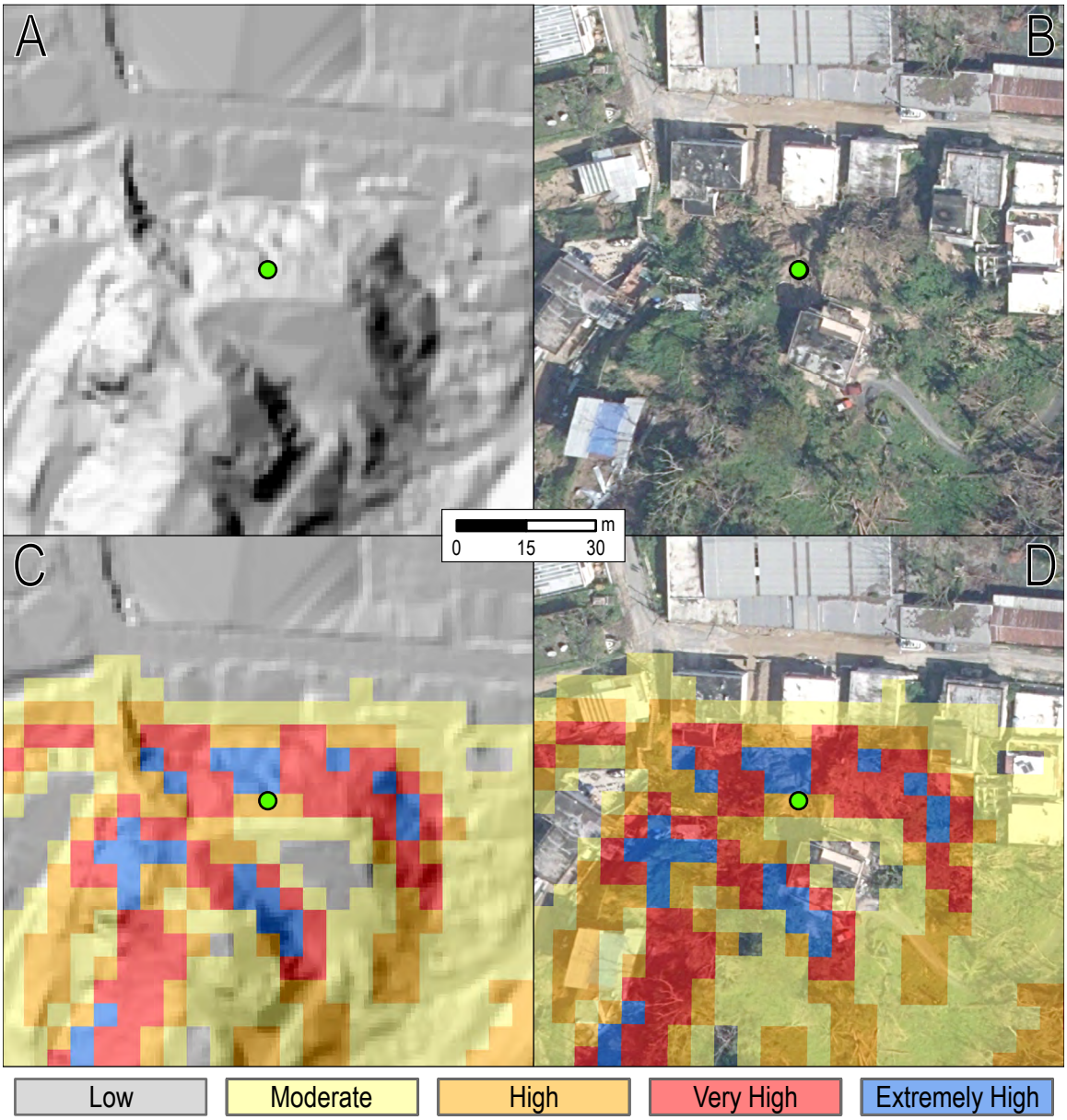
A
B
C
D
m
0 15 30
Low
Moderate
High
Very High
Extremely High


E

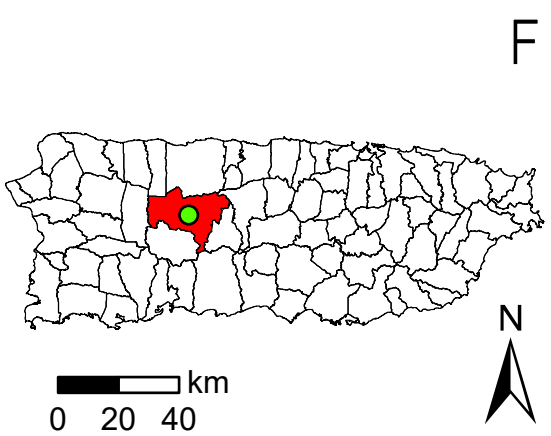
F
N
km
0 20 40

Figure 42 (previous page). Example of the Susceptibility Index model output for a landslide in the urban center of Utuado, Puerto Rico, caused by Hurricane María on 20 September 2017. This site (18.264, –66.698) resulted in the death of three residents when the cut bank behind their house mobilized and filled part of the lower level of the structure. Panes A–D show the same extent. The green marker is presented in the center of each image and does not necessarily correspond to any landslide feature. *A*, Hillshade raster of the 2016 lidar survey data. *B*, Aerial view of the same location. The imagery was acquired on 12 October 2017 and shows the scar of the landslide between the upper (south) and lower (north) houses. *C*, The final susceptibility map dataset overlayed on the hillshade raster. This site is classified as having Very High to Extremely High failure susceptibility. *D*, The final susceptibility map dataset overlayed on the aerial imagery. *E*, Photograph of the site on 2 November 2017 by Dr. Daniel Pradel (photo used with permission). *F*, Location map of the area with the municipality of Utuado is highlighted in red, and the location of the landslide is denoted by the green marker. (m, meter; km, kilometer)

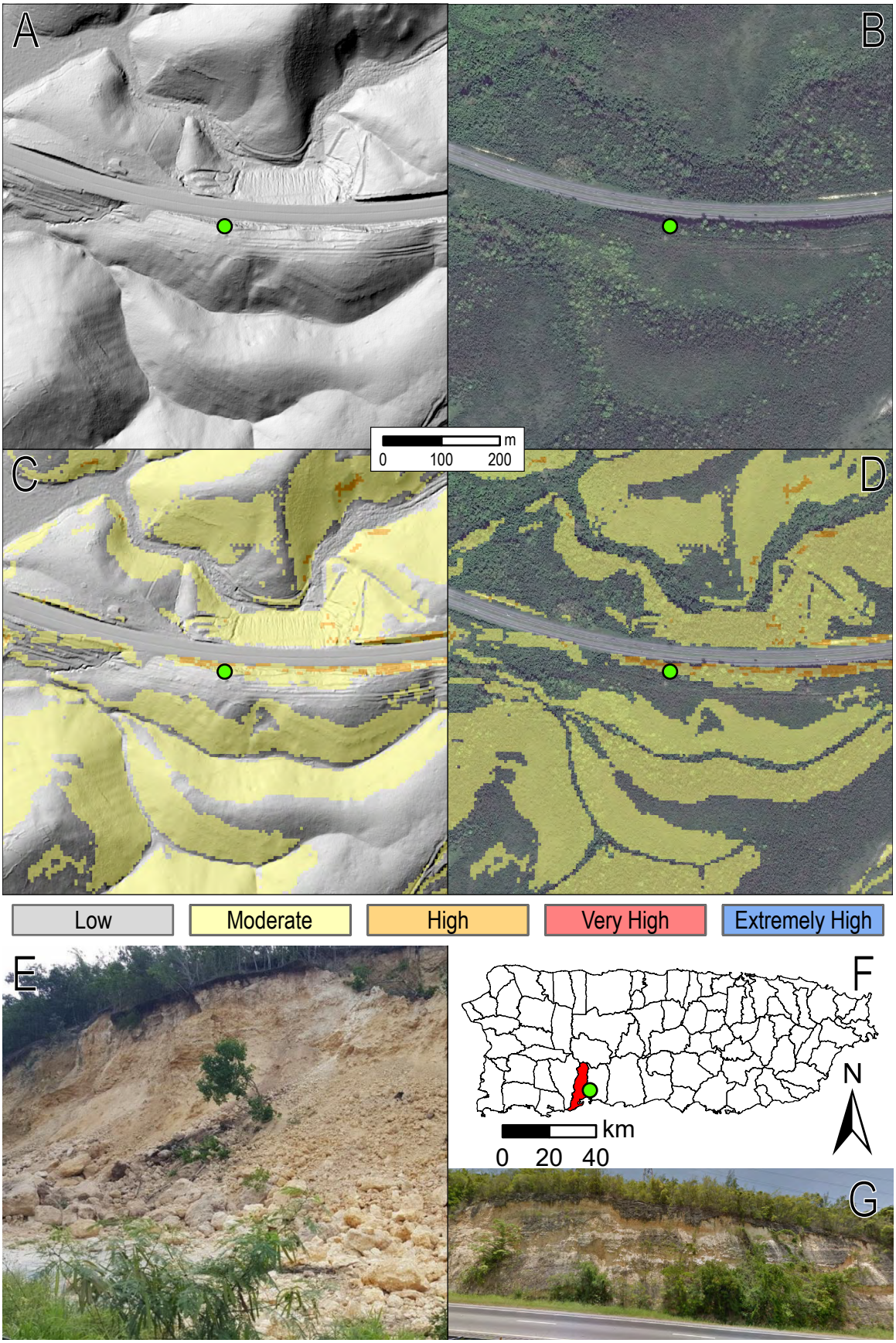
A
B
m
0 100 200
C
D
Low
Moderate
High
Very High
Extremely High
E
F
N
km
0 20 40
G

Figure 43 (previous page). Example of the Susceptibility Index model output for a landslide at kilometer 209.3 along Highway PR–2 in the municipality of Guayanilla, Puerto Rico, that occurred on 6 December 2017. This site (18.0112, –66.7569) resulted in the temporary closure of the regional highway, and the headscarp was very near a transmission tower of the electrical distribution system. Panes A–D show the same extent. The green marker is presented in the center of each image and does not necessarily correspond to any landslide feature. *A*, Hillshade raster of the 2016 lidar survey data. *B*, Aerial view of the same location. The imagery was acquired between October and December of 2017 by DigitalGlobe. *C*, The final susceptibility map dataset overlayed on the hillshade raster. This site is classified as having Moderate to High susceptibility to landslides. *D*, The final susceptibility map dataset overlayed on the aerial imagery. *E*, Photograph of the site on 6 December 2017 (Metro Puerto Rico, 2017). *F*, Location map of the area with the municipality of Guayanilla is highlighted in red, and the location of the landslide is denoted by the green marker. *G*, Image from Google Street View of the future failure site from May 2016. (m, meter; km, kilometer)

Use and Limitations of the Landslide Susceptibility Map

Plate 1 and geographic information system (GIS) files that accompany this report (Hughes and Schulz, 2020) depict estimated relative susceptibility to landslide occurrence during or soon after intense rainfall, such as that produced during tropical storms including hurricanes. The data are intended to illustrate relative potential landslide hazard to help guide site-specific landslide susceptibility assessments, and plan for future development and future widespread landslide events. For example, locations with higher landslide susceptibility could (1) be excluded from future development; (2) require slope-stability studies prior to development, and grading, foundation, and drainage design and construction that considers potential slope instability; (3) be targeted for evaluation and mitigation of potentially adverse conditions; (4) be monitored for signs of incipient landsliding, such as cracks in roadways and structures, leaning utility poles and trees, and broken water or sewer lines; and (or) (5) be considered for evacuation prior to forecasted landslide-inducing rainfall events and for emergency response activities after such rainfall. The map is not a substitute for site-specific, slope-stability investigations by licensed geologists and engineers. Additionally, many landslides in Puerto Rico move far from the locations where they originate and can destroy structures and injure and kill people as they move downslope; the map does not depict this significant hazard resulting from mobile landslides. Finally, locations of landslides triggered by earthquakes or prolonged, relatively low-intensity rainfall may significantly differ from High, Very High, and Extremely High susceptibility locations shown on the map.

For best use during emergency response to specific rainfall events, the map should be evaluated alongside event-specific rainfall conditions, with landslides being more likely where higher amounts of rainfall occur in locations with higher landslide susceptibility. As described herein, root-zone soil moisture estimated by the NASA SMAP mission correlated well with landslide locations during Hurricane María, and professionals may utilize event-specific soil moisture for more quantitative assessment of potential locations of landslides that result from future rainfall. Such use requires expertise in GIS data manipulation. Interested professionals may obtain root-zone soil moisture data from the NASA SMAP mission (https://smap.jpl.nasa.gov/, last accessed 26 December 2019), ensure that the data projection matches that of the *SI*_raster_for_SMAP files available with this report, reclassify the NASA SMAP data to the appropriate *SI* values provided in table 3, sum the *SI*_raster_for_SMAP and reclassified NASA SMAP data, and reclassify the sum by area percentile to obtain susceptibility rankings as provided in table 5.

Most landslides in Puerto Rico triggered by intense rainfall are shallow (to several meters deep) and occur in unconsolidated material (soil and saprolite) overlying rock (for example, Jibson, 1989; Larsen and Torres Sanchez, 1992; Bessette-Kirton and others, 2019). These are the types of landslides most well represented by the landslide susceptibility map because the map was produced using an inventory of landslides triggered by Hurricane María (Hughes and others, 2019) and most of those landslides were shallow. Hurricane María also triggered landslides in rock and some reached depths of approximately 30 m (Bessette-Kirton and others, 2019), so the map also depicts susceptibility to deeper landslides and those in rock. The tragic landslide that occurred at Mameyes in Ponce municipality during 1985, which killed more than 129 people (Silva-Tulla, 1986), is an example of a type of landslide that is likely poorly represented by the susceptibility map. Additionally, many landslides worldwide are triggered by human activities, such as hillslope grading and redirection of drainage. Local activities such as these cannot be accounted for on the map.

Common to nearly all modeling efforts, accuracy of the landslide susceptibility map relies upon accuracy and completeness of the input data utilized for its development. Among others, we expect that the following omissions and conditions detract from accuracy of the map: (1) variability within given geological terranes of bedrock strength and hydrologic properties, discontinuity orientation, and condition; (2) variability within given soil types of soil strength and hydrologic properties; (3) consideration of only part of the road network, including omission of most undocumented farm roads, paths, and trails; and (4) use of a 2015–2016 topographic model that predates landslides triggered by Hurricane María and other topographic changes.

Conclusion

Landslides are a common occurrence in Puerto Rico, with nearly two widespread landslide events occurring annually during recent decades. The high susceptibility of landslides in Puerto Rico primarily results from the island's topographic disequilibrium, rapid bedrock weathering, high-frequency intense rainfall events, and intense agrarian and urbanization practices during the past centuries. The high population density of Puerto Rico places many of its citizens and much of its infrastructure at risk to landslide events, as was well illustrated by the more than 70,000 landslides triggered during September 2017 by Hurricane María.

A digital inventory of those landslides was used alongside geospatial data that included land surface slope and curvature calculated from a light detection and ranging digital elevation model, mean annual precipitation, proximity to roadways and streams, geologic terrane, soil classification, land cover, and estimated soil moisture immediately following Hurricane María to develop a map depicting relative susceptibility to landslide occurrence during and following future intense rainfall events. The frequency-ratio statistical approach was utilized to identify relationships between landslide location and the geospatial data attributes and to develop the map. Results from analysis of soil moisture were used in an attempt to generalize the map by removing

the effects of variable soil moisture resulting from Hurricane María. Analysis using 25 percent of the landslide inventory sites that were not utilized for development of the map demonstrates that the map is statistically viable. Results of the analyses of these specific factors for Puerto Rico may potentially be adaptable for other tropical regions with comparable climate, topography, and geology.

The final map product depicts the susceptibility to landslide occurrence as Low (40 percent of the main island), Moderate (30 percent), High (20 percent), Very High (9 percent), and Extremely High (1 percent). Areas where landslides might travel after they occur are not shown on the map, although hazards may be extremely high in these areas. The map is intended to serve as a general guide for development planning, assessments of potential landslides and mitigation strategies across large areas, and emergency planning. The map is not a replacement for site-specific, slope-stability evaluations that should be performed by licensed geologists and engineers.

References Cited

Acevido, G., 1982, Soil survey of Arecibo area of northern Puerto Rico: U.S. Department of Agriculture Soil Conservation Service, 169 p. [Also available at https://www.nrcs.usda.gov/Internet/FSE_MANUSCRIPTS/puerto_rico/PR682/0/Arecibo.pdf.]

Bawiec, W.J., 1998, Geologic terranes of Puerto Rico, *in* Bawiec, W.J., ed., Geology, geochemistry, geophysics, mineral occurrences and mineral resource assessment for the Commonwealth of Puerto Rico: U.S. Geological Survey Open-File Report 98–038, p. 59–71, accessed February 28, 2020, at https://pubs.usgs.gov/of/1998/of98-038/.

Bayouth García, D., Rodríguez Feliciano, C.A., and Hughes, K.S., 2018, Event-specific and annual precipitation controls on mass wasting sites in Puerto Rico after the passage of Hurricane María, *in* Geological Society of America Annual Meeting, Indianapolis, Ind., 2018, Abstracts with Programs: Boulder, Colo., Geological Society of America, Paper 171-12, v. 50, no. 6, accessed February 28, 2020, at https://doi.org/10.1130/abs/2018AM-320596.

Berryhill, H.L., Jr., 1965, Geology of the Ciales quadrangle, Puerto Rico: U.S. Geological Survey Bulletin 1184, 116 p., 3 pls. [Also available at https://doi.org/10.3133/b1184.]

Bessette-Kirton, E.K., Cerovski-Darriau, C., Schulz, W.H., Coe, J.A., Kean, J.W., Godt, J.W., Thomas, M.A., and Hughes, K.S., 2019, Landslides triggered by Hurricane María—Assessment of an extreme event in Puerto Rico: GSA Today, v. 29, no. 6, p. 4–10. [Also available at https://www.geosociety.org/gsatoday/science/G383A/article.htm.]

Boccheciamp, R.A., 1977, Soil survey of the Humacao area of eastern Puerto Rico: U.S. Department of Agriculture Soil Conservation Service, 103 p. [Also available at https://www.nrcs.usda.gov/Internet/FSE_MANUSCRIPTS/puerto_rico/PR689/0/Humacao.pdf.]

Boccheciamp, R.A., 1978, Soil survey of San Juan area of Puerto Rico: U.S. Department of Agriculture Soil Conservation Service, 141 p. [Also available at https://www.nrcs.usda.gov/Internet/FSE_MANUSCRIPTS/puerto_rico/PR686/0/San_Juan.pdf.]

Brabb, E.E., 1984, Innovative approaches to landslide hazard and risk mapping, *in* Fourth International Symposium on Landslides, Toronto, Ontario, Canada, 1984, Proceedings: Toronto, Canadian Geotechnical Society, v. 1, p. 307–324.

Briggs, R.P., 1965, Geologic map of the Barceloneta quadrangle, Puerto Rico: U.S. Geological Survey Miscellaneous Geologic Investigations Map I-421, scale 1:20,000. [Also available at https://doi.org/10.3133/i421.]

Briggs, R.P., 1968, Geologic map of the Arecibo quadrangle Puerto Rico: U.S. Geological Survey Miscellaneous Geologic Investigations Map I-551, scale 1:20,000. [Also available at https://doi.org/10.3133/i551.]

Brocard, G.Y., Willenbring, J.K., Scatena, F.N., and Johnson, A.H., 2015, Effects of a tectonically-triggered wave of incision on riverine exports and soil mineralogy in the Luquillo Mountains of Puerto Rico: Applied Geochemistry, v. 63, p. 586–598. [Also available at https://doi.org/10.1016/j.apgeochem.2015.04.001.]

Campbell, R.H., Herd, D.G., and Alonso, R.M., 1985, Preliminary response activities and recommendations of the USGS Landslide Hazard Research Team to the Puerto Rico landslide disaster of October 7, 1985: U.S. Geological Survey Open-File Report 85–719, 13 p. [Also available at https://doi.org/10.3133/ofr85719.]

Carson, M.A., and Petley, D.J., 1970, The existence of threshold hillslopes in the denudation of the landscape: Translations of the Institute of British Geographers, v. 49, p. 71–95. [Also available at http://doi.org/10.2307/621642.]

Carter, O.R., 1965, Soil survey of the Lajas Valley area, Puerto Rico: U.S. Department of Agriculture Soil Conservation Service, Series 1961, no. 23, 170 p. [Also available at https://www.nrcs.usda.gov/Internet/FSE_MANUSCRIPTS/puerto_rico/lajasPR1965/Lajas.pdf.]

Chalkias, C., Kalogirou, S., and Ferentinou, M., 2014, Landslide susceptibility, Peloponnese Peninsula in south Greece: Journal of Maps, v. 10, no. 2, p. 211–222. [Also available at https://doi.org/10.1080/17445647.2014.884022.]

Civil Air Patrol, 2017, CAP imagery—Hurricane María: Civil Air Patrol web page, accessed January 13, 2020, at https://www.arcgis.com/home/webmap/viewer.html?webmap=3218d1cb022d4534be0c7d6833c0adf1.

Deere, D.U., Jimenez, P., and Hernandez, D., 1989, Complex landslides at plateau margins with an example from Puerto Rico, chap. 19 *of* Cording, E.J., Hall, W.J., Haltiwanger, J.D., Hendron, A.J., Jr., and Mesri, G., eds., The art and science of geotechnical engineering—At the dawn of the twenty-first century—A volume honoring Ralph B. Peck: Englewood Cliffs, N.J., Prentice-Hall, p. 349–366.

Dietz, J.L., 1986, Economic history of Puerto Rico—Institutional change and capitalist development: Princeton, N.J., Princeton University Press, 337 p.

Dorsey, C.W., Mesmer, L., and Caine, T.A., 1903, Soil survey from Arecibo to Ponce, Porto Rico: U.S. Department of Agriculture Bureau of Soils Field Operation 1902 Report no. 4, p. 793–839. [Also available at https://www.nrcs.usda.gov/Internet/FSE_MANUSCRIPTS/puerto_rico/areciboponcePR1902/areciboponcePR1902.pdf.]

Doser, D.I., Rodríguez, C.M., and Flores, C., 2005, Historical earthquakes of the Puerto Rico-Virgin Islands region (1915–1963), *in* Mann, P., ed., Active tectonics and seismic hazards of Puerto Rico, the Virgin Islands, and offshore areas: Geological Society of America Special Paper 385, p. 103–114. [Also available at https://doi.org/10.1130/0-8137-2385-X.103.]

Fawcett., T., 2006, An introduction to ROC analysis: Pattern Recognition Letters, v. 27, no. 8, p. 861–874. [Also available at https://doi.org/10.1016/j.patrec.2005.10.010.]

Fick, S.E., and Hijmans, R.J., 2017, WorldClim 2—New 1-km spatial resolution climate surfaces for global land areas: International Journal of Climatology, v. 37, no. 12, p. 4302–4315. [Also available at https://doi.org/10.1002/joc.5086.]

García López, X.A., 2018, Lidar and RTK GPS SfM monitoring of the PR-9 landslide in Ponce, Puerto Rico (2016–2018): University of Puerto Rico at Mayagüez, Undergraduate research thesis, 23 p.

Gierbolini, R.E., 1975, Soil survey of Mayaguez area of western Puerto Rico: U.S. Department of Agriculture Soil Conservation Service, 296 p. [Also available at https://www.nrcs.usda.gov/Internet/FSE_MANUSCRIPTS/puerto_rico/PR684/0/Mayaguez.pdf.]

Gierbolini, R.E., 1979, Soil survey of the Ponce area of southern Puerto Rico: U.S. Department of Agriculture Soil Conservation Service, 80 p. [Also available at https://www.nrcs.usda.gov/Internet/FSE_MANUSCRIPTS/puerto_rico/PR688/0/Ponce.pdf.]

Gould, W.A., Alarcón, C., Fevold, B., Jiménez, M.E., Martinuzzi, S., Potts, G., Quiñones, M., Solórzano, M., and Ventosa, E., 2008, Puerto Rico 2000 GAP Land Cover: U.S. Geological Survey web page, accessed September 12, 2019, at https://www.sciencebase.gov/catalog/item/560c3b2de4b058f706e5411e.

Grau, H.R., Aide, T.M., Zimmerman, J.K., Thomlinson, J.R., Helmer, E., and Zou, X., 2003, The ecological consequences of socioeconomic and land-use changes in postagriculture Puerto Rico: BioScience, v. 53, no. 12, p. 1159–1168. [Also available at https://doi.org/10.1641/0006-3568(2003)053[1159:TECOSA]2.0.CO;2.]

Grindlay, N.R., Abrams, L.J., Del Greco, L., and Mann, P., 2005, Toward an integrated understanding of Holocene fault activity in western Puerto Rico—Constraints from high-resolution seismic and sidescan sonar data, *in* Mann, P., ed., Active tectonics and seismic hazards of Puerto Rico, the Virgin Islands, and offshore areas: Geological Society of America Special Paper 385, p. 139–160. [Also available at https://doi.org/10.1130/0-8137-2385-X.139.]

He, Y., and Beighley, R.E., 2008, GIS-based regional landslide susceptibility mapping—A case study in southern California: Earth Surface Processes and Landforms, v. 33, no. 3, p. 380–393. [Also available at https://doi.org/10.1002/esp.1562.]

Huffaker, L., 2002, Soil survey of Caribbean National Forest and Luquillo Experimental Forest, Commonwealth of Puerto Rico: U.S. Department of Agriculture Natural Resources Conservation Service, 181 p. [Also available at https://www.nrcs.usda.gov/Internet/FSE_MANUSCRIPTS/puerto_rico/caribbeanNF_PR2002/CNF.pdf.]

Hughes, K.S., Bayouth García, D., Martínez Milian, G.O., Schulz, W.H., and Baum, R.L., 2019, Map of slope-failure locations in Puerto Rico after Hurricane María: U.S. Geological Survey data release, accessed September 12, 2019, at https://doi.org/10.5066/P9BVMD74.

Hughes, K.S., and Morales Vélez, A.C., 2017, Characterization of landslide sites in Puerto Rico after Hurricanes Irma and María, *in* American Geophysical Union Fall Meeting 2017, New Orleans, La., 2017, Abstracts: American Geophysical Union, Abstract NH23E-2859.

Hughes, K.S., and Schulz, W.H., 2020, Results from frequency-ratio analyses of soil classification and land use related to landslide locations in Puerto Rico following Hurricane María: U.S. Geological Survey data release, https://www.sciencebase.gov/catalog/item/5e2f53f5e4b0a79317d42330.

Irizarry Álvarez, F., 2017, Mueren tres hermanas por derrumbe en Utuado tras paso de María: Primera Hora, September 21, 2017, accessed September 12, 2019, at https://www.primerahora.com/noticias/puerto-rico/nota/muerentreshermanasporderrumbeenutuadotraspasodeMaría -1246727/.

Jennings, L.N., Douglas, J., Treasure, E., and González, G., 2014, Climate change effects in El Yunque National Forest, Puerto Rico, and the Caribbean region: Asheville, N.C., U.S. Department of Agriculture Forest Service, Southern Research Station, General Technical Report SRS-193, 47 p. [Also available at https://www.fs.usda.gov/treesearch/pubs/45918.]

Jibson, R.W., 1986, Evaluation of landslide hazards resulting from the 5–8 October 1985 storm in Puerto Rico: U.S. Geological Survey Open-File Report 86–26, 40 p. [Also available at https://doi.org/10.3133/ofr8626.]

Jibson, R.W., 1987, Landslide hazards of Puerto Rico, *in* Hays, W.W., and Gori, P.L., eds., Proceedings of Conference XXXVI—A workshop on "Assessment of geologic hazards and risk in Puerto Rico": U.S. Geological Survey Open-File Report 87–008, p. 183–188. [Also available at https://pubs.usgs.gov/of/1987/0008/report.pdf.]

Jibson, R.W., 1989, Debris flows in southern Puerto Rico, *in* Schultz, A.P., and Jibson, R.W., eds., Landslide processes of the eastern United States and Puerto Rico: Geological Society of America Special Paper 236, p. 29–55. [Also available at https://doi.org/10.1130/SPE236-p29.]

Jolly, W.T., Lidiak, E.G., Dickin, A.P., and Wu, T., 1998a, Geochemical diversity of Mesozoic island arc tectonic blocks in eastern Puerto Rico, *in* Lidiak, E.G., and Larue, D.K., eds., Tectonics and geochemistry of the northeastern Caribbean: Geological Society of America Special Paper 322, p. 67–98. [Also available at https://doi.org/10.1130/0-8137-2322-1.67.]

Jolly, W.T., Lidiak, E.G., Schellekens, J.H., and Santos, H., 1998b, Volcanism, tectonics, and stratigraphic correlations in Puerto Rico, *in* Lidiak, E.G., and Larue, D.K., eds., Tectonics and geochemistry of the northeastern Caribbean: Geological Society of America Special Paper 322, p. 1–34. [Also available at https://doi.org/10.1130/0-8137-2322-1.1.]

Kamal, S.A., 2008, Development of a landslide hazard map for the island of Puerto Rico: Massachusetts Institute of Technology, M.S. thesis, 58 p. [Also available at http://hdl.handle.net/1721.1/43886.]

Keellings, D., and Hernández Ayala, J.J., 2019, Extreme rainfall associated with Hurricane María over Puerto Rico and its connections to climate variability and change: Geophysical Research Letters, v. 46, no. 5, p. 2964–2973. [Also available at https://doi.org/10.1029/2019GL082077.]

Knutson, T.R., McBride, J.L, Chan, J., Emanuel, K., Holland, G., Landsea, C., Held, I., Kossin, J.P., Srivastava, A.K., and Sugi, M., 2010, Tropical cyclones and climate change: Nature Geoscience, v. 3, p. 157–163. [Also available at https://doi.org/10.1038/ngeo779.]

Larsen, M.C., 2012, Landslides and sediment budgets in four watersheds in eastern Puerto Rico, chap. F *of* Murphy, S.F., and Stallard, R.F., eds., Water quality and landscape processes of four watersheds in eastern Puerto Rico: U.S. Geological Survey Professional Paper 1789, p. 153–178. [Also available at https://doi.org/10.3133/pp1789F.]

Larsen, M.C., and Parks, J.E., 1997, How wide is a road? The association of roads and mass-wasting in a forested montane environment: Earth Surface Processes and Landforms, v. 22, no. 9, p. 835–848. [Also available at https://doi.org/10.1002/(SICI)1096-9837(199709)22:9%3C835::AID-ESP782%3E3.0.CO;2-C.]

Larsen, M.C., and Parks, J.E., 1998, Map showing landslide susceptibility in the Comerio municipality, Puerto Rico: U.S. Geological Survey Open-File Report 98–566, 1 map sheet, scale 1:20,000. [Also available at https://doi.org/10.3133/ofr98566.]

Larsen, M.C., and Santiago Román, A., 2001, Mass wasting and sediment storage in a small montane watershed—An extreme case of anthropogenic disturbance in the humid tropics, *in* Dorava, J. M., Fitzpatrick, F., Palcsak, B.B., and Montgomery, D.R., eds., Geomorphic processes and riverine habitat: American Geophysical Union, Water Science and Application Series, v. 4, p. 119–138. [Also available at https://pdfs.semanticscholar.org/6c39/1b6cb4c6de01c1f0468851df37e84a0f2ced.pdf.]

Larsen, M.C., Santiago, M., Jibson, R., and Questell, E., 2004, Map showing susceptibility to rainfall-triggered landslides in the municipality of Ponce, Puerto Rico: U.S. Geological Survey Scientific Investigations Map I-2818, 1 pl., scale 1:30,000. [Also available at https://pubs.usgs.gov/sim/2005/2818/.]

Larsen, M.C., and Simon, A., 1990, Landslide processes in saprolitic soils of a tropical rain forest, Puerto Rico *in* Larue, D.K., and Draper, G., eds., Transactions of the 12th Caribbean Conference, August 7–11, 1989, St. Croix, V.I.: Miami Geological Society, p. 217–222.

Larsen, M.C., and Simon, A., 1993, A rainfall intensity-duration threshold for landslides in a humid-tropical environment, Puerto Rico: Geografiska Annaler, Series A—Physical Geography, v. 75, no. 1-2, p. 13–23.

Larsen, M.C., and Torres-Sanchez, A.J., 1992, Landslides triggered by Hurricane Hugo in eastern Puerto Rico, September 1989: Caribbean Journal of Science, v. 28, no. 3-4, p. 113–125.

Lee, S., and Pradhan, B., 2006, Probabilistic landslide hazards and risk mapping on Penang Island, Malaysia: Journal of Earth System Science, v. 115, no. 6, p. 661–672. [Also available at https://doi.org/10.1007/s12040-006-0004-0.]

Lee, S., Ryu, J.H., and Kim, I.S., 2007, Landslide susceptibility analysis and its verification using likelihood ratio, logistic regression, and artificial neural network models—Case study of Youngin, Korea: Landslides, v. 4, no. 4, p. 327–338. [Also available at https://doi.org/10.1007/s10346-007-0088-x.]

Lepore, C., Kamal, S.A., Shanahan, P., and Bras, R.L., 2012, Rainfall-induced landslide susceptibility zonation of Puerto Rico: Environmental Earth Sciences, v. 66, p. 1667–1681. [Also available at https://doi.org/10.1007/s12665-011-0976-1.]

Li, L., Lan, H., Guo, C., Zhang, Y., Li, Q., and Wu, Y., 2016, A modified frequency ratio method for landslide susceptibility assessment: Landslides, v. 14, no. 2, p. 727–741. [Also available at https://doi.org/10.1007/s10346-016-0771-x.]

Lobeck, A.K., 1922, The physiography of Porto Rico: New York Academy of Sciences, Scientific Survey of Porto Rico and the Virgin Islands, v. 1, no. 4, p. 301–379.

López, A.M., Hughes, K.S., and Vanacore, E., 2020, Puerto Rico's winter 2019–2020 seismic sequence leaves the island on edge: Temblor, January 7, 2020, accessed January 13, 2020, at http://doi.org/10.32858/temblor.064. [Also available at https://temblor.net/earthquake-insights/puerto-ricos-winter-2019-2020-seismic-sequence-leaves-the-island-on-edge-10321/.]

Lugo Bendezú, R., Martinez, G., Ortiz Carrero, P., Torres Angleró, K.H., and Hughes, K.S., 2018, Assessing Puerto Rico's physical topography in relation to rainfall-induced mass wasting sites post Hurricane María, *in* Geological Society of America Annual Meeting, Indianapolis, Ind., 2018, Abstracts with Programs: Boulder, Colo., Geological Society of America, Paper 171-12, v. 50, no. 6, accessed February 28, 2020, at https://doi.org/10.1130/abs/2018AM-320601.

Lugo-Camacho, J.L., 2008, Soil survey of San Germán area, Puerto Rico: U.S. Department of Agriculture Natural Resources Conservation Service, 964 p. [Also available at https://www.nrcs.usda.gov/Internet/FSE_MANUSCRIPTS/puerto_rico/PR787/0/SanGerman.pdf.]

Mann, P., Prentice, C.S., Hippolyte, J.C., Grindlay, N.R., Abrams, L.J., and Laó-Dávila, D., 2005, Reconnaissance study of Late Quaternary faulting along Cerro Goden fault zone, western Puerto Rico, *in* Mann, P., ed., Active tectonics and seismic hazards of Puerto Rico, the Virgin Islands, and offshore areas, Geological Society of America Special Paper 385, p. 115–138. [Also available at https://doi.org/10.1130/0-8137-2385-X.115.]

Mattson, P.H., 1968, Geologic map of the Adjuntas quadrangle, Puerto Rico: U.S. Geological Survey Miscellaneous Geologic Investigations Map IMAP 519, 1 pl., scale 1:20,000. [Also available at https://doi.org/10.3133/i519.]

McIntyre, D.H., Geologic map of the central La Plata quadrangle, Puerto Rico: U.S. Geological Survey Miscellaneous Geologic Investigations Map IMAP 660, 1 pl., scale 1:20,000. [Also available at https://doi.org/10.3133/i660.]

Metro Puerto Rico, 2017, Derrumbe en carretera de Guayanilla hacia Peñuelas: Metro Puerto Rico, December 6, 2017, accessed September 12, 2019, at https://www.metro.pr/pr/noticias/2017/12/06/derrumbe-carretera-guayanilla-hacia-penuelas.html.

Meyerhoff, H.A., 1927, Tertiary physiographic development of Porto Rico and the Virgin Islands: Geological Society of America Bulletin, v. 38, no. 4, p. 557–576. [Also available at https://doi.org/10.1130/GSAB-38-557.]

Milken Institute School of Public Health, 2018, Ascertainment of the estimated excess mortality from Hurricane María in Puerto Rico: Washington, D.C., George Washington University, 69 p. [Also available at https://www.preventionweb.net/publications/view/60237.]

Monroe, W.H., 1963, Geology of the Camuy quadrangle, Puerto Rico: U.S. Geological Survey Map GQ-197, 1 pl., scale 1:20,000. [Also available at https://doi.org/10.3133/gq197.]

Monroe, W.H., 1964, Large retrogressive landslides in north-central Puerto Rico, *in* U.S. Geological Survey, Geological Survey Research 1964—Chapter B: U.S. Geological Survey Professional Paper 501-B, p. B123–B125. [Also available at https://doi.org/10.3133/pp501B.]

Monroe, W.H., 1967, Geologic map of the Quebradillas quadrangle, Puerto Rico: U.S. Geological Survey Miscellaneous Geologic Investigations Map IMAP 498, 1 pl., scale 1:20,000. [Also available at https://doi.org/10.3133/i498.]

Monroe, W.H., 1969a, Geologic map of the Aguadilla quadrangle, Puerto Rico: U.S. Geological Survey Miscellaneous Geologic Investigations Map IMAP 569, 1 pl., scale 1:20,000. [Also available at https://doi.org/10.3133/i569.]

Monroe, W.H., 1969b, Geologic map of the Moca and Isabela quadrangles, Puerto Rico: U.S. Geological Survey Miscellaneous Geologic Investigations Map IMAP 565, 1 pl., scale 1:20,000. [Also available at https://doi.org/10.3133/i565.]

Monroe, W.H., 1979, Map showing landslides and areas of susceptibility to landsliding in Puerto Rico: U.S. Geological Survey IMAP 1148, 1 pl., scale 1:240,000. [Also available at https://doi.org/10.3133/i1148.]

Monroe, W.H., 1980a, Geology of the middle Tertiary formations of Puerto Rico: U.S. Geological Survey Professional Paper 953, 1 pl., 93 p. [Also available at https://doi.org/10.3133/pp953.]

Monroe, W.H., 1980b, Some tropical landforms of Puerto Rico: U.S. Geological Survey Professional Paper 1159, 1 pl., 39 p. [Also available at https://doi.org/10.3133/pp1159.]

Morales-Vélez, A.C., and Hughes, K.S., 2018, Comprehensive Hurricane María mass wasting inventory and improved frequency ratio landslide hazard mapping—Status update from the University of Puerto Rico at Mayagüez: Dimension, Colegio de Ingenieros y Agrimensores de Puerto Rico, v. 1, p. 23–26. [Also available at https://docs.google.com/a/upr.edu/viewer?a=v&pid=sites&srcid=dXByLmVkdXxnZW9sb2d5fGd4OjY5MDk0MWM0OTg0OGRlZDE.]

Moul-Bogunovic, M., 2019, Timing and modern character of the western Puerto Rico fault system using carbonate stratigraphy and fluvial terrace chronology for the Río Culebrinas fault valley: University of Puerto Rico at Mayagüez, M.S. thesis, 105 p. [Also available at https://scholar.uprm.edu/handle/20.500.11801/2442.]

Muñoz, M.A., Lugo, W.I., Santiago, C., Matos, M., Ríos, S., and Lugo, J., 2018, Taxonomic classification of the soils of Puerto Rico, 2017: San Juan, Puerto Rico, University of Puerto Rico, Mayagüez Campus, College of Agricultural Sciences, Agricultural Experiment Station, Bulletin 313, 73 p. [Also available at https://scholar.uprm.edu/handle/20.500.11801/817.]

National Aeronautics and Space Administration [NASA], 2017, SMAP L4 Global 3-hourly 9 km EASE-Grid Surface and Root Zone Soil Moisture Analysis Update, Version 4: National Snow & Ice Data Center web page, accessed September 12, 2019, at https://nsidc.org/data/SPL4SMAU/versions/4.

National Weather Service, 2017, Update—Impacts of TJUA NEXRAD outage on quantitative precipitation estimates: San Juan, Puerto Rico, National Weather Service Public Information Sheet, October 3, 2017, accessed September 12, 2019, at http://www.weather.gov/media/serfc/PNSQPESJU2.pdf.

NationMaster, 2017, Transport > Road density > Km of road per 100 sq. km of land area—Countries compared: Nation Master website, accessed September 12, 2019, at http://www.nationmaster.com/country-info/stats/Transport/Road-density/Km-of-road-per-100-sq.-km-of-land-area.

Nelson, A.E., 1967, Geologic map of the Corozal quadrangle, Puerto Rico: U.S. Geological Survey Miscellaneous Geologic Investigations Map IMAP 473, 1 pl., scale 1:20,000. [Also available at https://doi.org/10.3133/i473.]

Nelson, A.E., and Tobisch, O.T., 1968, Geologic map of the Bayaney quadrangle, Puerto Rico: U.S. Geological Survey Miscellaneous Geologic Investigations Map IMAP 525, 1 pl., scale 1:20,000. [Also available at https://doi.org/10.3133/i525.]

Ortega-Ariza, D., Franseen, E.K., Santos-Mercado, H., Ramírez-Martínez, W.R., and Core-Suárez, E.E., 2015, Strontium isotope stratigraphy for Oligocene-Miocene carbonate systems in Puerto Rico and the Dominican Republic—Implications for Caribbean processes affecting depositional history: The Journal of Geology, v. 123, no. 6, p. 539–560. [Also available at https://www.journals.uchicago.edu/doi/abs/10.1086/683335.]

Pando, M.A., Ruiz, M.E., and Larsen, M.C., 2005, Rainfall-induced landslides in Puerto Rico—An overview in Geo-Frontiers Congress 2005, Austin, Tex., 2005, Abstracts: Reston, Va., American Society of Civil Engineers, p. 2911–2925. [Also available at https://doi.org/10.1061/40787(166)25.]

Pease, M.H., Jr., 1968, Geologic map of the Naranjito quadrangle, Puerto Rico: U.S. Geological Survey Miscellaneous Geologic Investigations Map IMAP 508, 1 pl., scale 1:20,000. [Also available at https://doi.org/10.3133/i508.]

Philpott, S.M., Lin, B.B., Jha, S., and Brines, S.J., 2008, A multi-scale assessment of hurricane impacts on agricultural landscapes based on land use and topographic features: Agriculture, Ecosystems & Environment, v. 128, no. 1–2, p. 12–20. [Also available at https://doi.org/10.1016/j.agee.2008.04.016.]

Porder, S., Johnson, A.H., Xing, H.X., Brocard, G., Goldsmith, S., and Pett-Ridge, J., 2015, Linking geomorphology, weathering and cation availability in the Luquillo Mountains of Puerto Rico: Geoderma, v. 249–250, p. 100–110. [Also available at https://doi.org/10.1016/j.geoderma.2015.03.002.]

Prentice, C.S., and Mann, P., 2005, Paleoseismic study of the South Lajas fault—First documentation of an onshore Holocene fault in Puerto Rico, *in* Mann, P., ed., Active tectonics and seismic hazards of Puerto Rico, the Virgin Islands, and offshore areas, Geological Society of America Special Paper 385, p. 215–222. [Also available at https://doi.org/10.1130/0-8137-2385-X.215.]

Puerto Rico Centro de Recaudación de Ingresos Municipales, 1998, Mapa base del CRIM (1996–98), accessed September 12, 2019, at http://gis.otg.pr.gov/downloads/CRIM_Basemap_Project_1996-98/DEM_CRIM.zip.

Puerto Rico Oficina de Gerencia y Presupuesto, 2018, Geología detallada: Government of Puerto Rico, accessed September 12, 2019, at http://gis.otg.pr.gov/downloads/geology/geology20k20181031_gdb.zip.

Ramos-Scharrón, C.E., and Arima, E., 2019, Hurricane María's precipitation signature in Puerto Rico—A conceivable presage of rains to come: Scientific Reports, v. 9, no. 1, article no. 15612, accessed February 28, 2020, at https://doi.org/10.1038/s41598-019-52198-2.

Ramos-Scharrón, C.E., and LaFevor, M.C., 2016, The role of unpaved roads as active source areas of precipitation excess in small watersheds drained by ephemeral streams in the northeastern Caribbean: Journal of Hydrology, v. 533, p. 168–179. [Also available at https://doi.org/10.1016/j.jhydrol.2015.11.051.]

Regmi, A.D., and Poudel, K., 2016, Assessment of landslide susceptibility using GIS-based evidential belief function in Patu Khola watershed, Dang, Nepal: Environmental Earth Sciences, v. 75, article no. 743, accessed February 28, 2020, at https://doi.org/10.1007/s12665-016-5562-0.

Reid, H.F., and Taber, S., 1919, The Porto Rico earthquake of 1918 with descriptions of earlier earthquakes—Report of the Earthquake Investigation Commission: Washington, D.C., Government Printing Office, 74 p.

Rivera-Santiago, F.O., 2015, High precision GPS monitoring for landslide hazard and land stability evaluation in the Cerca del Cielo urbanization, Ponce, Puerto Rico: University of Puerto Rico at Mayagüez, M.S. thesis, 144 p. [Also available at https://scholar.uprm.edu/handle/20.500.11801/56.]

Roberts, R.C., 1942, Soil survey of Puerto Rico: U.S. Department of Agriculture Bureau of Plant Industry, Series 1936, no. 8, 253 p. [Also available at https://www.nrcs.usda.gov/Internet/FSE_MANUSCRIPTS/puerto_rico/PR1942/puertorico1942a.pdf.]

Rodríguez Feliciano, C.A., Bayouth García, D., and Hughes, K.S., 2019, Volume of slope failures caused by Hurricane María in Puerto Rico using lidar and SfM, *in* Geological Society of America Annual Meeting, Phoenix, Az., 2019, Abstracts with Programs: Boulder, Colo., Geological Society of America, Paper 42-2, v. 51, no. 5, accessed February 28, 2020, at https://doi.org/10.1130/abs/2019AM-335978.

Rodríguez-Pérez, C., Vázquez Castillo, L., Rodriguez-Molina, C., and Vázquez Castillo, A., 1988, A study of a road landslide in Puerto Rico, *in* Second International Conference on Case Histories in Geotechnical Engineering, St. Louis, Mo., 1988, Proceedings: St. Louis, Mo., Missouri University of Science and Technology, Paper 2.16, p. 151–157. [Also available at https://scholarsmine.mst.edu/cgi/viewcontent.cgi?article=1440&context=icchge.]

Sanger, J.P., Gannett, H., Willcox, W.F., and United States War Department, 1900, Report on the census of Porto Rico, 1899: Washington, D.C., Government Printing Office, 417 p.

Santiago, M., and Larsen, M.C., 2001, Map showing susceptibility to earthquake-induced landsliding, San Juan metropolitan area, Puerto Rico: U.S. Geological Survey Open-File Report 2001–39, 2 pls., scale 1:20,000, accessed February 28, 2020, at https://doi.org/10.3133/ofr200139.

Santiago-Pérez, Y., Odom, W.E., III, and Hughes, K.S., 2019, Relict Caribbean topography and tectonically triggered erosion rates in the Cordillera Central of Puerto Rico *in* Geological Society of America Annual Meeting, Phoenix, Az., 2019 Abstracts with Programs: Boulder, Colo., Geological Society of America, Paper 263-7, v. 51, no. 5, accessed February 28, 2020, at https://doi.org/10.1130/abs/2019AM-338288.

Schulz, W.H., 2007, Landslide susceptibility revealed by lidar imagery and historical records, Seattle, Washington: Engineering Geology, v. 89, no. 1–2, p. 67–87. [Also available at https://doi.org/10.1016/j.enggeo.2006.09.019.]

Schwartz, S.B., 1992, The Hurricane of San Ciriaco—Disaster, politics, and society in Puerto Rico, 1899–1901: Hispanic American Historical Review, v. 72, no. 3, p. 303–334. [Also available at http://doi.org/10.2307/2515987.]

Sidle, R.C., and Ochiai, H., 2006, Landslides—Processes, prediction, and land use: Washington, D.C., American Geophysical Union, Water Resources Monograph 18, 312 p. [Also available at http://doi.org/10.1029/WM018.]

Silva-Tulla, F., 1986, The October 1985 landslide at Barrio Mameyes, Ponce, Puerto Rico: Washington, D.C., National Academies Press, 14 p.

Silva-Tulla, F., Pando, M.A., Soto, A.E., Morales, A., Pradel, D., Inci, G., Sasanakul, I., Bernal, J.R., Kayen, R., Hughes, S., Adams, T., and Park, Y., 2018, Geotechnical impacts of Hurricane María in Puerto Rico: Geotechnical Extreme Events Reconnaissance, Association Report No. GEER-057, 120 p. [Also available at http://www.geerassociation.org/administrator/components/com_geer_reports/geerfiles/180629_GEER_PR_Report_No_GEER-057.pdf.]

Simon, A., Larsen, M.C., and Hupp, C.R., 1990, The role of soil processes in determining mechanisms of slope failure and hillslope development in a humid-tropical forest, eastern Puerto Rico: Geomorphology, v. 3, no. 3–4, p. 263–286. [Also available at https://doi.org/10.1016/0169-555X(90)90007-D.]

Soler-López, L.R., 2000, Sedimentation survey of Lago Dos Bocas, Puerto Rico, October 1999: U.S. Geological Survey Water Resources Investigations Report 00-4234, 19 p. [Also available at https://pubs.usgs.gov/wri/2000/4234/report.pdf.]

Taggart, B.E., and Joyce, J., 1990, Radiometrically dated marine terraces on northwestern Puerto Rico, *in* Larue, D.K., and Draper, G., eds., Transactions of the 12th Caribbean Conference, August 7–11, 1989, St. Croix, V.I.: Miami Geological Society, p. 248–258.

Terzaghi, K., 1950, Mechanism of landslides, *in* Paige, S., ed., Application of geology to engineering practice—Berkey volume: New York, Geological Society of America, p. 83–124. [Also available at https://doi.org/10.1130/Berkey.1950.]

Tobisch, O.T., and Turner, M.D., 1971, Geologic map of the San Sebastián quadrangle, Puerto Rico: U.S. Geological Survey Miscellaneous Geologic Investigations Map IMAP 661, 1 pl., scale 1:20,000. [Also available at https://doi.org/10.3133/i661.]

U.S. Census Bureau, 2010, 2010 Census—Population density data (text version): United States Census Bureau web page, accessed January 13, 2020, at https://www.census.gov/data/tables/2010/dec/density-data-text.html.

U.S. Census Bureau, 2015, 2015 TIGER/Line Shapefiles, State, Puerto Rico, primary and secondary roads State-based Shapefile: United States Census Bureau, accessed September 12, 2019, at http://www2.census.gov/geo/tiger/TIGER2015/PRISECROADS/tl_2015_72_prisecroads.zip.

U.S. Department of Agriculture [USDA], 2018, Web soil survey: U.S. Department of Agriculture Natural Resources Conservation Service web page, accessed September 12, 2019, at https://websoilsurvey.sc.egov.usda.gov/App/WebSoilSurvey.aspx.

U.S. Geological Survey [USGS], 2017, 2015–2016 USGS Puerto Rico lidar: U.S. Geological Survey, accessed September 12, 2019, at ftp://rockyftp.cr.usgs.gov/vdelivery/Datasets/Staged/Elevation/OPR/PR_PuertoRico_2015/.

U.S. Geological Survey [USGS], 2019, NHD 20190815 for Puerto Rico State or territory Shapefile model version 2.2.1: U.S. Geological Survey web page, accessed September 12, 2019, at https://www.sciencebase.gov/catalog/item/5a96cdc6e4b06990606c4d7c.

Varnes, D.J., 1984, Landslide hazard zonation—A review of principles and practice: Paris, United Nations, Natural Hazards, no. 3, 63 p.

Vazquez Torres, J., 2013, Tremenda desgracia en Bayamón—Fotos y videos: Primera Hora, August 21, 2013, accessed September 12, 2019, at https://www.primerahora.com/noticias/policia-tribunales/nota/tremendadesgraciaenbayamon-fotosyvideos-947498/.

Wang, G., 2012, Kinematics of the Cerca del Cielo, Puerto Rico landslide derived from GPS observations: Landslides, v. 9, no. 1, p. 117–130. [Also available at https://doi.org/10.1007/s10346-011-0277-5.]

Wang, G., 2013, Millimeter-accuracy GPS landslide monitoring using Precise Point Positioning with Single Receiver Phase Ambiguity (PPP-SRPA) resolution—A case study in Puerto Rico: Journal of Geodetic Science, v. 3, no. 1, p. 22–31. [Also available at https://doi.org/10.2478/jogs-2013-0001.]

Wang, G., Joyce, J., Phillips, D., Shrestha, R., and Carter, W., 2013, Delineating and defining the boundaries of an active landslide in the rainforest of Puerto Rico using a combination of airborne and terrestrial lidar data: Landslides, v. 10, no. 4, p. 503–513. [Also available at https://doi.org/10.1007/s10346-013-0400-x.]

White, A.F., and Blum, A.E., 1995, Effects of climate on chemical weathering in watersheds: Geochimica et Cosmochimica Acta, v. 59, no. 9, p. 1729–1747. [Also available at https://doi.org/10.1016/0016-7037(95)00078-E.]

White, A.F., Blum, A.E., Schulz, M.S., Vivit, D.V., Stonestrom, D.A., Larsen, M., Murphy, S.F., and Eberl, D., 1998, Chemical weathering in a tropical watershed, Luquillo Mountains, Puerto Rico—I. Long-term versus short-term weathering fluxes: Geochimica et Cosmochimica Acta, v. 62, no. 2, p. 209–226. [Also available at https://doi.org/10.1016/S0016-7037(97)00335-9.]

Xu, C., Xu, X., Dai, F., and Saraf, A.K., 2012, Comparison of different models for susceptibility mapping of earthquake triggered landslides related with the 2008 Wenchuan earthquake in China: Computers & Geosciences, v. 46, p. 317–329. [Also available at https://doi.org/10.1016/j.cageo.2012.01.002.]

Zachariasen, J., and von Hillebrandt-Andrade, C.G., 2005, Holocene faulting of the Cero Goden fault, western Puerto Rico: National Earthquake Hazards Reduction Program, Final Technical Report, Grant Award Number 05HQGR0082, 27 p., accessed February 5, 2020, at https://earthquake.usgs.gov/cfusion/external_grants/reports/05HQGR0082.pdf.

Publishing support provided by the Science Publishing Network,
Denver Publishing Service Center
For more information concerning the research in this report, contact the
Center Director, USGS Geologic Hazards Science Center
Box 25046, Mail Stop 966
Denver, CO 80225
(303) 273-8579
Or visit Geologic Hazards Science Center website at
https://www.usgs.gov/centers/geohazards

Appendix 1. Key for Municipality Abbreviations

Abbreviation	Name	Abbreviation	Name	Abbreviation	Name
ADJ	Adjuntas	FLO	Florida	NAR	Naranjito
AGA	Aguada	GUA	Guánica	ORO	Orocovis
AGL	Aguadilla	GMA	Guayama	PAT	Patillas
AGB	Aguas Buenas	GNA	Guayanilla	PEN	Peñuelas
AIB	Aibonito	GYB	Guaynabo	PON	Ponce
ARE	Arecibo	GUR	Gurabo	QUE	Quebradillas
ARY	Arroyo	HAT	Hatillo	RIN	Rincón
ANA	Añasco	HOR	Hormigueros	RIO	Rio Grande
BAR	Barceloneta	HUM	Humacao	SAL	Salinas
BAQ	Barranquitas	ISA	Isabela	SAB	Sabana Grande
BAY	Bayamón	JAY	Jayuya	SGM	San Germán
CAG	Caguas	JDZ	Juana Díaz	SJU	San Juan
CBR	Cabo Rojo	JUN	Juncos	SLO	San Lorenzo
CAM	Camuy	LAJ	Lajas	SSB	San Sebastián
CAN	Canóvanas	LAR	Lares	SIB	Santa Isabel
CAR	Carolina	LMA	Las Marías	TAL	Toa Alta
CAT	Cataño	LPI	Las Piedras	TBA	Toa Baja
CAY	Cayey	LOI	Loíza	TRU	Trujillo Alto
CEI	Ceiba	LUQ	Luquillo	UTU	Utuado
CIA	Ciales	MAN	Manatí	VAL	Vega Alta
CID	Cidra	MAR	Maricao	VBA	Vega Baja
COA	Coamo	MAU	Maunabo	VIL	Villalba
COM	Comerío	MAY	Mayagüez	YAB	Yabucoa
COR	Corozal	MOC	Moca	YAU	Yauco
DOR	Dorado	MOR	Morovis		
FAJ	Fajardo	NAG	Naguabo		

Appendix 2. Results from Analyses of Land Cover

[km^2, square kilometer; %, percent; #, number; FR, frequency ratio; *SI*, Susceptibility Index]

VALUE	CLASS_NAME	Area (km^2)	Area (%)	Landslides (#)	Landslides (%)	FR	*SI*
43	Montane wet evergreen abandoned and active coffee plantation	548.9	0.063	13920	0.2598	4.12	1.42
39	Montane wet noncalcareous evergreen shrubland and woodland	241.1	0.0277	5831	0.1088	3.93	1.37
38	Young secondary montane wet noncalcareous evergreen forest	216.7	0.0249	4018	0.075	3.02	1.1
32	Montane wet alluvial shrubland and woodland	9	0.001	120	0.0022	2.17	0.77
30	Mature secondary montane wet alluvial evergreen forest	6.1	0.0007	80	0.0015	2.12	0.75
42	Wet serpentine shrubland and woodland	3.6	0.0004	42	0.0008	1.91	0.64
29	Lowland moist abandoned and active coffee plantations	110.8	0.0127	1269	0.0237	1.86	0.62
33	Mature secondary montane wet noncalcareous evergreen forest	252.3	0.029	2672	0.0499	1.72	0.54
31	Young secondary montane wet alluvial evergreen forest	9.9	0.0011	92	0.0017	1.51	0.41
36	Mature primary Sierra Palm and secondary montane wet noncalcareous evergreen forest	119.7	0.0137	869	0.0162	1.18	0.17
50	Moist grasslands and pastures	2184.6	0.2507	14547	0.2715	1.08	0.08
28	Lowland moist noncalcareous shrubland and woodland	438.6	0.0503	2850	0.0532	1.06	0.06
27	Young secondary lowland moist noncalcareous evergreen forest	530.5	0.0609	3077	0.0574	0.94	-0.06
40	Mature secondary montane wet serpentine evergreen forest	33.8	0.0039	198	0.0037	0.95	-0.05
26	Mature secondary lowland moist noncalcareous evergreen forest	378.5	0.0434	1671	0.0312	0.72	-0.33
41	Young secondary montane wet serpentine evergreen forest	6.5	0.0007	25	0.0005	0.62	-0.47
64	Low-density urban development	369.3	0.0424	990	0.0185	0.44	-0.83
22	Lowland moist alluvial shrubland and woodland	51.2	0.0059	123	0.0023	0.39	-0.94
65	Artificial barrens	85.8	0.0098	198	0.0037	0.38	-0.98
20	Mature secondary lowland moist alluvial evergreen forest	21.3	0.0024	49	0.0009	0.37	-0.98
37	Mature primary elfin woodland and secondary montane wet noncalcareous evergreen cloud forest	15.4	0.0018	34	0.0006	0.36	-1.02
21	Young secondary lowland moist alluvial evergreen forest	66.7	0.0077	137	0.0026	0.33	-1.1
34	Mature primary Tabonuco and secondary montane wet noncalcareous evergreen forest	87.3	0.01	177	0.0033	0.33	-1.11
35	Mature primary Palo Colorado and secondary montane wet noncalcareous evergreen forest	37.2	0.0043	49	0.0009	0.21	-1.54
16	Mature secondary dry and moist serpentine semideciduous forest	18.4	0.0021	22	0.0004	0.19	-1.64
24	Young secondary moist limestone evergreen and semideciduous forest	155	0.0178	136	0.0025	0.14	-1.95
17	Young secondary dry and moist serpentine semideciduous forest	19.6	0.0023	10	0.0002	0.08	-2.49
18	Dry and moist serpentine woodland and shrubland	8.4	0.001	4	0.0001	0.08	-2.56
25	Moist limestone shrubland and woodland	103.4	0.0119	58	0.0011	0.09	-2.39
7	Lowland dry limestone woodland and shrubland	50	0.0057	18	0.0003	0.06	-2.84
23	Mature secondary moist limestone evergreen and semideciduous forest	464.6	0.0533	130	0.0024	0.05	-3.09
6	Young secondary lowland dry limestone semideciduous forest	39.1	0.0045	8	0.0001	0.03	-3.4

VALUE	CLASS_NAME	Area (km^2)	Area (%)	Landslides (#)	Landslides (%)	FR	*SI*
15	Lowland dry noncalcareous shrubland and woodland	104.7	0.012	21	0.0004	0.03	-3.42
13	Mature secondary lowland dry noncalcareous semideciduous forest	21.6	0.0025	3	0.0001	0.02	-3.79
14	Young secondary lowland dry noncalcareous semideciduous forest	36.1	0.0041	3	0.0001	0.01	-4.3
59	Fine to coarse sandy beaches, mixed sand and gravel beaches	6.7	0.0008	1	0	0.02	-3.71
48	Dry grasslands and pastures	406.9	0.0467	36	0.0007	0.01	-4.24
3	Lowland dry alluvial shrubland and woodland	42.4	0.0049	5	0.0001	0.02	-3.95
66	Freshwater	44.2	0.0051	5	0.0001	0.02	-4
63	High-density urban development	522.8	0.06	38	0.0007	0.01	-4.44
53	Seasonally flooded herbaceous nonsaline wetlands	182.4	0.0209	15	0.0003	0.01	-4.31
55	Hay and row crops	257.9	0.0296	16	0.0003	0.01	-4.6
5	Mature secondary lowland dry limestone semideciduous forest	93.4	0.0107	6	0.0001	0.01	-4.56
1	Mature secondary lowland dry alluvial semideciduous forest	5.1	0.0006	0	0	0	-5
2	Young secondary lowland dry alluvial semideciduous forest	28.8	0.0033	0	0	0	-5
4	Mature secondary lowland dry limestone evergreen forest	8.8	0.001	0	0	0	-5
8	Lowland dry limestone shrubland	36.8	0.0042	0	0	0	-5
10	Coastal dwarf woodland and shrubland	0.1	0	0	0	0	-5
44	Mangrove forest and shrubland	76	0.0087	0	0	0	-5
45	Freshwater Pterocarpus swamp	2.6	0.0003	0	0	0	-5
46	Lowland dry riparian forest	6.9	0.0008	0	0	0	-5
47	Lowland dry riparian shrubland and woodland	4.2	0.0005	0	0	0	-5
49	Dry cactus grassland and shrubland	2.1	0.0002	0	0	0	-5
51	Emergent herbaceous nonsaline wetlands	11	0.0013	0	0	0	-5
52	Emergent herbaceous saline wetlands	8.8	0.001	0	0	0	-5
54	Seasonally flooded herbaceous saline wetlands	48.5	0.0056	0	0	0	-5
56	Woody agriculture and plantations: Palm plantations	4.9	0.0006	0	0	0	-5
57	Rocky cliffs and shelves	1.4	0.0002	0	0	0	-5
58	Gravel beaches and stony shoreline	0.3	0	0	0	0	-5
60	Riparian and other natural barrens	4.5	0.0005	0	0	0	-5
61	Salt and mudflats	12.4	0.0014	0	0	0	-5
62	Salt production	0.2	0	0	0	0	-5
67	Salt water	32.6	0.0037	0	0	0	-5
68	Lowland moist riparian forest	9.1	0.001	0	0	0	-5
69	Lowland moist riparian shrubland and woodland	5.1	0.0006	0	0	0	-5
70	Aquiculture	1	0.0001	0	0	0	-5

Appendix 3. Results from Analyses of Soil Class

[MUKEY, mapunit key; MUSYM, mapunit symbol; MUNAME, mapunit name; km^2, square kilometer; %, percent; #, number; FR, frequency ratio; *SI*, Susceptibility Index; >, greater than]

MUKEY	MUSYM	MUNAME	Area (km^2)	Area (%)	Landslides (#)	Landslides (%)	FR	SI
326463	PeF	Pellejas clay loam, 40 to 60 percent slopes	98.9	0.0114	8524	0.1591	14.01	2.64
326577	MrF2	Maricao clay, 20 to 60 percent slopes	3.8	0.0004	295	0.0055	12.65	2.54
326445	LcF2	Lirios clay loam, 40 to 60 percent slopes, eroded	59.1	0.0068	3802	0.071	10.47	2.35
326566	LuF2	Los Guineos clay, 20 to 60 percent slopes, eroded	6.9	0.0008	374	0.007	8.78	2.17
326444	LcE2	Lirios clay loam, 20 to 40 percent slopes, eroded	3	0.0003	146	0.0027	7.85	2.06
326536	CwF	Cuchillas silty clay loam, 20 to 60 percent slopes	0.4	0	16	0.0003	7.05	1.95
1386404	MkF	Maricao clay, 20 to 60 percent slopes	11.1	0.0013	452	0.0084	6.63	1.89
326414	CoF	Consejo clay, 40 to 60 percent slopes	9.1	0.001	361	0.0067	6.42	1.86
326702	PeF	Pellejas clay loam, 40 to 60 percent slopes	2.7	0.0003	105	0.002	6.3	1.84
326437	InE	Ingenio clay loam, 20 to 40 percent slopes	1.7	0.0002	66	0.0012	6.22	1.83
1379815	CvF	Cuchillas silty clay loam, 20 to 60 percent slopes	2.3	0.0003	85	0.0016	5.92	1.78
326574	MoF2	Maresua silty clay loam, 20 to 60 percent slopes, eroded	0	0	1	0	5.71	1.74
326416	CpF	Consumo clay, 40 to 60 percent slopes	11.7	0.0013	362	0.0068	5.04	1.62
326530	CoF2	Consumo clay, 40 to 60 percent slopes	157.6	0.0181	4863	0.0908	5.02	1.61
326550	HmF2	Humatas clay, 40 to 60 percent slopes	120	0.0138	3594	0.0671	4.87	1.58
1385065	HmF	Humatas clay, 40 to 60 percent slopes	6.4	0.0007	191	0.0036	4.84	1.58
326435	HmF	Humatas clay, 40 to 60 percent slopes	82.9	0.0095	2468	0.0461	4.84	1.58
326608	RsF2	Rosario clay, 40 to 60 percent slopes, eroded	0.1	0	3	0.0001	4.77	1.56
1379812	CsF	Consumo clay, 40 to 60 percent slopes	5.6	0.0006	161	0.003	4.64	1.54
326656	CuF	Consumo clay, 40 to 60 percent slopes	68.6	0.0079	1946	0.0363	4.61	1.53
1385087	AbF	Agueybana clay, 12 to 60 percent slopes	13.1	0.0015	351	0.0066	4.35	1.47
326591	MxF	Mucara clay, 40 to 60 percent slopes	20	0.0023	475	0.0089	3.87	1.35
326382	AdF2	Adjuntas clay, 40 to 60 percent slopes, eroded	7.2	0.0008	170	0.0032	3.82	1.34
326448	LgF	Los Guineos clay, 40 to 60 percent slopes	30.8	0.0035	666	0.0124	3.52	1.26
326839	PeF2	Pellejas clay loam, 40 to 60 percent slopes, eroded	3	0.0003	62	0.0012	3.37	1.21
326687	MoF	Maricao clay, 20 to 60 percent slopes	80.2	0.0092	1553	0.029	3.15	1.15
326401	CaF	Caguabo clay loam, 20 to 60 percent slopes	4.4	0.0005	82	0.0015	3.04	1.11
326830	MkF2	Maricao clay, 20 to 60 percent slopes	34	0.0039	615	0.0115	2.94	1.08
326587	MwF2	Morado clay loam, 40 to 60 percent slopes	26.7	0.0031	466	0.0087	2.84	1.04
326447	LgE	Los Guineos clay, 20 to 40 percent slopes	9.4	0.0011	156	0.0029	2.71	1
326449	MaF2	Maraguez silty clay loam, 40 to 60 percent slopes, eroded	24.5	0.0028	393	0.0073	2.61	0.96
326511	AoF2	Anones clay loam, 40 to 60 percent slopes, eroded	10.5	0.0012	166	0.0031	2.56	0.94
326812	HmF2	Humatas clay, 40 to 60 percent slopes	66.6	0.0076	1047	0.0195	2.56	0.94
326458	MuF	Mucara clay, 40 to 60 percent slopes	54.3	0.0062	816	0.0152	2.45	0.89
326415	CpE	Consumo clay, 20 to 40 percent slopes	0.6	0.0001	9	0.0002	2.42	0.88
326517	CbF	Caguabo clay loam, 20 to 60 percent slopes	51.1	0.0059	753	0.0141	2.4	0.87
326507	AdE2	Aibonito clay, 20 to 40 percent slopes, eroded	0.5	0.0001	7	0.0001	2.39	0.87
326701	PaF	Pandura sandy loam, 40 to 60 percent slopes	52.6	0.006	697	0.013	2.16	0.77
326413	CoE	Consejo clay, 20 to 40 percent slopes	0.7	0.0001	9	0.0002	2.08	0.73
328582	NOTCOM	No Digital Data Available	1.6	0.0002	20	0.0004	2.02	0.7

MUKEY	MUSYM	MUNAME	Area (km^2)	Area (%)	Landslides (#)	Landslides (%)	FR	SI
326392	AoF2	Alonso clay, 40 to 60 percent slopes, eroded	12	0.0014	149	0.0028	2.02	0.7
326600	QuF2	Quebrada silty clay, 40 to 60 percent slopes, eroded	1.1	0.0001	13	0.0002	1.99	0.69
326446	LgD	Los Guineos clay, 12 to 20 percent slopes	3.4	0.0004	40	0.0007	1.91	0.65
326436	InD	Ingenio clay loam, 5 to 20 percent slopes	8.5	0.001	99	0.0018	1.91	0.64
326599	QuE2	Quebrada silty clay, 20 to 40 percent slopes, eroded	2.3	0.0003	27	0.0005	1.9	0.64
326668	HtF	Humatas clay, 40 to 60 percent slopes	83.8	0.0096	965	0.018	1.87	0.63
326549	HmE2	Humatas clay, 20 to 40 percent slopes	76.9	0.0088	865	0.0161	1.83	0.6
326825	LuF	Los Guineos clay, 40 to 60 percent slopes	20.4	0.0023	229	0.0043	1.83	0.6
326821	LmF2	Lirios clay loam, 40 to 60 percent slopes, eroded	2.3	0.0003	26	0.0005	1.8	0.59
326824	LuE	Los Guineos clay, 20 to 40 percent slopes	7.8	0.0009	85	0.0016	1.77	0.57
326789	AaF2	Adjuntas clay, 40 to 60 percent slopes, eroded	1.8	0.0002	19	0.0004	1.74	0.55
1887168	RuG	Rubias-Chiquito complex, 60 to 90 percent slopes	0.1	0	1	0	1.73	0.55
326698	NaF	Naranjito silty clay loam, 40 to 60 percent slopes	109.5	0.0126	1155	0.0216	1.72	0.54
326708	RpF2	Rio Piedras clay, 40 to 60 percent slopes, eroded	4.9	0.0006	51	0.001	1.7	0.53
326529	CoE	Consumo clay, 20 to 40 percent slopes	83.2	0.0096	869	0.0162	1.7	0.53
326502	VoE2	Voladora clay, 20 to 40 percent slopes, eroded	4.2	0.0005	43	0.0008	1.68	0.52
1884759	AlF	Aljibe-Guama-Indiera complex, 20 to 60 percent slopes	0.3	0	3	0.0001	1.66	0.51
326434	HmE	Humatas clay, 20 to 40 percent slopes	10.1	0.0012	102	0.0019	1.65	0.5
326422	CvF	Cuchillas-Rock outcrop complex, 40 to 60 percent slopes	5.2	0.0006	50	0.0009	1.56	0.45
326667	HtE	Humatas clay, 20 to 40 percent slopes	87.5	0.01	801	0.015	1.49	0.4
326811	HmE2	Humatas clay, 20 to 40 percent slopes	15.5	0.0018	139	0.0026	1.46	0.38
326538	DaE2	Daguey clay, 20 to 40 percent slopes, eroded	15	0.0017	129	0.0024	1.4	0.34
1386662	EcG	El Cacique-La Taina complex, 60 to 90 percent slopes	9.4	0.0011	79	0.0015	1.36	0.31
326802	CuF2	Consumo clay, 40 to 60 percent slopes	4.7	0.0005	39	0.0007	1.35	0.3
1884723	EdF	El Descanso-Hoconuco complex, 20 to 60 percent slopes	2.4	0.0003	20	0.0004	1.33	0.28
326895	HuF	Humatas-Stony land complex, 40 to 60 percent slopes	7.1	0.0008	58	0.0011	1.33	0.28
326616	So	Serpentinite outcrop	18.5	0.0021	148	0.0028	1.3	0.27
326677	LmE	Limones clay, 20 to 40 percent slopes	1.6	0.0002	13	0.0002	1.3	0.26
1379811	CsE	Consumo clay, 20 to 40 percent slopes	7.5	0.0009	58	0.0011	1.26	0.23
326639	AbE	Aibonito clay, 20 to 40 percent slopes	2.7	0.0003	21	0.0004	1.25	0.22
326421	CuF	Cuchillas silty clay loam, 40 to 60 percent slopes	2.7	0.0003	20	0.0004	1.22	0.2
326565	LuD	Los Guineos clay, 12 to 20 percent slopes	0.4	0	3	0.0001	1.2	0.18
326695	MxF	Mucara clay, 40 to 60 percent slopes	298.9	0.0343	2154	0.0402	1.17	0.16
326634	VoE2	Voladora silty clay, 20 to 40 percent slopes, eroded	14.8	0.0017	106	0.002	1.16	0.15
326658	DaC	Daguey clay, 2 to 12 percent slopes	0.4	0	3	0.0001	1.16	0.15
326837	MuF2	Mucara silty clay, 40 to 60 percent slopes, eroded	108.3	0.0124	769	0.0144	1.16	0.14
326655	CuE	Consumo clay, 20 to 40 percent slopes	8	0.0009	54	0.001	1.1	0.1
326692	MuF2	Morado clay loam, 40 to 60 percent slopes	10.5	0.0012	71	0.0013	1.1	0.1
326546	GoC	Guanajibo loam, 2 to 12 percent slopes	0.6	0.0001	4	0.0001	1.1	0.1
326450	McF	Maricao clay, 20 to 60 percent slopes	3.6	0.0004	24	0.0004	1.09	0.08
326456	MpF2	Morado clay loam, 40 to 60 percent slopes	33.1	0.0038	219	0.0041	1.07	0.07
1907042	EdG	El Descanso-Hoconuco complex, 60 to 90 percent slopes	1.5	0.0002	10	0.0002	1.07	0.06
2706232	SoE	Sonadora-Caguabo complex, 20 to 40 percent slopes	0.8	0.0001	5	0.0001	1.05	0.05
326391	AoE2	Alonso clay, 20 to 40 percent slopes, eroded	4.1	0.0005	26	0.0005	1.04	0.04

MUKEY	MUSYM	MUNAME	Area (km^2)	Area (%)	Landslides (#)	Landslides (%)	FR	SI
1379816	CvG	Cuchillas silty clay loam, 60 to 90 percent slopes	0.5	0.0001	3	0.0001	1.03	0.03
326681	LsF	Los Guineos clay, 40 to 60 percent slopes	53.8	0.0062	338	0.0063	1.02	0.02
326697	NaE	Naranjito silty clay loam, 20 to 40 percent slopes	24	0.0027	150	0.0028	1.02	0.02
326510	AoE2	Anones clay loam, 20 to 40 percent slopes, eroded	9.6	0.0011	60	0.0011	1.02	0.02
2706238	YqE	Yunque-Los Guineos-Moteado complex, 5 to 40 percent slopes	0.5	0.0001	3	0.0001	0.99	-0.01
326455	MoE2	Moca clay, 20 to 40 percent slopes, eroded	1.7	0.0002	10	0.0002	0.98	-0.02
326500	VoC2	Voladora clay, 5 to 12 percent slopes, eroded	3	0.0003	18	0.0003	0.97	-0.03
326442	JuE2	Juncal clay, 20 to 40 percent slopes, eroded	0.7	0.0001	4	0.0001	0.95	-0.05
1356080	CbF	Caguabo clay loam, 20 to 60 percent slopes	49.9	0.0057	291	0.0054	0.95	-0.05
326390	AoD2	Alonso clay, 12 to 20 percent slopes, eroded	0.7	0.0001	4	0.0001	0.95	-0.05
1386546	QbF	Quebrada clay loam, 40 to 60 percent slopes	14.2	0.0016	81	0.0015	0.93	-0.07
326829	MeF2	Maraguez silty clay loam, 40 to 60 percent slopes, eroded	23.1	0.0027	128	0.0024	0.9	-0.11
326548	HmD	Humatas clay, 12 to 20 percent slopes	15.6	0.0018	86	0.0016	0.9	-0.11
1887167	RuF	Rubias-Chiquito complex, 40 to 60 percent slopes	8.8	0.001	48	0.0009	0.89	-0.12
2706236	HmE	Humatas-Zarzal complex, 5 to 40 percent slopes	11.5	0.0013	62	0.0012	0.88	-0.13
326680	LsE	Los Guineos clay, 20 to 40 percent slopes	12.7	0.0015	68	0.0013	0.87	-0.14
326937	Ru	Rough stony land	0.4	0	2	0	0.86	-0.15
326596	PlE2	Plata clay, 20 to 40 percent slopes, eroded	8	0.0009	42	0.0008	0.85	-0.16
326889	GuE2	Guayabota silty clay loam, 20 to 40 slopes, eroded	2.1	0.0002	11	0.0002	0.85	-0.17
326524	ClE	Colinas clay loam, 20 to 40 percent slopes	31.7	0.0036	164	0.0031	0.84	-0.17
2706233	SoG	Sonadora-Caguabo complex, 40 to 90 percent slopes	4.1	0.0005	21	0.0004	0.84	-0.18
326796	CdF	Caguabo-Rock land complex, 20 to 60 percent slopes	31.9	0.0037	161	0.003	0.82	-0.2
326793	AnE2	Alonso clay, 20 to 40 percent slopes, eroded	4	0.0005	20	0.0004	0.82	-0.2
326826	LyFX	Los Guineos-Maricao association, steep	26.6	0.003	133	0.0025	0.81	-0.21
2553832	CaD	Caguabo gravelly clay loam, 12 to 20 percent slopes	0.6	0.0001	3	0.0001	0.8	-0.22
326679	LoF2	Lirios silty clay loam, 20 to 60 percent slopes, eroded	17.9	0.002	86	0.0016	0.78	-0.24
1385063	HmE	Humatas clay, 20 to 40 percent slopes	5.7	0.0007	27	0.0005	0.77	-0.26
326402	CbF	Caguabo-Rock outcrop complex, 20 to 60 percent slopes	8.5	0.001	40	0.0007	0.76	-0.27
2706239	YuF	Yunque-Moteado complex, 20 to 60 percent slopes	0.4	0	2	0	0.76	-0.28
2553845	PcE	Picacho-Ciales complex, 5 to 40 percent slopes	4.8	0.0006	22	0.0004	0.75	-0.29
326527	CmE	Colinas cobbly clay loam, 20 to 40 percent slopes	10.1	0.0012	46	0.0009	0.74	-0.3
326678	LmF	Limones clay, 40 to 60 percent slopes	1.1	0.0001	5	0.0001	0.71	-0.34
2706242	ZcF	Zarzal-Cristal complex, 20 to 60 percent slopes	5.8	0.0007	25	0.0005	0.7	-0.35
326423	DaD2	Daguey clay, 12 to 20 percent slopes, eroded	5.1	0.0006	22	0.0004	0.7	-0.35
326726	VkC2	Via clay loam, 5 to 12 percent slopes, eroded	1.9	0.0002	8	0.0001	0.7	-0.36
326601	Re	Reilly gravelly loam	4.2	0.0005	18	0.0003	0.7	-0.36
326805	DaD	Daguey clay, 12 to 20 percent slopes	2.8	0.0003	12	0.0002	0.7	-0.36
326501	VoD2	Voladora clay, 12 to 20 percent slopes, eroded	0.7	0.0001	3	0.0001	0.69	-0.37
326894	HtF2	Humatas clay, 40 to 60 percent slopes	20.4	0.0023	86	0.0016	0.69	-0.38
326470	Rm	Riverwash	2.6	0.0003	11	0.0002	0.69	-0.38
326638	AbD	Aibonito clay, 12 to 20 percent slopes	1	0.0001	4	0.0001	0.68	-0.38
326590	MxE	Mucara clay, 20 to 40 percent slopes	9.6	0.0011	40	0.0007	0.67	-0.39
326794	AnF2	Alonso clay, 40 to 60 percent slopes, eroded	8	0.0009	33	0.0006	0.67	-0.4
326525	ClF2	Colinas clay loam, 20 to 60 percent slopes, eroded	4	0.0005	16	0.0003	0.66	-0.42

MUKEY	MUSYM	MUNAME	Area (km^2)	Area (%)	Landslides (#)	Landslides (%)	FR	SI
1386421	MuF	Mucara loam, 40 to 60 percent slopes	14.7	0.0017	59	0.0011	0.65	-0.42
326653	CrF2	Colinas clay loam, 40 to 60 percent slopes, eroded	3.2	0.0004	13	0.0002	0.65	-0.42
326645	CaF	Caguabo clay loam, 40 to 60 percent slopes	218.5	0.0251	877	0.0164	0.65	-0.43
2706234	CzE	Cristal-Zarzal complex, 5 to 40 percent slopes	2.8	0.0003	11	0.0002	0.64	-0.45
326843	Re	Reilly gravelly loam	4.3	0.0005	17	0.0003	0.64	-0.45
326597	PlF2	Plata clay, 40 to 60 percent slopes, eroded	1	0.0001	4	0.0001	0.63	-0.47
1884632	CjD	Cerro Gordo mucky peat, 2 to 20 percent slopes	1.1	0.0001	4	0.0001	0.6	-0.51
326923	PaF2	Pandura loam, 40 to 60 percent slopes, eroded	126.5	0.0145	462	0.0086	0.59	-0.52
326589	MxD	Mucara clay, 12 to 20 percent slopes	1.1	0.0001	4	0.0001	0.59	-0.53
326659	DaD	Daguey clay, 12 to 20 percent slopes	24.2	0.0028	86	0.0016	0.58	-0.55
326646	CbF	Caguabo-Rock outcrop complex, 40 to 60 percent slopes	9.3	0.0011	33	0.0006	0.57	-0.55
326907	LsF	Los Guineos clay, 40 to 60 percent slopes	46.5	0.0053	164	0.0031	0.57	-0.56
326443	LME	Los Guineos-Maricao-Rock outcrop association, steep	19	0.0022	65	0.0012	0.56	-0.58
326700	PaE	Pandura sandy loam, 20 to 40 percent slopes	12.8	0.0015	43	0.0008	0.54	-0.61
326691	MtC	Montegrande clay, 5 to 12 percent slopes	1.6	0.0002	5	0.0001	0.52	-0.65
326569	McF2	Malaya clay, 20 to 60 percent slopes, eroded	47.1	0.0054	150	0.0028	0.52	-0.66
2553834	SoE	Sonadora-Caguabo complex, 20 to 40 percent slopes	1.3	0.0001	4	0.0001	0.51	-0.68
326669	HuF	Humatas-Rock outcrop complex, 20 to 60 percent slopes	3.9	0.0004	12	0.0002	0.51	-0.68
2706231	CaD	Caguabo gravelly clay loam, 12 to 20 percent slopes	0.3	0	1	0	0.5	-0.7
2553844	PiG	Picacho-Utuado complex, 40 to 90 percent slopes	4.7	0.0005	14	0.0003	0.49	-0.72
326635	VrC2	Voladora clay, 5 to 12 percent slopes, eroded	1	0.0001	3	0.0001	0.49	-0.72
1386415	MrF	Morado clay loam, 40 to 60 percent slopes	4	0.0005	12	0.0002	0.48	-0.73
326499	Vm	Vivi loam	11.8	0.0014	35	0.0007	0.48	-0.73
326921	NaF	Naranjito silty clay loam, 40 to 60 percent slopes	23.2	0.0027	67	0.0013	0.47	-0.76
326543	Du	Dique silt loam	2.1	0.0002	6	0.0001	0.47	-0.76
326906	LsE	Los Guineos clay, 20 to 40 percent slopes	9	0.001	25	0.0005	0.45	-0.79
1386397	McF	Malaya clay, 20 to 60 percent slopes	19.1	0.0022	53	0.001	0.45	-0.8
1386551	RoF	Rosario silty clay, 40 to 60 percent slopes	4.3	0.0005	12	0.0002	0.45	-0.8
326606	RsD2	Rosario clay, 12 to 20 percent slopes, eroded	1.1	0.0001	3	0.0001	0.44	-0.81
326836	MuE2	Mucara silty clay, 20 to 40 percent slopes, eroded	8.2	0.0009	22	0.0004	0.44	-0.82
326904	LrE2	Lirios silty clay loam, 20 to 40 percent slopes, eroded	5.2	0.0006	14	0.0003	0.44	-0.83
326633	VoD2	Voladora silty clay, 12 to 20 percent slopes, eroded	6.8	0.0008	18	0.0003	0.43	-0.84
326924	PdF	Pandura-Very stony land complex, 40 to 60 percent slopes	41	0.0047	106	0.002	0.42	-0.87
326651	CrD2	Colinas clay loam, 12 to 20 percent slopes, eroded	6.2	0.0007	16	0.0003	0.42	-0.87
326842	QeF2	Quebrada silty clay loam, 40 to 60 percent slopes, eroded	55.6	0.0064	141	0.0026	0.41	-0.89
326709	SaF	Sabana silty clay loam, 40 to 60 percent slopes	3.2	0.0004	8	0.0001	0.41	-0.89
326795	CbF2	Caguabo gravelly clay loam, 20 to 60 percent slopes, eroded	88.4	0.0101	222	0.0041	0.41	-0.9
326844	Rw	Riverwash	0.8	0.0001	2	0	0.4	-0.91
1386556	SmE	Santa Marta gravelly clay loam, 20 to 40 percent slopes	1.2	0.0001	3	0.0001	0.4	-0.92
326694	MxE	Mucara clay, 20 to 40 percent slopes	71.5	0.0082	168	0.0031	0.38	-0.96
326417	CrC	Corozal clay, 5 to 12 percent slopes	2.6	0.0003	6	0.0001	0.38	-0.96
326863	CbF	Caguabo clay loam, 20 to 60 percent slopes	128.6	0.0148	297	0.0055	0.38	-0.98
326905	LsD	Los Guineos clay, 12 to 20 percent slopes	0.9	0.0001	2	0	0.37	-1
2706237	PrF	Prieto very cobbly clay loam, 20 to 60 percent slopes	0.5	0.0001	1	0	0.36	-1.03

MUKEY	MUSYM	MUNAME	Area (km^2)	Area (%)	Landslides (#)	Landslides (%)	FR	SI
2553846	PiE	Picacho-Utuado complex, 5 to 40 percent slopes	5.1	0.0006	11	0.0002	0.35	-1.04
326612	SdF2	San Sebastian gravelly clay, 20 to 60 percent slopes, eroded	26.7	0.0031	56	0.001	0.34	-1.08
2706240	PaG	Palm-Yunque complex, 40 to 90 percent slopes, extremelly stony	0.5	0.0001	1	0	0.34	-1.08
730211	GPQ	Gravel, pits and quarries	0.5	0.0001	1	0	0.34	-1.08
326878	DcE2	Daguao clay, 20 to 40 percent slopes, eroded	3.9	0.0004	8	0.0001	0.34	-1.09
326834	MtF2	Morado clay loam, 40 to 60 percent slopes	37.9	0.0043	78	0.0015	0.33	-1.09
326713	SoF	Soller clay loam, 40 to 60 percent slopes	14.6	0.0017	30	0.0006	0.33	-1.1
326899	JgE2	Jagueyes loam, 20 to 40 percent slopes, eroded	4	0.0005	8	0.0001	0.33	-1.12
1386661	EcF	El Cacique-La Taina complex, 20 to 60 percent slopes	46.6	0.0054	93	0.0017	0.32	-1.13
326583	MuE3	Moca clay, 20 to 40 percent slopes, severely eroded	1	0.0001	2	0	0.32	-1.14
326537	DaD2	Daguey clay, 12 to 20 percent slopes, eroded	6.2	0.0007	12	0.0002	0.32	-1.15
326648	ClC	Catalina clay, 4 to 12 percent slopes	1	0.0001	2	0	0.32	-1.15
326920	NaE	Naranjito silty clay loam, 20 to 40 percent slopes	24.1	0.0028	45	0.0008	0.3	-1.19
326441	JuD2	Juncal clay, 12 to 20 percent slopes, eroded	9.1	0.001	17	0.0003	0.3	-1.19
326939	SaF2	Sabana silty clay loam, 40 to 60 percent slopes, eroded	27.6	0.0032	51	0.001	0.3	-1.2
2706235	ZaG	Zarzal very cobbly clay, 40 to 90 percent slopes	3.3	0.0004	6	0.0001	0.29	-1.22
326637	AaC	Aceitunas clay, 5 to 12 percent slopes	18.8	0.0022	32	0.0006	0.28	-1.28
326484	SpF	Soller cobbly clay, 20 to 60 percent slopes	2.4	0.0003	4	0.0001	0.28	-1.29
326607	RsE2	Rosario clay, 20 to 40 percent slopes, eroded	0.6	0.0001	1	0	0.27	-1.3
326720	Um	Urban land-Mucara complex	16.1	0.0018	27	0.0005	0.27	-1.3
326686	MlF	Malaya clay loam, 40 to 60 percent slopes	2.5	0.0003	4	0.0001	0.26	-1.33
326644	CaE	Caguabo clay loam, 20 to 40 percent slopes	11.9	0.0014	19	0.0004	0.26	-1.35
326581	MuD2	Moca clay, 12 to 20 percent slopes, eroded	4.4	0.0005	7	0.0001	0.26	-1.35
326896	InE2	Ingenio silty clay loam, 20 to 40 percent slopes, eroded	5.7	0.0007	9	0.0002	0.26	-1.36
326919	MuE2	Mucara silty clay loam, 20 to 40 percent slopes, eroded	61.9	0.0071	96	0.0018	0.25	-1.38
326593	NcD2	Nipe clay, 5 to 20 percent slopes, eroded	2.6	0.0003	4	0.0001	0.25	-1.39
2553838	HmE	Humatas-Zarzal complex, 5 to 40 percent slopes	7.8	0.0009	12	0.0002	0.25	-1.39
326647	Ce	Candelero loam	2.6	0.0003	4	0.0001	0.25	-1.4
326902	LeE2	Limones silty clay, 20 to 40 percent slopes, eroded	7.3	0.0008	11	0.0002	0.25	-1.4
326619	SsD2	Soller cobbly clay, 5 to 20 percent slopes, eroded	2.7	0.0003	4	0.0001	0.24	-1.41
326567	MaB	Mabi clay, 2 to 5 percent slopes	0.7	0.0001	1	0	0.24	-1.41
326467	Pt	Pits, sand	2.7	0.0003	4	0.0001	0.24	-1.43
326699	PaD	Pandura sandy loam, 12 to 20 percent slopes	6.1	0.0007	9	0.0002	0.24	-1.43
326410	ClF2	Colinas clay loam, 40 to 60 percent slopes, eroded	24.8	0.0028	35	0.0007	0.23	-1.47
1386412	MrE	Morado clay loam, 20 to 40 percent slopes	3	0.0003	4	0.0001	0.22	-1.52
2553836	CzE	Cristal-Zarzal complex, 5 to 40 percent slopes	9.1	0.001	12	0.0002	0.22	-1.53
336722	GPQ	Canteras and Graveros	1.5	0.0002	2	0	0.21	-1.54
2553833	GuF	Guayabota-Yunque complex, 20 to 60 percent slopes	0.8	0.0001	1	0	0.21	-1.56
326631	ToA	Toa silty clay loam, 0 to 2 percent slopes, occasionally flooded	12.5	0.0014	16	0.0003	0.21	-1.57
326660	DeF	Descalabrado clay loam, 40 to 60 percent slopes	6.4	0.0007	8	0.0001	0.2	-1.59
1384368	LpG	Los Penones-Limestone outcrop complex, 60 to 90 percent slopes	0.8	0.0001	1	0	0.2	-1.6
326657	CzC	Corozal clay, 5 to 12 percent slopes	0.9	0.0001	1	0	0.19	-1.67
326849	To	Toa silty clay loam, 0 to 2 percent slopes, occasionally flooded	5.2	0.0006	6	0.0001	0.19	-1.68
1386545	QbE	Quebrada clay loam, 20 to 40 percent slopes	3.6	0.0004	4	0.0001	0.18	-1.71

MUKEY	MUSYM	MUNAME	Area (km^2)	Area (%)	Landslides (#)	Landslides (%)	FR	SI
1407041	MfF	Maresua gravelly clay loam, 20 to 60 percent slopes	2.7	0.0003	3	0.0001	0.18	-1.71
326714	TaF	Tanama-Rock outcrop complex, 20 to 60 percent slopes	26.3	0.003	29	0.0005	0.18	-1.72
2553843	PaG	Palm-Yunque complex, 40 to 90 percent slopes, extremelly stony	8.4	0.001	9	0.0002	0.17	-1.75
326604	RpD2	Rio Piedras clay, 12 to 20 percent slopes, eroded	4.7	0.0005	5	0.0001	0.17	-1.75
326556	JuD2	Juncal clay, 12 to 20 percent slopes, eroded	3.9	0.0004	4	0.0001	0.17	-1.79
326627	TcC2	Tanama clay, 5 to 12 percent slopes, eroded	3	0.0003	3	0.0001	0.16	-1.82
326705	RoC2	Rio Arriba clay, 5 to 12 percent slopes, eroded	12.1	0.0014	12	0.0002	0.16	-1.83
326454	MoD2	Moca clay, 12 to 20 percent slopes, eroded	10.1	0.0012	10	0.0002	0.16	-1.83
1386420	MuE	Mucara loam, 20 to 40 percent slopes	33.5	0.0038	33	0.0006	0.16	-1.83
326489	TaD2	Tanama clay, 12 to 20 percent slopes, eroded	7.2	0.0008	7	0.0001	0.16	-1.84
326650	Co	Cayagua sandy loam	8.2	0.0009	8	0.0001	0.16	-1.85
326521	CfC2	Cidral clay, 2 to 12 percent slopes, eroded	6.2	0.0007	6	0.0001	0.16	-1.85
326893	HtE2	Humatas clay, 20 to 40 percent slopes	16.5	0.0019	16	0.0003	0.16	-1.85
326595	PeD2	Perchas clay, 12 to 20 percent slopes, eroded	11.5	0.0013	11	0.0002	0.16	-1.86
326665	GuF	Guayama clay loam, 20 to 60 percent slopes	1	0.0001	1	0	0.16	-1.86
326730	YeF	Yunes silty clay loam, 40 to 60 percent slopes	4.2	0.0005	4	0.0001	0.16	-1.86
326558	LaD2	Lares clay, 5 to 20 percent slopes, eroded	5.5	0.0006	5	0.0001	0.15	-1.91
326799	CoF2	Callabo silty clay loam, 40 to 60 percent slopes eroded	114.7	0.0132	103	0.0019	0.15	-1.92
326922	PaE2	Pandura loam, 12 to 40 percent slopes, eroded	61.1	0.007	53	0.001	0.14	-1.96
326835	MuD2	Mucara silty clay, 12 to 20 percent slopes, eroded	2.3	0.0003	2	0	0.14	-1.97
326790	AgD	Aguilita gravelly clay loam, 12 to 20 percent slopes	3.5	0.0004	3	0.0001	0.14	-1.98
326652	CrE2	Colinas clay loam, 20 to 40 percent slopes, eroded	14.1	0.0016	12	0.0002	0.14	-1.98
326853	AcC	Aceitunas silty clay loam, 5 to 12 percent slopes	11.9	0.0014	10	0.0002	0.14	-1.99
326477	SgF	San German gravelly clay loam, 20 to 60 percent slopes	10.9	0.0013	9	0.0002	0.13	-2.01
2553847	IcA	Icacos loam, occasionally flooded	1.2	0.0001	1	0	0.13	-2.01
326429	EcC	Espinosa clay, 5 to 12 percent slopes	6.1	0.0007	5	0.0001	0.13	-2.02
1386544	QbD	Quebrada clay loam, 12 to 20 percent slopes	1.2	0.0001	1	0	0.13	-2.03
326810	GoF	Guanabano clay, 40 to 60 percent slopes	3.8	0.0004	3	0.0001	0.13	-2.05
326460	NaE	Naranjo clay, 20 to 40 percent slopes	6.4	0.0007	5	0.0001	0.13	-2.06
326486	TP	Tropopsamments	1.3	0.0002	1	0	0.12	-2.1
326468	Re	Reilly gravelly silt loam	5.4	0.0006	4	0.0001	0.12	-2.11
326592	NaD	Naranjo clay, 12 to 20 percent slopes	5.4	0.0006	4	0.0001	0.12	-2.12
326494	VaC2	Vega Alta sandy clay loam, 5 to 12 percent slopes, eroded	2.8	0.0003	2	0	0.12	-2.14
326791	AgF	Aguilita gravelly clay loam, 20 to 60 percent slopes	57.6	0.0066	40	0.0007	0.11	-2.18
1386550	RoE	Rosario silty clay, 20 to 40 percent slopes	1.5	0.0002	1	0	0.11	-2.24
2553837	ZaG	Zarzal very cobbly clay, 40 to 90 percent slopes	10.7	0.0012	7	0.0001	0.11	-2.24
326641	AmC	Almirante clay, 5 to 12 percent slopes	4.6	0.0005	3	0.0001	0.11	-2.25
679205	LeF	La Tea-Limestone outcrop complex, 20 to 60 percent slopes	4.6	0.0005	3	0.0001	0.11	-2.25
334735	SdF	San German cobbly clay loam, 20 to 60 percent slopes	3.1	0.0004	2	0	0.1	-2.26
326806	EnC	Ensenada gravelly clay, 2 to 12 percent slopes	1.6	0.0002	1	0	0.1	-2.28
2553848	ZcF	Zarzal-Cristal complex, 20 to 60 percent slopes	26.1	0.003	16	0.0003	0.1	-2.31
326696	NaD2	Naranjito silty clay loam, 12 to 20 percent slopes, eroded	4.9	0.0006	3	0.0001	0.1	-2.31
2553842	YuF	Yunque-Moteado complex, 20 to 60 percent slopes	11.5	0.0013	7	0.0001	0.1	-2.32
326951	VeC	Vega Alta silty clay loam, 5 to 12 percent slopes	3.4	0.0004	2	0	0.1	-2.34

MUKEY	MUSYM	MUNAME	Area (km^2)	Area (%)	Landslides (#)	Landslides (%)	FR	SI
1385059	HmD	Humatas clay, 12 to 20 percent slopes	3.4	0.0004	2	0	0.1	-2.34
326461	NaF	Naranjo clay, 40 to 60 percent slopes	1.7	0.0002	1	0	0.1	-2.34
326818	JzD	Juana Diaz clay loam, 12 to 20 percent slopes	1.7	0.0002	1	0	0.1	-2.35
326568	MaC2	Mabi clay, 5 to 12 percent slopes, eroded	3.4	0.0004	2	0	0.09	-2.35
326928	PmE2	Patillas clay loam, 20 to 40 percent slopes, eroded	10.6	0.0012	6	0.0001	0.09	-2.39
326881	DgF2	Descalabrado and Guayama soils, 20 to 60 percent slopes, eroded	36.1	0.0041	20	0.0004	0.09	-2.41
326729	YeE	Yunes silty clay loam, 20 to 40 percent slopes	1.8	0.0002	1	0	0.09	-2.41
2553841	YnG	Yunque cobbly clay,40 to 90 percent slopes, extremely stony	7.4	0.0009	4	0.0001	0.09	-2.43
326961	YuF2	Yunes silty clay loam, 20 to 60 percent slopes, eroded	11.2	0.0013	6	0.0001	0.09	-2.44
326483	SpD	Soller cobbly clay, 12 to 20 percent slopes	5.7	0.0006	3	0.0001	0.09	-2.45
326724	VaC2	Vega Alta clay, 2 to 5 percent slopes	7.6	0.0009	4	0.0001	0.09	-2.46
1386406	MkG	Maricao clay, 60 to 90 percent slopes	1.9	0.0002	1	0	0.08	-2.47
1386422	NpD	Nipe clay, 5 to 20 percent slopes	5.8	0.0007	3	0.0001	0.08	-2.47
326471	Ro	Rock outcrop, limestone	1.9	0.0002	1	0	0.08	-2.47
326383	AgC	Algarrobo fine sand, 2 to 12 percent slopes	8	0.0009	4	0.0001	0.08	-2.51
326466	Ps	Pits, gravel	2	0.0002	1	0	0.08	-2.51
326618	SrE	Soller-Limestone rockland complex, 20 to 40 percent slopes	43.6	0.005	21	0.0004	0.08	-2.55
326427	EbC	Espinosa sandy clay loam, 5 to 12 percent slopes	2.1	0.0002	1	0	0.08	-2.55
326936	Rs	Rock land	46.6	0.0054	22	0.0004	0.08	-2.57
326509	AoD	Anones clay loam, 12 to 20 percent slopes	2.1	0.0002	1	0	0.08	-2.57
326942	TeE	Teja gravelly sandy loam, 12 to 40 percent slopes	30.4	0.0035	14	0.0003	0.07	-2.59
326632	Ts	Toa silty clay	2.2	0.0003	1	0	0.07	-2.6
326603	RpC2	Rio Piedras clay, 5 to 12 percent slopes, eroded	2.3	0.0003	1	0	0.07	-2.63
326832	MsC	Montegrande clay, 2 to 12 percent slopes	11.5	0.0013	5	0.0001	0.07	-2.65
326684	MaC	Mabi clay, 5 to 12 percent slopes	11.7	0.0013	5	0.0001	0.07	-2.67
326693	MxD	Mucara clay, 12 to 20 percent slopes	12	0.0014	5	0.0001	0.07	-2.69
326428	EcB	Espinosa clay, 2 to 5 percent slopes	14.5	0.0017	6	0.0001	0.07	-2.7
326488	TaC2	Tanama clay, 5 to 12 percent slopes, eroded	7.4	0.0008	3	0.0001	0.07	-2.72
326480	SoC	Soller clay, 5 to 12 percent slopes	2.5	0.0003	1	0	0.07	-2.72
326523	ClD	Colinas clay loam, 12 to 20 percent slopes	5.1	0.0006	2	0	0.06	-2.74
326562	Lm	Leveled sandy land	2.6	0.0003	1	0	0.06	-2.76
1385084	LkB	Lares clay, 0 to 5 percent slopes	2.6	0.0003	1	0	0.06	-2.76
326399	ByB	Bayamon clay, 2 to 5 percent slopes	38.9	0.0045	15	0.0003	0.06	-2.77
326873	Cn	Cobbly alluvial land	13	0.0015	5	0.0001	0.06	-2.77
326411	CmF2	Colinas cobbly clay loam, 20 to 60 percent slopes, eroded	31.3	0.0036	12	0.0002	0.06	-2.78
326676	LaC2	Lares clay, 5 to 12 percent slopes, eroded	7.9	0.0009	3	0.0001	0.06	-2.78
2553840	YqE	Yunque-Los Guineos-Moteado complex, 5 to 40 percent slopes	7.9	0.0009	3	0.0001	0.06	-2.79
326491	To	Toa silty clay loam, 0 to 2 percent slopes, occasionally flooded	26.8	0.0031	10	0.0002	0.06	-2.8
326703	Re	Reilly sandy loam	2.7	0.0003	1	0	0.06	-2.81
326869	CgD2	Cayagua sandy loam, 12 to 20 percent slopes, eroded	5.4	0.0006	2	0	0.06	-2.81
326563	Lo	Limestone outcrop	115.9	0.0133	42	0.0008	0.06	-2.83
326664	Es	Estacion silty clay loam	8.4	0.001	3	0.0001	0.06	-2.84
326712	SoE	Soller clay loam, 20 to 40 percent slopes	2.8	0.0003	1	0	0.06	-2.85
326868	CgC2	Cayagua sandy loam, 5 to 12 percent slopes, eroded	14.1	0.0016	5	0.0001	0.06	-2.85

MUKEY	MUSYM	MUNAME	Area (km^2)	Area (%)	Landslides (#)	Landslides (%)	FR	SI
730214	W	Water > 40 acres	5.7	0.0007	2	0	0.06	-2.87
326496	VcC2	Vega Alta clay, 5 to 12 percent slopes, eroded	8.8	0.001	3	0.0001	0.06	-2.9
326405	CeC	Carrizales fine sand, 2 to 12 percent slopes	11.9	0.0014	4	0.0001	0.05	-2.9
1379827	DsF	Descalabrado clay, 20 to 60 percent slopes	47.8	0.0055	16	0.0003	0.05	-2.91
326586	MwE	Morado clay loam, 20 to 40 percent slopes	3.1	0.0004	1	0	0.05	-2.94
2553831	DwF	Dwarf-El Duque complex, 5 to 60 percent slopes, windswept	3.1	0.0004	1	0	0.05	-2.95
1386660	EcD	El Cacique-La Taina complex, 5 to 20 percent slopes	3.1	0.0004	1	0	0.05	-2.95
326809	FtC2	Fraternidad clay, 5 to 12 percent slopes, eroded	12.4	0.0014	4	0.0001	0.05	-2.95
326792	AhF	Aguilita stony clay loam, 20 to 60 percent slopes	44	0.005	14	0.0003	0.05	-2.96
326833	MtE	Morado clay loam, 20 to 40 percent slopes	3.2	0.0004	1	0	0.05	-2.96
326398	BsC	Bayamon sandy clay loam, 5 to 12 percent slopes	19.1	0.0022	6	0.0001	0.05	-2.97
326412	Cn	Coloso silty clay	25.8	0.003	8	0.0001	0.05	-2.99
326481	SoD	Soller clay, 12 to 20 percent slopes	9.8	0.0011	3	0.0001	0.05	-3
326387	AmC	Almirante sandy clay loam, 5 to 12 percent slopes	3.5	0.0004	1	0	0.05	-3.06
326672	JnD2	Juncal clay, 5 to 20 percent slopes, eroded	3.6	0.0004	1	0	0.04	-3.11
326408	ClD2	Colinas clay loam, 12 to 20 percent slopes, eroded	3.8	0.0004	1	0	0.04	-3.14
326813	HxF	Humatas complex, 20 to 60 percent slopes	3.9	0.0004	1	0	0.04	-3.17
326485	SrF	Soller-Rock outcrop complex, 5 to 60 percent slopes	118.6	0.0136	30	0.0006	0.04	-3.19
326453	MoC2	Moca clay, 2 to 12 percent slopes, eroded	8	0.0009	2	0	0.04	-3.2
1690326	NOTCOM	No Digital Data Available	73.6	0.0084	18	0.0003	0.04	-3.22
326722	Uv	Urban land-Vega Alta complex	100.1	0.0115	24	0.0004	0.04	-3.24
730213	NOTCOM	No Digital Data Available	29.2	0.0034	7	0.0001	0.04	-3.25
326683	MaB	Mabi clay, 2 to 5 percent slopes	8.4	0.001	2	0	0.04	-3.25
326469	RlC	Rio Lajas sand, 2 to 12 percent slopes	4.2	0.0005	1	0	0.04	-3.26
326397	BsB	Bayamon sandy clay loam, 2 to 5 percent slopes	4.4	0.0005	1	0	0.04	-3.29
326394	Ba	Bajura clay	13.5	0.0016	3	0.0001	0.04	-3.32
326617	SrD	Soller-Limestone rockland complex, 5 to 20 percent slopes	14.3	0.0016	3	0.0001	0.03	-3.38
326464	PhC2	Perchas clay, 2 to 12 percent slopes, eroded	4.8	0.0005	1	0	0.03	-3.38
326728	W	Water	14.4	0.0016	3	0.0001	0.03	-3.38
326661	DgF	Descalabrado-Rock outcrop complex, 40 to 60 percent slopes	5	0.0006	1	0	0.03	-3.42
326882	DrF	Descalabrado-Rock land complex, 40 to 60 percent slopes	51.5	0.0059	10	0.0002	0.03	-3.46
326474	RtF	Rock outcrop-Tanama complex, 12 to 60 percent slopes	239.4	0.0275	46	0.0009	0.03	-3.47
326473	RsF	Rock outcrop-San German complex, 20 to 60 percent slopes	10.9	0.0013	2	0	0.03	-3.52
326706	RpD2	Rio Piedras clay, 12 to 20 percent slopes, eroded	5.6	0.0006	1	0	0.03	-3.54
326935	RrC2	Rio Arriba clay, 5 to 12 percent slopes, eroded	17.3	0.002	3	0.0001	0.03	-3.57
326465	PhD2	Perchas clay, 12 to 20 percent slopes, eroded	5.9	0.0007	1	0	0.03	-3.59
326389	AnC	Almirante clay, 5 to 12 percent slopes	17.9	0.0021	3	0.0001	0.03	-3.6
326578	MsB	Matanzas clay, 2 to 5 percent slopes	6.1	0.0007	1	0	0.03	-3.62
326459	NaD	Naranjo clay, 5 to 20 percent slopes	6.2	0.0007	1	0	0.03	-3.64
326864	CdB	Candelero loam, 2 to 5 percent slopes	6.2	0.0007	1	0	0.03	-3.65
326396	BcC	Bayamon sandy loam, 5 to 12 percent slopes	18.8	0.0022	3	0.0001	0.03	-3.65
326478	SmF	San Sebastian gravelly clay, 20 to 60 percent slopes	94.7	0.0109	15	0.0003	0.03	-3.66
2812031	NOTPUB	Not Public Information	51.1	0.0059	8	0.0001	0.03	-3.67
326953	VlC	Via silty clay loam, 3 to 10 percent slopes	6.5	0.0007	1	0	0.02	-3.69

MUKEY	MUSYM	MUNAME	Area (km^2)	Area (%)	Landslides (#)	Landslides (%)	FR	SI
326910	MaC2	Mabi clay, 5 to 12 percent slopes, eroded	13.6	0.0016	2	0	0.02	-3.73
615218	W	Water >40 acres	7.1	0.0008	1	0	0.02	-3.77
326388	AnB	Almirante clay, 2 to 5 percent slopes	21.2	0.0024	3	0.0001	0.02	-3.77
326715	To	Toa silty clay loam, 0 to 2 percent slopes, occasionally flooded	21.5	0.0025	3	0.0001	0.02	-3.79
326704	RoB	Rio Arriba clay, 2 to 5 percent slopes	7.2	0.0008	1	0	0.02	-3.79
326841	QeE2	Quebrada silty clay loam, 20 to 40 percent slopes, eroded	7.3	0.0008	1	0	0.02	-3.8
326804	CyB	Cuyon loam, 0 to 5 percent slopes	7.6	0.0009	1	0	0.02	-3.85
326624	StE	Soller clay, 20 to 40 percent slopes	7.7	0.0009	1	0	0.02	-3.86
1386419	MuD	Mucara loam, 12 to 20 percent slopes	7.8	0.0009	1	0	0.02	-3.87
326519	Cd	Catano sand	7.8	0.0009	1	0	0.02	-3.87
326945	Tt	Toa silty clay loam, 0 to 2 percent slopes, occasionally flooded	23.6	0.0027	3	0.0001	0.02	-3.88
326629	TcE2	Tanama clay, 20 to 40 percent slopes, eroded	16	0.0018	2	0	0.02	-3.89
326938	SaE2	Sabana silty clay loam, 20 to 40 percent slopes, eroded	24.3	0.0028	3	0.0001	0.02	-3.91
326798	CoE	Callabo silty clay loam, 20 to 40 percent slopes	34.3	0.0039	4	0.0001	0.02	-3.96
326817	JnC	Jacana clay, 5 to 12 percent slopes	8.6	0.001	1	0	0.02	-3.97
615217	NOTCOM	No Digital Data Available	53.7	0.0062	6	0.0001	0.02	-4.01
326476	SgD	San German gravelly clay loam, 5 to 20 percent slopes	9	0.001	1	0	0.02	-4.01
328580	W	Water	9.4	0.0011	1	0	0.02	-4.06
326885	Fo	Fortuna clay	10.1	0.0012	1	0	0.02	-4.13
326852	YcC	Yauco silty clay loam, 5 to 12 percent slopes	10.8	0.0012	1	0	0.02	-4.2
326533	CuB2	Coto clay, 2 to 5 percent slopes, eroded	33.5	0.0038	3	0.0001	0.01	-4.23
326934	RrB	Rio Arriba clay, 2 to 5 percent slopes	12.6	0.0014	1	0	0.01	-4.35
326823	LnC2	Llanos clay, 5 to 12 percent slopes, eroded	26.2	0.003	2	0	0.01	-4.39
326640	AmB	Almirante clay, 2 to 5 percent slopes	15.5	0.0018	1	0	0.01	-4.56
326482	SoF	Soller clay, 20 to 60 percent slopes	16.1	0.0018	1	0	0.01	-4.6
326874	Co	Coloso silty clay loam, occasionally flooded	33.4	0.0038	2	0	0.01	-4.63
326492	Ur	Urban land	16.8	0.0019	1	0	0.01	-4.64
1379825	DsD	Descalabrado clay, 12 to 20 percent slopes	17.7	0.002	1	0	0.01	-4.69
326909	MaB	Mabi clay, 0 to 5 percent slopes	20.9	0.0024	1	0	0.01	-4.86
326528	Cn	Coloso silty clay loam	24.3	0.0028	1	0	0.01	-5.01
326816	Jg	Jacaguas silty clay loam	24.6	0.0028	1	0	0.01	-5.02
1386571	Ua	Urban land	60.4	0.0069	1	0	0	-5.92
2706241	PiG	Picacho-Utuado complex, 40 to 90 percent slopes	0.2	0	0	0	0	-5
326819	JzE	Juana Diaz clay loam, 20 to 40 percent slopes	1	0.0001	0	0	0	-5
2553835	SoG	Sonadora-Caguabo complex, 40 to 90 percent slopes	3	0.0003	0	0	0	-5
326545	GnC	Guanajibo sandy loam, 2 to 12 percent slopes	2.1	0.0002	0	0	0	-5
326559	Lc	Leveled clayey land	2.4	0.0003	0	0	0	-5
326673	JuC	Juncos clay, 5 to 12 percent slopes	3	0.0003	0	0	0	-5
1379902	DqA	Dique loam, 0 to 2 percent slopes, frequently flooded	3.8	0.0004	0	0	0	-5
326898	JaC2	Jacana clay, 5 to 12 percent slopes, eroded	10.2	0.0012	0	0	0	-5
326932	Re	Reilly soils	13.3	0.0015	0	0	0	-5
326797	CoD	Callabo silty clay loam, 12 to 20 percent slopes	22.5	0.0026	0	0	0	-5
326850	TuF	Tuque stony clay loam, 12 to 60 percent slopes	29.4	0.0034	0	0	0	-5
326503	AaC2	Aceitunas clay, 2 to 12 percent slopes, eroded	11.8	0.0014	0	0	0	-5

MUKEY	MUSYM	MUNAME	Area (km²)	Area (%)	Landslides (#)	Landslides (%)	FR	SI
326636	AaB	Aceitunas clay, 2 to 5 percent slopes	2.3	0.0003	0	0	0	-5
326381	AcC	Aceitunas clay, 5 to 12 percent slopes	0.5	0.0001	0	0	0	-5
326504	AbC2	Aceitunas sandy clay loam, 2 to 12 percent slopes, eroded	2.7	0.0003	0	0	0	-5
326380	AaC	Aceitunas sandy clay loam, 5 to 12 percent slopes	0.1	0	0	0	0	-5
326854	Ad	Aguadilla loamy sand	9.9	0.0011	0	0	0	-5
326855	Ag	Aguadilla sandy loam, moderately wet	2.8	0.0003	0	0	0	-5
334691	AgF	Aguilita silty clay loam, 20 to 60 percent slopes	0.6	0.0001	0	0	0	-5
334690	AgD	Aguilita silty clay loam, 5 to 20 percent slopes	3.1	0.0004	0	0	0	-5
334692	AkA	Aguirre clay, occasionally ponded	16.9	0.0019	0	0	0	-5
326508	An	Alluvial land	4	0.0005	0	0	0	-5
326386	AmB	Almirante sandy clay loam, 2 to 5 percent slopes	1.5	0.0002	0	0	0	-5
326384	AlB	Almirante sandy loam, 2 to 5 percent slopes	7.5	0.0009	0	0	0	-5
326385	AlC	Almirante sandy loam, 5 to 12 percent slopes	8.9	0.001	0	0	0	-5
1606301	AtD	Altamira gravelly clay, 2 to 20 percent slopes	15.9	0.0018	0	0	0	-5
1606302	AtF	Altamira gravelly clay, 20 to 60 percent slopes	1.6	0.0002	0	0	0	-5
326856	AmB	Amelia gravelly clay loam, 2 to 5 percent slopes	5.5	0.0006	0	0	0	-5
326857	AmC2	Amelia gravelly clay loam, 5 to 12 percent slopes, eroded	6.7	0.0008	0	0	0	-5
326393	ArC	Arecibo fine sand, 2 to 12 percent slopes	2.3	0.0003	0	0	0	-5
326858	An	Arenales sandy loam	1.6	0.0002	0	0	0	-5
326859	Ar	Arenales sandy loam, gravelly substratum	1.2	0.0001	0	0	0	-5
1316502	BaB	Bahia fine sand, 0 to 5 percent slopes	2.7	0.0003	0	0	0	-5
1385077	BhB	Bahia Salinas sand, 0 to 5 percent slopes, rarely flooded	2.2	0.0002	0	0	0	-5
326512	Ba	Bajura clay	9.3	0.0011	0	0	0	-5
326642	Ba	Bajura clay	15.9	0.0018	0	0	0	-5
1356074	BjA	Bajura clay, 0 to 1 percent slopes, frequently flooded	4.4	0.0005	0	0	0	-5
326861	Bc	Bajura clay, frequently flooded	21	0.0024	0	0	0	-5
326860	Ba	Bajura silty clay, saline	1	0.0001	0	0	0	-5
326643	BmB	Bayamon clay, 2 to 5 percent slopes	2.8	0.0003	0	0	0	-5
326400	ByC	Bayamon clay, 5 to 12 percent slopes	7.8	0.0009	0	0	0	-5
326395	BcB	Bayamon sandy loam, 2 to 5 percent slopes	2.8	0.0003	0	0	0	-5
1379803	BkB	Beaches, sand, 0 to 5 percent slopes	0.4	0	0	0	0	-5
326513	BcB	Bejucos sandy clay loam, 2 to 5 percent slopes	1.6	0.0002	0	0	0	-5
326514	BeB	Bejucos sandy loam, 2 to 5 percent slopes	10.6	0.0012	0	0	0	-5
1716033	BmD	Bermeja-Cerro Mariquita complex, 12 to 20 percent slopes	1.1	0.0001	0	0	0	-5
1716036	BmF	Bermeja-Cerro Mariquita complex, 20 to 60 percent slopes	0.8	0.0001	0	0	0	-5
1716034	BmC	Bermeja-Cerro Mariquita complex, 5 to 12 percent slopes	0.7	0.0001	0	0	0	-5
1716038	BrF	Bermeja-Rock outcrop complex, 20 to 60 percent slopes, extremely cobbly	0.6	0.0001	0	0	0	-5
1356075	CaC	Cabo Rojo clay, 2 to 12 percent slopes	3	0.0003	0	0	0	-5
326862	CbD	Caguabo clay loam, 12 to 20 percent slopes	0.5	0.0001	0	0	0	-5
1356078	CbD	Caguabo clay loam, 12 to 20 percent slopes	0.6	0.0001	0	0	0	-5
326518	CcB	Camaguey clay, 2 to 5 percent slopes	1.6	0.0002	0	0	0	-5
326865	CdC2	Candelero loam, 5 to 12 percent slopes, eroded	14.6	0.0017	0	0	0	-5
326404	CcE	Caracoles loam, 20 to 40 percent slopes	2.1	0.0002	0	0	0	-5
326403	CcD	Caracoles loam, 5 to 20 percent slopes	2.5	0.0003	0	0	0	-5

MUKEY	MUSYM	MUNAME	Area (km^2)	Area (%)	Landslides (#)	Landslides (%)	FR	SI
326866	Ce	Cartagena clay	5.9	0.0007	0	0	0	-5
1379800	CeA	Cartagena clay, 0 to 2 percent slopes	12.8	0.0015	0	0	0	-5
2023625	CgF	Casabe clay, 20 to 60 percent slopes	0.7	0.0001	0	0	0	-5
1884546	CgD	Casabe clay, 5 to 20 percent slopes	1.7	0.0002	0	0	0	-5
326649	Cn	Catano loamy sand	0.8	0.0001	0	0	0	-5
326867	Cf	Catano loamy sand	17.3	0.002	0	0	0	-5
326406	Cf	Catano sand	2.7	0.0003	0	0	0	-5
1379802	ChA	Catano sand, 0 to 2 percent slopes	0.9	0.0001	0	0	0	-5
326520	Ce	Catano sandy clay loam	1	0.0001	0	0	0	-5
1716016	CkD	Cerro Mariquita gravelly clay loam, 12 to 20 percent slopes	1.8	0.0002	0	0	0	-5
334712	CkF	Cerro Mariquita gravelly clay loam, 20 to 60 percent slopes	10.4	0.0012	0	0	0	-5
326800	Cr	Cintrona clay	5.5	0.0006	0	0	0	-5
326870	ClB	Coamo clay loam, 2 to 5 percent slopes	3.3	0.0004	0	0	0	-5
1379810	CmB	Coamo clay loam, 2 to 5 percent slopes	0.2	0	0	0	0	-5
326522	Ch	Coastal beach	1.8	0.0002	0	0	0	-5
326407	Cg	Coastal beaches	0.9	0.0001	0	0	0	-5
326872	Cm	Coastal beaches	2.7	0.0003	0	0	0	-5
326409	ClE2	Colinas clay loam, 20 to 40 percent slopes, eroded	10.4	0.0012	0	0	0	-5
326526	CmD	Colinas cobbly clay loam, 12 to 20 percent slopes	0.5	0.0001	0	0	0	-5
1379808	CoA	Coloso clay, 0 to 2 percent slopes, occasionally flooded	15.9	0.0018	0	0	0	-5
326875	Cr	Coloso silty clay	9.5	0.0011	0	0	0	-5
326654	Cs	Coloso silty clay loam	11	0.0013	0	0	0	-5
326801	Ct	Constancia silty clay	28.1	0.0032	0	0	0	-5
326876	Cs	Corcega sandy loam	5.1	0.0006	0	0	0	-5
326531	Cr	Corcega silty clay loam	1.3	0.0002	0	0	0	-5
326418	CsC	Corozo fine sand, 2 to 12 percent slopes	7	0.0008	0	0	0	-5
326803	Cx	Cortada silty clay loam	14.9	0.0017	0	0	0	-5
1386555	CtA	Cortada silty clay loam, 0 to 2 percent slopes, occasionally flooded	1	0.0001	0	0	0	-5
1716031	CuF	Costa-Pitahaya complex, 20 to 60 percent slopes	17.8	0.002	0	0	0	-5
1716030	CuD	Costa-Pitahaya complex, 5 to 20 percent slopes	6.1	0.0007	0	0	0	-5
326532	CtB2	Cotito clay, 0 to 5 percent slopes, eroded	2.7	0.0003	0	0	0	-5
326419	CtB	Coto clay, 2 to 5 percent slopes	0.2	0	0	0	0	-5
326420	CtC	Coto clay, 5 to 12 percent slopes	0	0	0	0	0	-5
326534	CuC2	Coto clay, 5 to 12 percent slopes, eroded	16.3	0.0019	0	0	0	-5
326535	CvB	Coto sandy clay loam, 2 to 5 percent slopes	0.7	0.0001	0	0	0	-5
326877	DaC	Daguao silty clay loam, deep variant, 2 to 12 percent slopes	1.3	0.0001	0	0	0	-5
1379822	DeD	Delicias clay, 5 to 20 percent slopes	2	0.0002	0	0	0	-5
326880	DeE2	Descalabrado clay loam, 20 to 40 percent slopes, eroded	14.3	0.0016	0	0	0	-5
326879	43801	Descalabrado clay loam, 5 to 12 percent slopes, eroded	3.4	0.0004	0	0	0	-5
1379824	DsC	Descalabrado clay, 2 to 12 percent slopes	8	0.0009	0	0	0	-5
326662	Dm	Dique loam	1.3	0.0001	0	0	0	-5
326663	Dr	Durados sandy loam	1.3	0.0001	0	0	0	-5
1884721	EdD	El Descanso-Hoconuco complex, 5 to 20 percent slopes	0.1	0	0	0	0	-5
1690984	EpD	El Papayo gravelly clay loam, 12 to 20 percent slopes	4.6	0.0005	0	0	0	-5

MUKEY	MUSYM	MUNAME	Area (km²)	Area (%)	Landslides (#)	Landslides (%)	FR	SI
1690982	EpC	El Papayo gravelly clay loam, 2 to 12 percent slopes	4.1	0.0005	0	0	0	-5
1716015	EpF	El Papayo gravelly clay loam, 20 to 60 percent slopes	4.1	0.0005	0	0	0	-5
326544	Es	Espinal sand	2.4	0.0003	0	0	0	-5
326426	EbB	Espinosa sandy clay loam, 2 to 5 percent slopes	1.8	0.0002	0	0	0	-5
326424	EaB	Espinosa sandy loam, 2 to 5 percent slopes	2.3	0.0003	0	0	0	-5
326425	EaC	Espinosa sandy loam, 5 to 12 percent slopes	4.8	0.0006	0	0	0	-5
328579	Es	Estacion silty clay loam	0	0	0	0	0	-5
326883	FaC	Fajardo clay, 2 to 10 percent slopes	1.3	0.0001	0	0	0	-5
326884	FaC2	Fajardo clay, 2 to 10 percent slopes, eroded	1.9	0.0002	0	0	0	-5
326807	Fe	Fe clay	2.6	0.0003	0	0	0	-5
334703	FeA	Fe clay, 0 to 2 percent slopes	4.3	0.0005	0	0	0	-5
326886	FrA	Fraternidad clay, 0 to 2 percent slopes	9.3	0.0011	0	0	0	-5
334704	FrA	Fraternidad clay, 0 to 2 percent slopes	20.7	0.0024	0	0	0	-5
326808	FtB	Fraternidad clay, 2 to 5 percent slopes	34.6	0.004	0	0	0	-5
326887	FrB	Fraternidad clay, 2 to 5 percent slopes	1.4	0.0002	0	0	0	-5
334705	FrB	Fraternidad clay, 2 to 5 percent slopes	9.9	0.0011	0	0	0	-5
326430	Ga	Garrochales muck	3.7	0.0004	0	0	0	-5
615215	GPQ	Gravel pits, quarry	2	0.0002	0	0	0	-5
1690325	GPQ	Gravel, Pits, Quarries	1.6	0.0002	0	0	0	-5
326888	Gm	Guamani silty clay loam	15.9	0.0018	0	0	0	-5
1379915	GbF	Guanabano clay, 20 to 60 percent slopes	1.5	0.0002	0	0	0	-5
1379916	GhC	Guanajibo gravelly sandy clay loam, 2 to 12 percent slopes	3.2	0.0004	0	0	0	-5
334709	GnA	Guanica clay, 0 to 1 percent slopes	16.3	0.0019	0	0	0	-5
334710	GuB	Guayabo fine sand, 0 to 5 percent slopes	1.2	0.0001	0	0	0	-5
1716028	GyB	Guayacan clay, 0 to 5 percent slopes	5.9	0.0007	0	0	0	-5
1716026	GyD	Guayacan clay, 12 to 20 percent slopes	1.2	0.0001	0	0	0	-5
1716024	GyC	Guayacan clay, 5 to 12 percent slopes	4.4	0.0005	0	0	0	-5
326891	GyC2	Guayama clay loam, moderately deep variant, 2 to 12 percent, slopes, eroded	3.3	0.0004	0	0	0	-5
326431	GeC	Guerrero sand, 2 to 12 percent slopes	13.4	0.0015	0	0	0	-5
326547	GuB	Guerrero sand, 2 to 5 percent slopes	3.3	0.0004	0	0	0	-5
326666	Hm	Humacao loam	0.3	0	0	0	0	-5
326892	HmB	Humacao loam, 2 to 5 percent slopes	4.3	0.0005	0	0	0	-5
2706245	HtF2	Humatas clay, 40 to 60 percent slopes	0	0	0	0	0	-5
326551	HuE	Humatas gravelly clay, 12 to 40 percent slopes	0	0	0	0	0	-5
326814	Hy	Hydraquents	0.7	0.0001	0	0	0	-5
326432	HD	Hydraquents, frequently flooded	2.1	0.0002	0	0	0	-5
326433	HS	Hydraquents, saline	1.3	0.0002	0	0	0	-5
326670	Hy	Hydraquents, saline	3.5	0.0004	0	0	0	-5
326815	Hz	Hydraquents, saline	8.2	0.0009	0	0	0	-5
326552	Ig	Igualdad clay	1.5	0.0002	0	0	0	-5
326438	IsC	Islote sandy clay loam, 2 to 12 percent slopes	3.9	0.0005	0	0	0	-5
334713	JaB	Jacana clay, 0 to 5 percent slopes	5.7	0.0007	0	0	0	-5
326897	JaB	Jacana clay, 2 to 5 percent slopes	3	0.0003	0	0	0	-5
334714	JaC	Jacana clay, 5 to 12 percent slopes	6.2	0.0007	0	0	0	-5

MUKEY	MUSYM	MUNAME	Area (km^2)	Area (%)	Landslides (#)	Landslides (%)	FR	SI
326671	JaE2	Jagueyes loam, 20 to 40 percent slopes, eroded	0.7	0.0001	0	0	0	-5
326439	Ja	Jareales clay	7.5	0.0009	0	0	0	-5
326440	JoC	Jobos sandy loam, 2 to 12 percent slopes	11.1	0.0013	0	0	0	-5
326555	JoB	Jobos sandy loam, 2 to 5 percent slopes	9.6	0.0011	0	0	0	-5
1407076	JBA	Joyuda, Atolladero, and Bajura soils, very frequently flooded	2.5	0.0003	0	0	0	-5
326674	JuD	Juncos clay, 12 to 20 percent slopes	3.1	0.0004	0	0	0	-5
326900	JuC	Junquitos gravelly clay loam, 5 to 12 percent slopes	6.3	0.0007	0	0	0	-5
1716023	LcE	La Covana-Limestone outcrop-Seboruco complex, 12 to 40 percent slopes	8.9	0.001	0	0	0	-5
1857273	LdA	La Luna silty clay loam, 0 to 2 percent slopes, occasionally flooded	3.9	0.0004	0	0	0	-5
328581	LDF	Landfill	0.2	0	0	0	0	-5
730212	LFD	Landfill	0	0	0	0	0	-5
615216	LFD	Landfill	0.2	0	0	0	0	-5
1386581	LfC	Landfill, 0 to 8 percent slopes	0.9	0.0001	0	0	0	-5
326557	LaB2	Lares clay, 0 to 5 percent slopes, eroded	5.7	0.0006	0	0	0	-5
326675	LaB	Lares clay, 2 to 5 percent slopes	1	0.0001	0	0	0	-5
326820	LeC	Lares clay, 5 to 12 percent slopes	1.3	0.0002	0	0	0	-5
326901	Lc	Leveled clayey land	2.1	0.0002	0	0	0	-5
326560	Le	Leveled clayey land, shallow	0.3	0	0	0	0	-5
326561	Lf	Leveled land, frequently flooded	2	0.0002	0	0	0	-5
326564	Lr	Limestone rock land	5.2	0.0006	0	0	0	-5
326903	LoC2	Lirios clay loam, 3 to 10 percent slopes, eroded	2.4	0.0003	0	0	0	-5
326822	LnB	Llanos clay, 2 to 5 percent slopes	11.8	0.0014	0	0	0	-5
334695	LnA	Llanos Costa loam, 0 to 2 percent slopes	2.6	0.0003	0	0	0	-5
1316499	LnB	Llanos Costa loam, 2 to 5 percent slopes	3.5	0.0004	0	0	0	-5
1316500	LnC	Llanos Costa loam, 5 to 12 percent slopes	6.3	0.0007	0	0	0	-5
326908	LyF	Los Guineos-Yunque-Stony rock land association steep	1.8	0.0002	0	0	0	-5
2706230	LuB	Luquillo-El Verde complex, 0 to 5 percent slopes, occasionally flooded	0.5	0.0001	0	0	0	-5
2553830	LuB	Luquillo-El Verde complex, 0 to 5 percent slopes, occasionally flooded	0.6	0.0001	0	0	0	-5
326682	MaA	Mabi clay, 0 to 2 percent slopes	1.2	0.0001	0	0	0	-5
326911	MaD2	Mabi clay, 12 to 20 percent slopes, eroded	3.2	0.0004	0	0	0	-5
1386391	MaB	Mabi clay, 2 to 5 percent slopes, rarely flooded	1.5	0.0002	0	0	0	-5
326912	McA	Machete loam, 0 to 2 percent slopes	4	0.0005	0	0	0	-5
326913	McB	Machete loam, 2 to 5 percent slopes	4.9	0.0006	0	0	0	-5
326828	Ma	Machuelo clay	7.5	0.0009	0	0	0	-5
326685	Md	Made land	0.6	0.0001	0	0	0	-5
326914	Md	Made land	15.4	0.0018	0	0	0	-5
1386393	MbA	Maguayo very gravelly sandy clay loam, 0 to 2 percent slopes	1.3	0.0002	0	0	0	-5
1386395	MbC	Maguayo very gravelly sandy clay loam, 2 to 12 percent slopes	2.1	0.0002	0	0	0	-5
326570	MdB	Maleza fine sandy loam, 2 to 5 percent slopes	2.7	0.0003	0	0	0	-5
334743	MDA	Manglillo, Boqueron and Serrano soils, very frequently flooded	11.4	0.0013	0	0	0	-5
326572	Mn	Mani clay	2.3	0.0003	0	0	0	-5

MUKEY	MUSYM	MUNAME	Area (km²)	Area (%)	Landslides (#)	Landslides (%)	FR	SI
1386398	MeA	Mani clay, 0 to 2 percent slopes, occasionally flooded	2.7	0.0003	0	0	0	-5
326571	Mh	Mani silty clay loam, overwash	0	0	0	0	0	-5
326573	MoD2	Maresua silty clay loam, 12 to 20 percent slopes, eroded	0	0	0	0	0	-5
1386561	MgF	Maresua-Serpentinite outcrop complex, 40 to 60 percent slopes	0.8	0.0001	0	0	0	-5
334720	MiD	Mariana gravelly clay loam, 12 to 20 percent slopes	2.1	0.0002	0	0	0	-5
334721	MiE	Mariana gravelly clay loam, 20 to 40 percent slopes	2.4	0.0003	0	0	0	-5
326688	Mp	Martin Pena muck	9	0.001	0	0	0	-5
326452	MnB	Matanzas clay, 2 to 5 percent slopes	2.9	0.0003	0	0	0	-5
326689	MsB	Matanzas clay, 2 to 5 percent slopes	3.5	0.0004	0	0	0	-5
326579	MtB	Matanzas-Limestone rockland complex, 0 to 5 percent slopes	3.1	0.0004	0	0	0	-5
326451	MmF	Matanzas-Rock outcrop complex, 5 to 60 percent slopes	4.1	0.0005	0	0	0	-5
326915	Me	Maunabo clay	20.2	0.0023	0	0	0	-5
326916	MlC	Mayo loam, 3 to 10 percent slopes	2.4	0.0003	0	0	0	-5
334717	MnA	Melones clay, 0 to 2 percent slopes	0.5	0.0001	0	0	0	-5
1602235	MnC	Melones clay, 2 to 12 percent slopes	4.7	0.0005	0	0	0	-5
326831	Mr	Meros sand	4.5	0.0005	0	0	0	-5
326917	MrB	Meros sand, 1 to 6 percent slopes	2.7	0.0003	0	0	0	-5
326582	MuD3	Moca clay, 12 to 20 percent slopes, severely eroded	1	0.0001	0	0	0	-5
326580	MuC2	Moca clay, 5 to 12 percent slopes, eroded	3	0.0003	0	0	0	-5
1716018	MoB	Montalva clay, 0 to 5 percent slopes	4.7	0.0005	0	0	0	-5
1716017	MoC	Montalva clay, 5 to 12 percent slopes	3.4	0.0004	0	0	0	-5
326584	MvC	Montegrande clay, 2 to 12 percent slopes	3.1	0.0004	0	0	0	-5
1386408	MqC	Montegrande clay, 2 to 12 percent slopes	8.5	0.001	0	0	0	-5
326690	MtB	Montegrande clay, 2 to 5 percent slopes	0.8	0.0001	0	0	0	-5
1386411	MrD	Morado clay loam, 12 to 20 percent slopes	1	0.0001	0	0	0	-5
326457	MuE	Mucara clay, 20 to 40 percent slopes	0.5	0.0001	0	0	0	-5
326588	MxC	Mucara clay, 5 to 12 percent slopes	0	0	0	0	0	-5
1386418	MuC	Mucara loam, 5 to 12 percent slopes	3.5	0.0004	0	0	0	-5
326918	MuD2	Mucara silty clay loam, 12 to 20 percent slopes, eroded	6.5	0.0008	0	0	0	-5
336721	NOTCOM	No Digital Data Available	63.2	0.0072	0	0	0	-5
2812030	NOTPUB	Not Public Information	3.7	0.0004	0	0	0	-5
1379801	OrA	Olivares muck, ponded	1.4	0.0002	0	0	0	-5
326462	Pa	Palmar muck	2.2	0.0002	0	0	0	-5
334722	PaA	Palmarejo loam, 0 to 2 percent slopes	0.8	0.0001	0	0	0	-5
334723	PaB	Palmarejo loam, 2 to 5 percent slopes	2.4	0.0003	0	0	0	-5
334724	PaC	Palmarejo loam, 5 to 12 percent slopes	0.8	0.0001	0	0	0	-5
2706244	PdF	Pandura-Very stony land complex, 40 to 60 percent slopes	0	0	0	0	0	-5
326925	PeC2	Parcelas clay, 5 to 12 percent slopes, eroded	4.6	0.0005	0	0	0	-5
1384474	PgA	Parguera clay, 0 to 2 percent slopes	1.4	0.0002	0	0	0	-5
334708	PgB	Parguera clay, 2 to 5 percent slopes	1.2	0.0001	0	0	0	-5
326926	PlB	Paso Seco clay, 0 to 5 percent slopes	11.6	0.0013	0	0	0	-5
326838	PaB	Paso Seco clay, 2 to 5 percent slopes	11.7	0.0013	0	0	0	-5
326927	PmD2	Patillas clay loam, 12 to 20 percent slopes, eroded	2	0.0002	0	0	0	-5
2706243	PcE	Picacho-Ciales complex, 5 to 40 percent slopes	0	0	0	0	0	-5

MUKEY	MUSYM	MUNAME	Area (km^2)	Area (%)	Landslides (#)	Landslides (%)	FR	SI
326929	Pn	Pinones silty clay	3.6	0.0004	0	0	0	-5
1407028	PsF	Pitahaya-Limestone outcrop-Seboruco complex, 40 to 60 percent slopes	33	0.0038	0	0	0	-5
1887151	PsG	Pitahaya-Limestone outcrop-Seboruco complex, 60 to 90 percent slopes	1.7	0.0002	0	0	0	-5
1386537	Pt	Pits and Quarries	1.4	0.0002	0	0	0	-5
326930	Po	Poncena clay	9.8	0.0011	0	0	0	-5
326931	PrC2	Pozo Blanco clay loam, 5 to 12 percent slopes, eroded	1.9	0.0002	0	0	0	-5
334728	PzB	Pozo Blanco clay, 0 to 5 percent slopes	0.7	0.0001	0	0	0	-5
334730	PzD	Pozo Blanco clay, 12 to 20 percent slopes	0.2	0	0	0	0	-5
334729	PzC	Pozo Blanco clay, 5 to 12 percent slopes	1.7	0.0002	0	0	0	-5
2553839	PrF	Prieto very cobbly clay loam, 20 to 60 percent slopes	0.8	0.0001	0	0	0	-5
326840	QeD2	Quebrada silty clay loam, 12 to 20 percent slopes, eroded	5.1	0.0006	0	0	0	-5
1386547	ReA	Reilly sandy loam, 0 to 2 percent slopes, frequently flooded	5.5	0.0006	0	0	0	-5
326933	Rp	Reparada clay	0.9	0.0001	0	0	0	-5
326602	RlB	Rio Lajas sand, 2 to 5 percent slopes	4.5	0.0005	0	0	0	-5
326707	RpE2	Rio Piedras clay, 20 to 40 percent slopes, eroded	3.3	0.0004	0	0	0	-5
326605	Rr	Riverwash	0	0	0	0	0	-5
326472	Rr	Rock outcrop, sandstone	0.6	0.0001	0	0	0	-5
1386549	RoD	Rosario silty clay, 12 to 20 percent slopes	1.2	0.0001	0	0	0	-5
326475	SaB	Sabana Seca clay, 2 to 5 percent slopes	5.3	0.0006	0	0	0	-5
326710	ScB	Sabana Seca clay, 2 to 8 percent slopes	3	0.0003	0	0	0	-5
326711	Sm	Saladar muck	6.2	0.0007	0	0	0	-5
1386543	Sa	Salt flats, ponded	5.1	0.0006	0	0	0	-5
1386554	Sb	Salt pits	1.2	0.0001	0	0	0	-5
326940	Sm	Salt water marsh	5.1	0.0006	0	0	0	-5
326845	Sa	San Anton clay loam	24.1	0.0028	0	0	0	-5
334731	ScA	San Anton clay loam, 0 to 2 percent slopes, occasionally flooded	10.9	0.0012	0	0	0	-5
334734	SdD	San German cobbly clay loam, 5 to 20 percent slopes	0.2	0	0	0	0	-5
326611	ScB	San German cobbly sandy loam, 0 to 5 percent slopes	0.1	0	0	0	0	-5
326609	SaD	San German gravelly clay loam, 12 to 20 percent slopes	14.2	0.0016	0	0	0	-5
326610	SaE	San German gravelly clay loam, 20 to 40 percent slopes	8.3	0.001	0	0	0	-5
1407068	SgF	San German-Duey complex, 20 to 60 percent slopes	18.7	0.0021	0	0	0	-5
1407070	SgD	San German-Duey complex, 5 to 20 percent slopes	1	0.0001	0	0	0	-5
326479	SnC	Santa Clara clay, 2 to 12 percent slopes	5	0.0006	0	0	0	-5
326613	SeB	Santa Clara silty clay loam, 2 to 5 percent slopes	2.1	0.0002	0	0	0	-5
334737	SiA	Santa Isabel clay, 0 to 2 percent slopes	2	0.0002	0	0	0	-5
326615	Sn	Santoni clay	3.5	0.0004	0	0	0	-5
1379905	SoC	Seboruco silty clay loam, 2 to 12 percent slopes	2	0.0002	0	0	0	-5
326846	Se	Serrano sand	3.4	0.0004	0	0	0	-5
326623	StD	Soller clay, 12 to 20 percent slopes	4	0.0005	0	0	0	-5
326621	StB	Soller clay, 2 to 5 percent slopes	0	0	0	0	0	-5
326622	StC	Soller clay, 5 to 12 percent slopes	1.3	0.0002	0	0	0	-5
326620	SsE2	Soller cobbly clay, 20 to 40 percent slopes, eroded	1.6	0.0002	0	0	0	-5
334739	SsB	Sosa sandy loam, 2 to 5 percent slopes	6.5	0.0007	0	0	0	-5

MUKEY	MUSYM	MUNAME	Area (km²)	Area (%)	Landslides (#)	Landslides (%)	FR	SI
334740	SsC	Sosa sandy loam, 5 to 12 percent slopes	0.5	0.0001	0	0	0	-5
326625	Ta	Talante loam	3.6	0.0004	0	0	0	-5
326941	Ta	Talante soils	20.1	0.0023	0	0	0	-5
326628	TcD2	Tanama clay, 12 to 20 percent slopes, eroded	3.8	0.0004	0	0	0	-5
326487	TaB	Tanama clay, 2 to 5 percent slopes	1.3	0.0001	0	0	0	-5
326626	TcB2	Tanama clay, 2 to 5 percent slopes, eroded	2	0.0002	0	0	0	-5
326847	Te	Teresa clay	14.4	0.0017	0	0	0	-5
334741	TeA	Teresa clay, 0 to 1 percent slopes	3.7	0.0004	0	0	0	-5
334742	TfA	Teresa clay, ponded	0.7	0.0001	0	0	0	-5
326490	Tb	Tiburones muck	14.1	0.0016	0	0	0	-5
326848	Tf	Tidal flats	1.8	0.0002	0	0	0	-5
326943	Tf	Tidal flats	4.7	0.0005	0	0	0	-5
326630	Td	Tidal swamp	2.4	0.0003	0	0	0	-5
326944	Ts	Tidal swamp	49.5	0.0057	0	0	0	-5
1386570	ToA	Toa clay loam, 0 to 2 percent slopes, occasionally flooded	17.1	0.002	0	0	0	-5
326716	TrB	Torres loamy sand, 2 to 5 percent slopes	3.6	0.0004	0	0	0	-5
326717	Ts	Tropopsamments	0.5	0.0001	0	0	0	-5
1386574	UbB	Urban land-Bahia complex, 0 to 5 percent slopes	0.4	0.0001	0	0	0	-5
326719	Ud	Urban land-Durados complex	14	0.0016	0	0	0	-5
1386576	UgB	Urban land-Guayabo complex, 0 to 5 percent slopes	0.1	0	0	0	0	-5
326721	Us	Urban land-Sabana Seca complex	8.6	0.001	0	0	0	-5
1386577	UsC	Urban land-Sosa complex, 5 to 12 percent slopes	0.2	0	0	0	0	-5
326946	UpF	Utuado-Picacho-Stony rockland association, very steep	0.3	0	0	0	0	-5
326948	Va	Vayas silty clay loam, occasionally flooded	1.7	0.0002	0	0	0	-5
1407077	VaA	Vayas silty clay, 0 to 2 percent slopes, occasionally flooded	2.7	0.0003	0	0	0	-5
326949	Vc	Vayas silty clay, frequently flooded	5.4	0.0006	0	0	0	-5
326495	VcB	Vega Alta clay, 2 to 5 percent slopes	5.4	0.0006	0	0	0	-5
326723	VaB	Vega Alta clay, 2 to 5 percent slopes	1.6	0.0002	0	0	0	-5
326493	VaB	Vega Alta sandy clay loam, 2 to 5 percent slopes	0.7	0.0001	0	0	0	-5
326950	VeB	Vega Alta silty clay loam, 2 to 5 percent slopes	3.3	0.0004	0	0	0	-5
326497	VeB	Vega Baja clay, 2 to 5 percent slopes	6.4	0.0007	0	0	0	-5
326725	Vg	Vega Baja silty clay	0.2	0	0	0	0	-5
326952	VgA	Vega Baja silty clay loam, 0 to 3 percent slopes	2	0.0002	0	0	0	-5
326498	Vg	Vigia muck	6.4	0.0007	0	0	0	-5
326957	VvA	Vives clay, 0 to 2 percent slopes	6.2	0.0007	0	0	0	-5
326958	VvB	Vives clay, 2 to 7 percent slopes	9.6	0.0011	0	0	0	-5
326956	Vs	Vives silty clay loam, high bottom	12	0.0014	0	0	0	-5
326727	Vv	Vivi loam	0.9	0.0001	0	0	0	-5
326959	Vw	Vivi loam	7	0.0008	0	0	0	-5
1386780	VoD	Voladora clay, 12 to 20 percent slopes	0.9	0.0001	0	0	0	-5
1386764	VoC	Voladora clay, 5 to 12 percent slopes	2.6	0.0003	0	0	0	-5
1690327	W	Water	18	0.0021	0	0	0	-5
334747	W	Water	5.3	0.0006	0	0	0	-5
326960	Wa	Wet alluvial land	14.2	0.0016	0	0	0	-5
326851	YcB	Yauco silty clay loam, 2 to 5 percent slopes	3.1	0.0004	0	0	0	-5

ISSN 2331-1258 (online)
https://doi.org/10.3133/ofr20201022